UNIVERSITÀ DI SIENA
1240

DEPARTMENT OF MEDICAL BIOTECHNOLOGY
Doctoral School in Biochemistry and Molecular Biology
XXXIII Cycle

The antimicrobial peptide SET-M33. Strategies to improve the manufacturing procedures and production of back-up molecules as novel antibiotics

SCIENTIFIC-DISCIPLINARY SECTOR: BIO/10

COORDINATOR
Prof. Lorenza Trabalzini

TUTOR:
Prof. Alessandro Pini

DOCTORAL THESIS OF:
Francesca Maria Castiglia

ACADEMIC YEAR: 2019-2020

A scientist in his laboratory is not a mere technician: he is also a child confronting natural phenomena that impress him as though they were fairy tales.

Marie Curie

ABSTRACT

The increasing frequency of multidrug-resistant (MDR) pathogens leads to an urgent need for the development of new antimicrobial drugs and new strategies for the treatment of infectious diseases. Antimicrobial peptides (AMPs) are described as a promising alternative to traditional antibiotics, powerful to address the increasing problem of antibiotic resistance and hold promise to be developed as novel antibiotics thanks to their antimicrobial, immunomodulatory and anti-inflammatory combined properties. However, despite their desirable characteristic, AMPs show limited pharmaceutical development due to their toxicity, instability, manufacturing costs and systemic administration. Researchers and industry have been seeking news AMPs of natural or synthetic origin with low toxicity and longer half-life necessary for drug development. SET-M33 peptide, optimized version of an artificial peptide sequence isolated from a random phage library, is a synthetic cationic peptide obtained in tetra-branched form for making it more resistant to degradation in biological fluids and more suitable for clinical applications than its linear analogue. SET-M33 shows broadly high antimicrobial activity, both *in vitro* and *in vivo*, against Gram-negative bacteria, anti-inflammatory activity through selective LPS neutralization, low hemolytic activity, lack of immunogenicity and ability to eradicate biofilms.

In this thesis are reported strategies focused to improve the biopharmaceutical development and manufacturing procedures of the peptide SET-M33.

First, the secondary structure of the peptide was investigated by NMR to fully characterize the product in the framework of preclinical studies. The formation of helixes or β-sheets in the structure had to be explored to predict the behavior of the branched peptide in solution, with a view to designing a formulation for parenteral administration.

Salt formation is important in biopharmaceutical drug development as it modulates drug solubility, stability and bioavailability. Since the final formulation of SET-M33 had to be strictly defined in terms of counter-ions, a novel salt form, SET-M33 chloride was synthetized and characterized. SET-M33 chloride retains its activity against Gram-negative bacteria and gains in solubility, with a possible improvement in the pharmacokinetic profile. The opportunity of using a chloride counter-ion is very convenient from a process development point of view and did not increase the toxicity of the antimicrobial drug.

In addition, to identify back-up molecules, a panel of modified versions of SET-M33 was tested in order to produce new molecules with better performance in terms of pharmaceutical profile and manufacturing costs. Amongst them, the opportunity of using SET-M33D-L-Ile and SET-M33D-Leu/Ile will allow to decrease the costs in the synthesis process and SET-M33-Gly/Ala, to eliminate the degradation site for bacterial proteases, without altering the strong antimicrobial activity of the original peptide.

INDEX

INTRODUCTION

Antimicrobial resistance

Antimicrobial resistance is currently evaluated one of the main threats to global public health by the World Health Organization (WHO) [1], particularly for the global spread of multidrug-resistant (MDR) bacterial pathogens causing increases in nosocomial infections and in hospital mortality [2-5]. The resistance is the ability of bacteria to grow in the presence of high concentrations of an antibiotic and it is caused by reduced permeability of the membrane or by increased efflux that block the access of antibiotic to its targets, by inherited mutations and post-translational modifications of antibiotic targets and also by enzyme-catalized modification/degradation of the antibiotic molecule itself [6-7]. According to the Infectious Diseases Society of America (IDSA), the most worrying MDR bacterial pathogens are *Enterococcus faecium*, *Staphylococcus aureus*, *Klebsiella pneumoniae*, *Acinetobacter baumannii*, *Pseudomonas aeruginosa*, and *Enterobacter* spp., known as the "ESKAPE" pathogens [8]. Some other opportunistic pathogens, like *Escherichia coli*, *Enterococcus faecalis*, and *Burkholderia cepacia* can also become MDR strains and are able to cause severe infections. The failure of the most traditional antibiotics for killing bacteria leads to an urgent need to develop new antimicrobial drugs and new strategies for the treatment of infectious diseases [9-10]; the increasing antibiotic resistance, due to the inability and the shortage of new antibiotics, suggests that we are heading for a "post-antibiotics era", where the previously effective therapeutic strategies are no longer relevant [11]. Moreover, the number of new antibiotics approved by the U.S. Food and Drug Administration (FDA) has steadily declined every year since 1980 and the major part of therapeutics in clinical development are modified derivatives of already existing antibiotics, which improve the activity and reduce the toxicity of the respective parent molecules [12-13]. Unfortunately, this procedure has led to the same undesired result namely bacterial resistance has developed also against these modified classes, either by alterations of the same resistance mechanisms observed with the original compounds or horizontal acquisition of new resistance genes [14]. Therefore, the need for novel and effective alternatives is essential [15-18].

Antimicrobial peptides

Since their isolation and characterization in the late 1980, antimicrobial peptides (AMPs) have been evaluated one of the most important solutions to overcome the crisis of antimicrobial resistance [19-25]. AMPs are described as a promising alternative to traditional antibiotics, powerful to address the increasing problem of antibiotic resistance and hold promise to be developed as novel antibiotics [16]. Moreover, these precious molecules can act on multiple-fronts; indeed, in addition to their antimicrobial properties, they have been shown to possess immunomodulatory functions, to have anti-inflammatory properties, to demonstrate anti-cancer activity and to inhibit and eradicate biofilms [27-31]. Therefore, this ability to address different perspectives makes the AMPs very attractive [16, 18] and has led to them being referred to as host defense peptides (HDPs) [16, 32-34].

Properties of antimicrobial peptides

Antimicrobial peptides (AMPs) are produced naturally by all organisms ranging from bacteria to plants, vertebrates and invertebrates or they also can be designed and chemically synthetized in the laboratory. They can kill bacteria directly, by either targeting a wide spectrum of bacteria, or by being selective for Gram-positive and Gram-negative bacteria. Moreover, these peptides are also active against pathogenic species like viruses, fungi and parasites [16, 35-37]. Antimicrobial peptides are composed by a short amino acid sequence (between 12-50 aa) carrying a substantial portion of hydrophobic residues (50% or more), and most AMPs have a net positive charge, although a few anionic peptides are known [38]. The major part of antimicrobial peptides is amphipathic and this characteristic leads to their ability to fold in different conformations often induced by selective interaction with the bacterial membrane [39]. The cationic nature is ascribed to the presence of lysine and arginine (and sometimes histidine) residues while the hydrophobicity to the percent of hydrophobic residues like valine, leucine, isoleucine, alanine, methionine, phenylalanine, tyrosine and tryptophan in the peptide sequence. The amphipathicity can be thought of as the balance between the cationic and hydrophobic residues, not just at the sequence level but also in terms of the 2D or 3D structure of the AMPs [40].

To date, an analysis in the Antimicrobial Peptide Database (APD) has revealed that the peptide average length is 33 amino acids and more than 90% of these peptides have no more than 50 amino acids. Moreover, APD has showed that the mean peptide net charge is +3, the average hydrophobic content is 54% and about 45% of the peptides do not have cysteine [41]. Finally, the APD has revealed that these peptides all have different structures and sequence motifs and show the ability to kill a range of pathogens [42-43]. The structure, the sequence and the amphipathicity of the antimicrobial peptides all play a key role to determine the peptide's activity. Therefore, it is important to take these properties into account.

Structural features of antimicrobial peptides

The AMPs, both natural and synthetic, are divided into four major classes based on their structure: α-helical, β-sheet, not α or β extended and mixed structures peptides [44]. The structural representation of these classes is reported in Figure 1. The shared ability amongst cationic AMPs to fold into respective amphipathic or amphiphilic conformations is often induced by interaction with the membranes or membrane mimics.

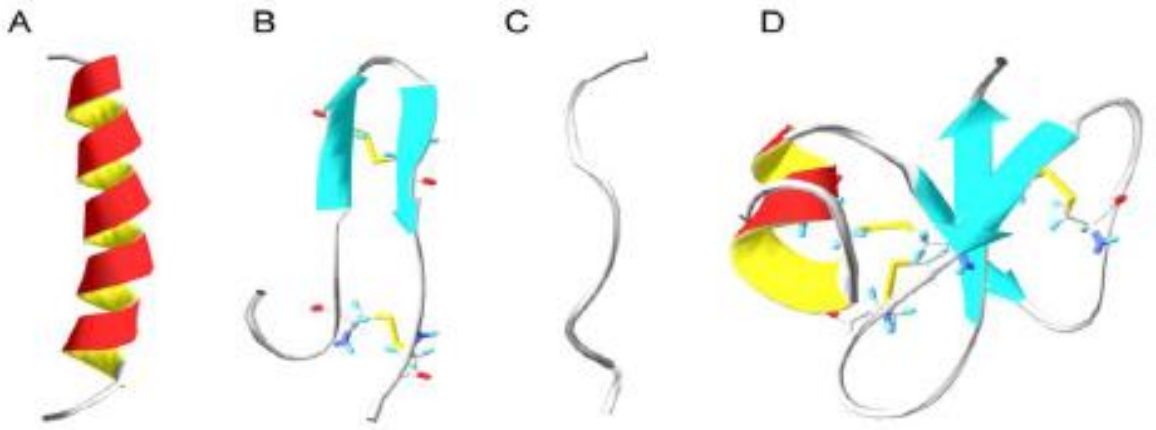

Figure 1. Structural classes of antimicrobial peptides; (A) α-helical, human cathelicidin LL-37 [48]; (B) β-sheet, Polyphemusin I [52]; (C) extended, indolicidin [54]; (D) mixed structure, human β-defensin-2[57]. Disulfide bonds are indicated in yellow.

α-Helical peptides

The α-Helical peptides are characterized by their α-helical conformation and predominantly found in the matrix of frogs and insects. The major part of these peptides are unstructured in aqueous solution but become structured upon contact with detergents/surfactants above critical micellar concentration like sodium dodecyl sulfate (SDS), micelles and liposomes [45]. These peptides have an efficient solubility into the microbial membrane due to the two opposite different faces of their helix containing hydrophobic and polar residues, respectively [46]. Generally, peptides belonging to this class do not have cysteine residues; thus, they are unable to form disulfide bridges [47]. An extensively studied human AMP in this class is cathelicidin LL37 (Figure 1A) that plays an important role in immunomodulatory and inflammation responses [48-49]; this class also includes the α-helical magainins which show antimicrobial activity against Gram-negative and Gram-positive bacteria, fungi, yeast and viruses [50].

β-Sheet peptides

The β-sheet peptides are characterized by the presence of an antiparallel β-sheet, generally stabilized by conserved disulfide bonds. β sheet AMPs are more structured in solution and do not

undergo major conformational changes when going from an aqueous environment to a membrane environment [51]. This class includes polyphemusin, tachyplesins, defensins and protegrins. The polyphemusin I peptide, isolated from hemocytes of horseshoe crabs, shows an amphipathic antiparallel β-hairpin structure connected by a type I-β-turn stabilized by two disulfide bonds (Figure 1B) [52]; this peptide shows antimicrobial activity against Gram-negative and Gram-positive species and fungi [53]. Interestingly, this disulfide-constrained, β-sheet structure of polyphemusin I is required for maximal antimicrobial activity [52].

Extended peptides

The extended peptides are characterized by the lack of classical secondary structures, generally due to their high contents of proline and/or glycine. Therefore, these peptides form their final structures by hydrogen bond and Van der Waals interaction with membrane lipids. This class includes the tryptophan rich indolicidin, a member of the cathelicidins, isolated from bovine neutrophils (Figure 1C) [54]; this peptide exhibits membrane permeabilization effects and antimicrobial activity against Gram-negative and Gram-positive bacteria, fungi, HIV-1 virus and protozoa [55-56].

Mixed peptides

The mixed peptides are characterized by the presence of several structural elements. A good example of this class is the human β-defensin 2, isolated from leukocytes and epithelial cells [57]; this peptide is rich of cysteine and arginine residues and it is composed by three-stranded β-sheets stabilized by three disulfide bonds and an α-helical region (Figure 1D). The human β-defensin 2 has strong antimicrobial and immunomodulatory functions and also it has further effects on healing and protection of the intestinal epithelial barrier [58].

The α-helical and the β-sheet classes are the most common in nature.

The sequence and the conformation of the peptide affect peptide's activity.

Mechanism of antimicrobial peptide activity

It was originally thought that the only mechanism of antimicrobial peptide action was membrane targeting but now other modes of action have been discovered [59]; the mechanism of action of these peptides can be thereby classified into direct killing and immune modulation (Figure 2).

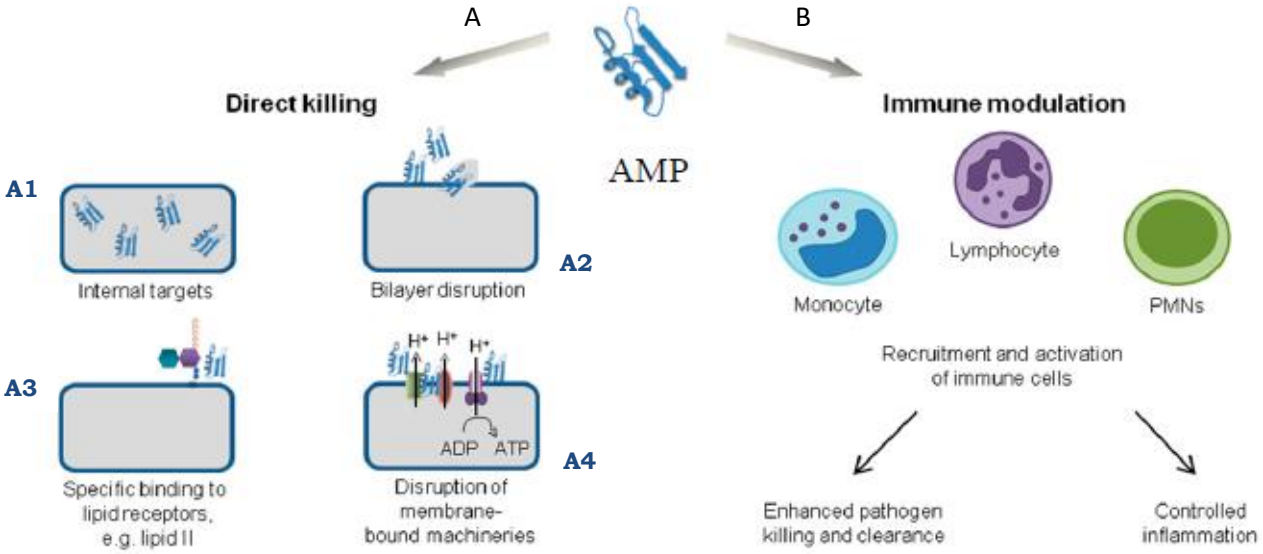

Figure 2. Mechanisms of antimicrobial peptide action [40].

Direct killing action

The direct killing is principally characterized by the specific interactions of the cationic peptide character with the model membrane systems, figure 2A; therefore, the design of membrane, then the different lipid bilayer composition, in eukaryotic and prokaryotic ones, has a key role to define the activity of antimicrobial peptides. The outer monolayer (leaflet) of the lipid bilayer in bacterial membranes is mainly composed by lipids with negatively charged head groups, as phospholipid sphosphatidylglycerol and cardiolipin [60]; in mammalian membranes most of these anionic lipids are in the inner leaflet facing the cytoplasm whereas their outer leaflet is made up of zwitterionic phospholipids like phosphatidylcholine, sphingomyelin and other neutral components as cholesterol [61]. Therefore, the positively charged AMPs have a strong electrostatic interaction with the negatively charged phospholipids on the outer leaflet of the bacterial membrane (Figure 3).

Moreover, some AMPs are even sensitive to other lipid properties, not just the charge but also the shape depending on the relative size of the head group and hydrophobic tails [62-63]; the different shapes of lipids can display several membrane curvature properties [64]. Therefore, for the initial interaction, in addition to the membrane charge properties, it is also important the membrane curvature [62,65-66].

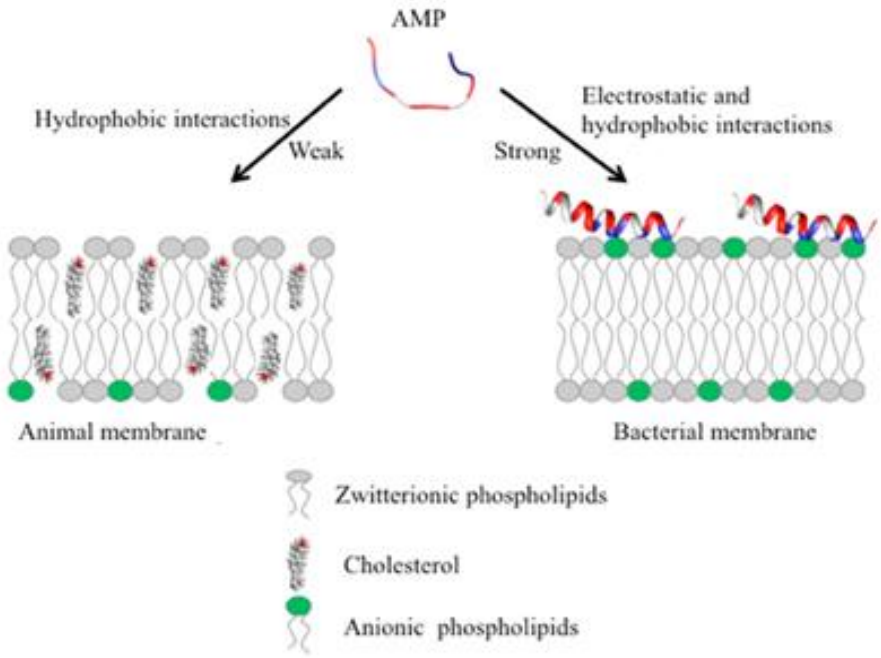

Figure 3. Initial interaction of cationic AMPs with the mammalian or bacterial membrane [40].

The next section will be focused in particular on the interaction of the antimicrobial peptides with the Gram-negative bacterial membrane.

Mechanism of action: interaction of AMPs with bacterial membrane

The initial electrostatic attraction of AMPs, primarily unfolded, with the bacterial membranes is allowed by the interaction of the peptide positive charge with negative charge of lipopolysaccharide (LPS) or lipoteichoic acid (LTA), which are on the outer surface of Gram-negative and Gram-positive bacteria, respectively [67-68]. This interaction leads to membrane perturbation due to the higher affinity of peptides with LPS (in the case of Gram-negative bacteria) than those by the native divalent cations like Mg^{2+} and Ca^{2+} [69]; this propensity disrupts the stabilizing effect of the divalent cations and perturbs the normal barrier properties of the outer membrane [70]. The formation of destabilized areas allows the peptides to translocate into the outer membrane in a process termed self-promoted uptake [71]. The peptides then associate with the monolayer of the cytoplasmic membrane after reaching a certain concentration [72-73]. At this stage different models have been proposed to describe the mechanism of action of AMPs; these models can be divided in two classes as transmembrane pore and non-pore mechanistic models depending on whether the orientation of peptides leads to a perturbation of the cytoplasmic membrane's integrity or peptide translocation in the cytoplasm. All models lead to the lipid bilayer disruption (Fig. 2, A2).

The transmembrane pore models can be further divided into the barrel stave and toroidal pore models.

Barrel-stave pore model

In the barrel-stave model the AMPs are initially oriented parallel to the membrane but eventually they are inserted perpendicularly in the lipid bilayer like the staves in a barrel (Figure 4a) [74]; this orientation promotes lateral peptide-peptide interactions, similar to that of membrane protein ion channels, in which the hydrophobic regions interact with the membrane lipids and hydrophilic residues form the lumen of the pore. The arrangement of the lipid bilayer is conserved. In this pore formation mechanism is then necessary the peptide amphipathic structure (α helix and/or β sheet) [75-76].

Toroidal pore model

In the toroidal pore model the AMPs, also perpendicularly inserted in the lipid bilayer, induce a local curvature of the lipid bilayer which lead to the pores partly formed by peptides and partly by the phospholipids head group (Figure 4b). Unlike the barrel stave, this model is not characterized by specific peptide-peptide interactions instead by the formation of lipid-peptide supramolecule termed "toroidal pore" that disrupts the arrangement of lipid bilayer [77]. This formation provides alternate surfaces for the lipid tail and the lipid head group to interact with.

Both pore forming models cause the membrane depolarization and eventually cell death. As the pores are transient upon disintegration, some peptides translocate to the inner cytoplasmic leaflet entering the cytoplasm and potentially targeting intracellular components [78].

The transmembrane non-pore models are instead divided in carpet and micellar aggregate models; in these mechanisms antimicrobial peptides do not insert in the lipid bilayer to form transmembrane channels/pore or specific peptide structures.

Carpet model

In the carpet model AMPs are oriented parallel to the lipid bilayer and after reaching a threshold concentration they cover the surface of the membrane, thus, forming a "carpet" (Figure 4c); this tendency causes local perturbation in membrane stability, formation of large cracks, disruption of the membrane potential and, ultimately, disintegration of the membrane [51,67-68, 79].

Micellar aggregate

In the micellar aggregate model, the antimicrobial peptides reorient and associate in an informal membrane-spanning micellar or aggregate-like arrangement leading to a final collapse of the membrane bilayer structure (Figure 4d) [69,80].

In some cases, there are not distinctions amongst the described mechanisms; for example, it has been suggested that the carpet mechanism is a prerequisite step for the micellar aggregate and toroidal pore models [51].

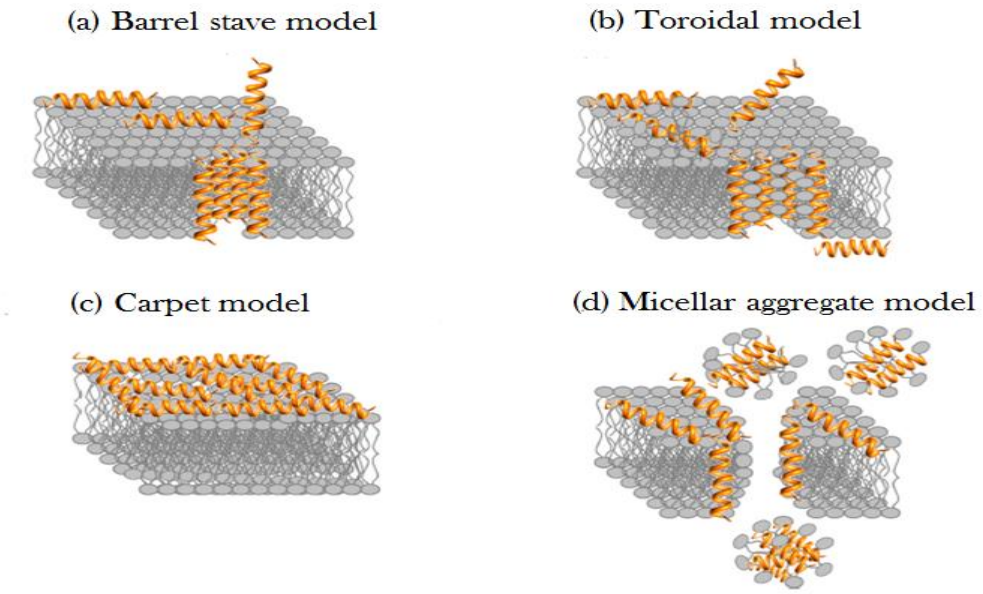

Figure 4. Proposed mechanisms of action for AMPs in bacteria [40].

Moreover, the action of AMPs on the disruption of the target membrane can also be mediated by receptor interactions; this pathway includes AMPs produced by bacteria that are active in vitro in the nanomolar range, like nisin peptide [81]. The nisin peptide is composed by two domains, the first has high affinity to a membrane anchored cell wall precursor, known as lipid II molecule and the second one, membrane embedded, forms the pores (Fig. 2, A3).

Although the bacterial membrane is the main AMP target, intracellular targets that lead to the block critical cellular processes like inhibition of protein/nucleic acid synthesis and disruption of enzymatic/protein activity (Fig. 2, A1, A4) have been reported [75]. Therefore, in this case, AMPs do not cause membrane permeability but still cause bacterial death.

Immune modulation and inflammatory actions

In addition to the direct killing action, AMPs can also have an important role in the immune modulation. In an infection, it is important to produce an immune response to attract other immune cells and control inflammation. It has been shown that most AMPs interact with components of innate immune system, like macrophages and neutrophils. They recruit and activate immune cell resulting in enhanced pathogen killing and/or controlled inflammation (Fig. 2, B) [82-84]. Antimicrobial peptides can lead to a variety of immune responses as activation, attraction and differentiation of white blood cells. Moreover, they can also produce stimulation of angiogenesis, reduce the inflammation lowering the expression of pro-inflammatory cytokines, control the expression of chemokines and reactive oxygen/nitrogen species [33, 82, 83, 85-86]. For example, human chatelicidin LL37 and human β defensins activate the toll-like receptor signal in the innate immune system [87-88] and synthetic versions of natural AMPs, known as innate defense regulators (IDR), suppress pro-inflammatory cytokines in mice infection models [89-90].

There is also evidence that AMPs are involved in modulation of adaptive immune system, inducing the recruitment of T cells [89].

Furthermore, AMPs have an important role in the promotion of wound healing. These peptides act directly on epithelial and endothelial cells which lead to the process of re-growth of epithelial layers and the formation of new blood resulting re-epithelialization and angiogenesis [91].

Finally, the AMPs are involved in the modulation of pyroptosis, a type of cellular death that is induced by pathogen- and damage-associated molecules, due to the binding of peptides with LPS [92].

Interestingly, all studies of AMPs point out their ability to act with independent or co-operative “multi-hit” mechanism, making them ideal candidates for further development [93].

Challenges of antimicrobial peptides for therapeutic application

Antimicrobial peptides are promising candidates as new therapeutic agents to face infections and antimicrobial resistance thanks to their antimicrobial, immunomodulatory and anti-inflammatory combined properties; none of the antibiotics used in clinical trials has these characteristics [94].

Although many eukaryotic AMPs have been discovered and characterized, only a few have been approved by US Food and Drug Administration for clinical use [41]. The principal drawbacks of AMPs in clinical applications are due to systemic toxicity, low stability and systemic administration [36, 73, 95]. Natural antimicrobial peptides show a certain degree of toxicity for eukaryotic cells due to their low selectivity that leads to a high degree of hemolysis. The low stability is due to susceptibility of these peptides to protease degradation by enzymes in the digestive tract, as trypsin and pepsin, if peptides are administered orally. Finally, the systemic administration of these peptides, e.g. by intravenous injection, results in short half lives in vivo due to the rapid renal or hepatic clearances, also quick protease degradation and cytotoxic profiles in blood [24]. Therefore, antimicrobial peptides are usually administered like dermal creams and emollients at the wound bed or like nasal spray for mucosal application [11]. To overcome these issues and to improve the efficacy of AMPs different strategies have been examined; these refer chemical modification of AMPs [96] and the use of delivery vehicles [97].

Chemical modification of AMPs

Several chemical modifications of AMPs, allowed by solid phase synthesis, have been used to improve the performance of these peptides. The most important include:

- incorporation of D and non-natural amino acids (1)
- peptide cyclization (2)
- acetylation of the N-terminus and polymer conjugation (3)
- peptidomimetics (4)
- Multiple Antigen Peptide forms (MAPs) (5)
- different salt formulations (6)

(1) The incorporation of D amino acids in the sequence of peptides improves their stability against proteolytic enzymes, as the latter are stereospecific, because these enzymes do not recognize the cutting site in the peptide sequence due to these incorporations. Although this strategy improves the stability and retains the antimicrobial activity of peptides, the synthesis containing D-amino acids is very costly [98]. Thus, alternative strategies have to

be find for reducing the economic impact. The substitution of positively-charged arginine with other non-natural amino acids like L-ornithine and L-homoarginine also increases the proteolysis stability of AMPs [99].

(2) The peptide cyclization, joining the backbone N- and C-termini or by disulfide bridges, is a common strategy to increase the serum stability of AMPs preventing protease degradation [100].

(3) The acetylation of the N-terminus leads to the block of the aminopeptidase activity increasing the proteolytic stability of peptides; however, in most cases this results in the decrease of the antimicrobial activity due to the removal of a positive charge [101-102]. Another common strategy to improve pharmaceutical properties of AMPs is the PEGylation, a process by which polyethylene glycol (PEG) chain is covalently or not covalently bound to the peptides. The advantages of this strategy are provided water solubility, reduced non-specific uptake in tissue, reduced cell toxicity, increased blood half-life and reduced proteolytic degradation [103-104]. However, the site and the nature of the conjugation chemistry affect the antimicrobial activity of the resulting peptide [105].

(4) Peptidomimetics are peptide-like polymers composed by a backbone altered when compared to a peptide [106-108]. The use of peptidomimetics allow to conserve the 2D and 3D spatial arrangement of the side chains modifying the backbone to prevent proteolysis maintaining the antimicrobial activity; some example are peptoids, ceragenins, oligocyllysines and β-peptides [107-108].

(5) A promising strategy is the synthesis of peptides in branched form, known as multiple antigen peptides (MAPs). These peptides are characterized by peptidyl core of branched lysine amino acids in which peptide sequences can be added using solid phase synthesis (Figure 5). Bracci *et al.* demonstrated that the MAPs make peptides more resistant to degradation in biological fluid and more efficient, due to the increase of the positive charges ascribed to lysine residues and to their ability to have polyvalent interactions, compared to the respective linear forms [109].

(6) The salt formulations, defined in terms of counter-ions and additives, are important in developing a medicinal product. Various salt formulations, e.g. trifluoroacetate, acetate, sulfate, chloride, differently affect the solubility, the antimicrobial activity, the toxicity and the treatment of the resulting peptides. Therefore, it is strictly important to find the better salt formulation of the peptide in terms of pharmacological profile.

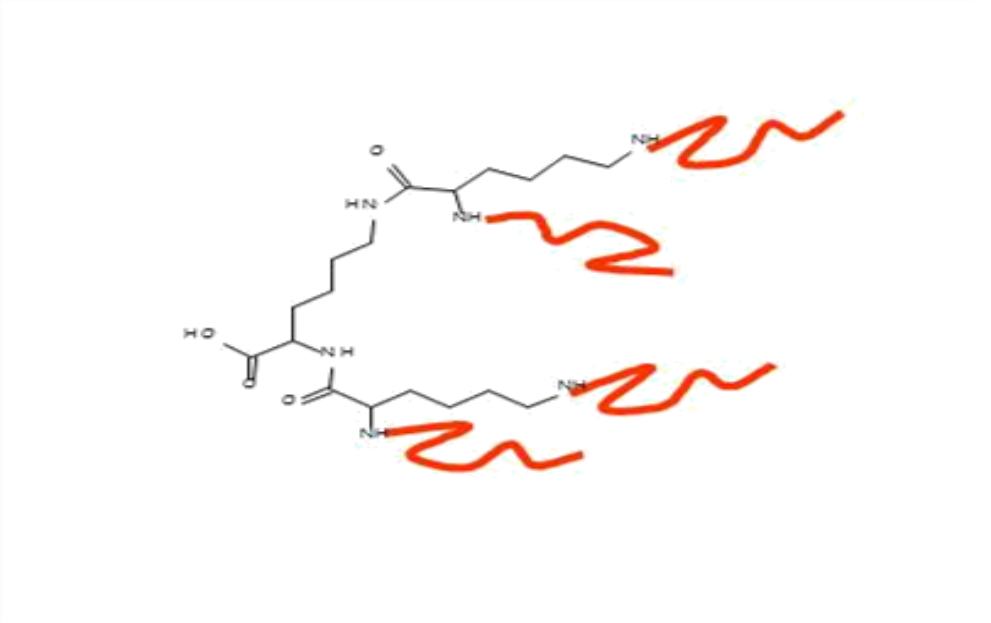

Figure 5. Structure of tetra-branched Multiple Antigen Peptide (MAP).

Delivery systems for AMPs

Delivery systems are another strategy to improve the properties of AMPs; in particular, they can improve the stability, toxicity, half-life and release profile of antimicrobial peptides. The delivery systems include inorganic and polymer materials, from surfactant/lipid self-assembly to peptide self-assembly system [97,103]. AMPs can be covalently bind to the delivery system or non-covalently encapsulated by them. Amongst inorganic materials there are mesoporous silica particles [110], titanium [111], metal Au and Ag nanoparticles [112-113], quantum dots [114], graphene [115] and carbon nanotubes [116]. Polymeric materials include polymer particles and fibers, polymer gels, polymer multilayers and polymer conjugates [97]. To date, poly(lactic-co-glycolic acid) (PLGA) nanoparticles aroused lot of interest; in particular, d'Angelo *et al.* investigated colistin-loaded-PLGA particles coated with chitosan or poly(vinyl alcohol) for their ability to improve the transport (artificial) efficiency through cystic fibrosis mucus [117]. It was found that these particles coated with chitosan were active against *Pseudomonas aeruginosa* biolfilms and exhibited prolonged efficacy in the biofilm eradication compared to the free colistin. These results can be ascribed to nanoparticle penetration into bacterial biofilm, as well as, sustained colistin release within the biofilms.

Antimicrobial peptides for therapeutic application

It is not surprising that the FDA-approved antimicrobial peptides are composed by different noncanonical amino acids and show chemical modifications or cyclic structures to optimize their pharmacological properties. They are colistin, gramicidin, daptomicin, vancomycin and vancomycin's derivatives oritavancin, dalbavancin and telavancin (Figure 6) [41].

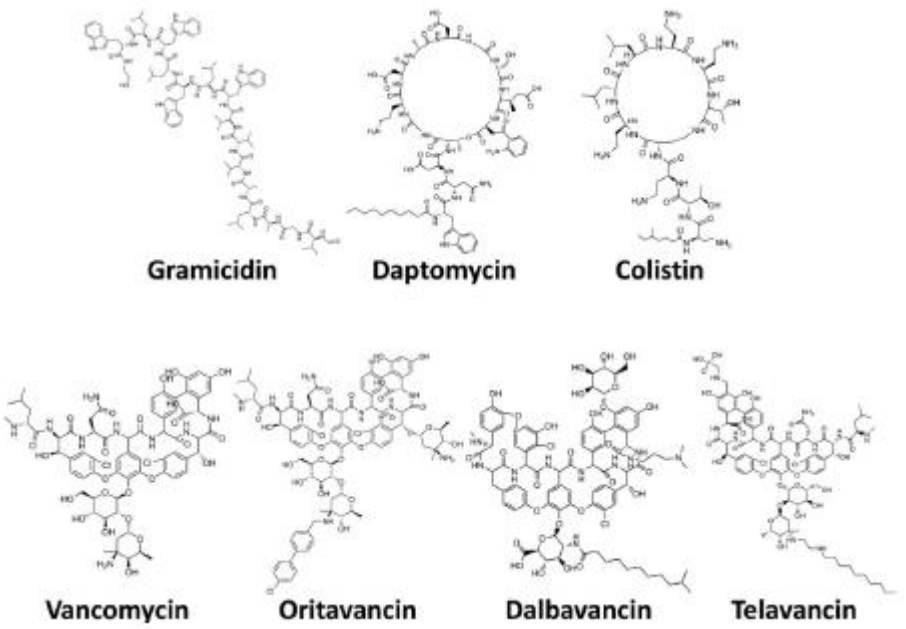

Figure 6. Chemical structures of seven FDA-approved AMPs [41].

Of these, only cyclic lipopeptides polymyxin B and **colistin**, also known as polymixin E, are included in the category of small cationic amphipathic peptides; colistin is a cyclic lipopeptide composed of 10 amino acids (KTKKKLLKKT) and one fatty acid (6-methyl octanoic acid) that was FDA approved in 1962; it is commercially available as the product Coly-Mycins (colistin sulfate). Colistin is used in the treatment of acute infections due to *P. aeruginosa* and other several Gram-negative bacteria for their antimicrobial activity against various Gram-negative pathogens [118]. In particular, this peptide shows a transmembrane pore mechanism, thus, it forms pore-like aggregates in the bacterial cell membrane and disrupts the membrane resulting in lytic cell death [119-120]. **Gramicidin** is a small hydrophobic linear peptide composed of 10 amino acids and FDA approved in 1955 as a constituent in Neosporin®, a triple antibiotic ointment used for treating bacterial conjunctivitis [121]; gramicidin is a pore-forming peptide that forms ion channels as a transmembrane dimer. **Daptomycin** is a small amphipathic cyclic lipopeptide, composed of 13 residues, that shows neutral net charge. Daptomycin and its derivative Cubicin were FDA approved in 2003 to treat or prevent infectious diseases [122-123]. Cubicin and its new formulation Cubicin

RF are antibiotics used for the treatment of complicated skin structure infections (cSSSI) and *S. aureus* bloodstream infections. Daptomycin is a membrane lytic peptide that forms co-clusters with anionic lipids and lyses the membrane. Vancomycin and its derivatives telavancin, oritavancin and dalbavancin are small lipoglycopeptides, which are FDA approved in 1983, 2009, 2014 and 2014, respectively. The derivative lipoglycopeptides are more efficient and bactericidal compared to their prototype vancomycin, indeed, they are also active against vancomycin-resistant bacteria. The therapeutic products Orbactiv® (oritavancin), Dalvance™ (dalbavancin) and Vibativ® (telavancin) are used for treating Gram-positive bacterial infections and in particular for injection against cSSSI caused by *S. aureus*. These peptides inhibit the bacterial cell wall formation and oritavancin and telavancin also disrupt bacterial cell membranes and affect membrane permeability [124-127].

The FDA-approved AMPs were discovered in or derived from Gram-positive bacteria commonly found in the soil; they, except gramicidin, are characterized by longer elimination half-life (ranging from hours to days) and better pharmakocinetics than other AMPs [100, 128-131].

However, these peptides show some issues as few of them have been administered as oral solutions or tablets due to their poor penetration of the intestinal mucosa [132] and the major part of them (except colistin) are used against Gram-positive bacterial infections. Therefore, AMPs for treating infection caused by Gram-negative pathogens are strictly needed. Vancomycin can cause kidney damage in high doses and in some patients, telavancin can induce acute kidney injury and oritavancin and dalbavancin show some side effects that have to be study deeper [133-137]. Moreover, the clinical use of colistin is mainly limited by nephrotoxicity and neurotoxicity and its heavy use leads to colistin-resistant bacteria, making it problematic for regular use [118,138-139].

Many peptides have been currently studied in clinical phase and many are in pre-clinical development; among the first ones there are the indolicidin derivative termed Omiganan, the magainin analoge termed Pexiganan and the proteigrin analog termed Iseganan. They are used for treat severe acne, rosacea, atopic dermatitis (Omiganan), for treat diabetic foot ulcers infections (Pexiganan) and for the treatment of inflammation and ulceration of digestive system mucous membrane (Iseganan) [24, 83, 140-141]. Instead among the peptides under pre-clinical development there are Novarifyn® [142], PXL150 [143], MU1140 (Mutacin) [144] and SET-M33 [145].

In conclusion, it is right to say finding antimicrobial peptides used in human medicines, which show a good stability, a low toxicity and low unexpected side effects, is an arduous challenge. The general goal to face this challenge is to perform the synthesis of a handful of peptide sequences, and then, find the peptide that display a good stability, a broad spectrum antimicrobial activity toward antibiotic resistant pathogens and especially a low toxicity amongst them.

SET-M33 peptide

Structure and synthesis

The SET-M33 peptide [146], obtained by the optimization of a phage library, is identified as a possible candidate for the development of a new antibacterial drug [147]. SET-M33 is a cationic synthetic peptide obtained in a branched form (MAP) in which four copies of the same peptide sequence (KKIRVRLSA), containing all amino-acids in L isomeric version, are linked by a three lysine core (Figure 7) [148]. This tetra-branched form makes the peptide more resistant to proteases, thus improving its half-life, and more suitable for clinical applications than its linear analogues [149].

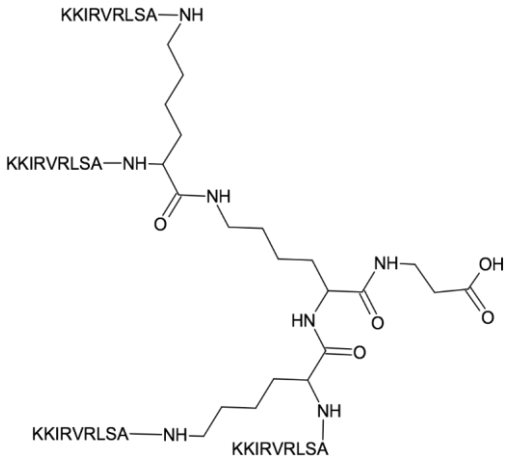

Figure 7. Structure of the tetra-branched SET-M33 peptide.

The peptide is obtained by solid phase synthesis, carried out by an automated Syro multiple peptide synthesizer, using standard 9-fluorenylmethyloxycarbonyl (Fmoc) strategy [150]. The amino acid sequences are build up stepwise on a solid support resin by successive cycles of Fmoc deprotection, with Piperidine 20%/dimethylformamide (DMF), and coupling of the following amino acid by the activation of the respective carboxylic group with O-(benzotriazol- 1-yl)-N,N,N,N-tetramethyluronium hexafluorophosphate (HBTU)/1,3-isopropylethylamine (DIPEA). SET-M33, as almost all synthetic peptides, is obtained as trifluoroacetate salt (SET-M33 TFA), due to the cleavage and purification conditions that requires trifluoroacetic acid. Preliminary studies, on the efficacy and toxicity of SET-M33 revealed that the acetate form of the peptide (SET-M33 acetate) was less toxic to human cells and animals than SET-M33 TFA [151]. Thus, SET-M33 peptide is traditionally converted to the acetate form at the end of synthesis.

In vitro antimicrobial activity

The peptide showed strong antimicrobial activity against various multi-resistant Gram-negative bacteria, including clinical isolates of *Pseudomonas aeruginosa, Klebsiella pneumoniae*, *Acinetobacter baumannii* and some enterobacteriaceae; in particular, SET-M33 showed a minimum inhibitory concentration (MIC)90 below 1.5 μM and 3 μM for *P. aeruginosa* and *K. pneumoniae*, respectively [145]. The peptide was also active against *P. aeruginosa* strains of clinical isolates from cystic fibrosis (CF) patients, which are resistant to currently available antibiotics (Figure 8) [145-146, 151]. Moreover, the peptide showed strong antimicrobial activity against other Gram-negative clinical isolates, including MDR strains of *Escherichia coli* [152].

Bacterial species and strains			MIC (μM)	
			M33	Colistin
Pseudomonas aeruginosa ATCC 27853	Reference strain, wild type		1.5	1.5
P. aeruginosa PAO-1	Reference strain, wild type		1.5	1.5
P. aeruginosa VR-143/97	FQ^r AG^r ESC^r NEM^r (MBL/VIM-1)	Cystic Fibrosis	1.5	1.5
P. aeruginosa SC-MDr03-06[b]	FQ^r AG^r ESC^r NEM^r	Cystic Fibrosis	3	1.5
P. aeruginosa SC-VMr04-05[b]	FQ^r AG^r ESC^r NEM^r	Cystic Fibrosis	3	1.5
P. aeruginosa SC-DMr05-04[b]	FQ^r AG^r ESC^r NEM^r	Cystic Fibrosis	1.5	1.5
P. aeruginosa SC-BGr12-02[b]	FQ^r AG^r ESC^r NEM^r	Cystic Fibrosis	1.5	1.5
P. aeruginosa EF-OBG6-1[b]	FQ^r AG^r ESC^r NEM^r (MBL/IMP-13)	Cystic Fibrosis	1.5	0.7
P. aeruginosa SC-MDm03-02[b,c]	FQ^r AG^r ESC^r NEM^r	Cystic Fibrosis	3	1.5
P. aeruginosa SC-GMm03-05[b,c]	FQ^r AG^r ESC^r NEM^r	Cystic Fibrosis	1.5	1.5
P. aeruginosa SC-CNm03-07[b,c]	FQ^r AG^r ESC^r NEM^r	Cystic Fibrosis	0.3	0.7
Klebsiella pneumoniae ATCC 13833	Reference strain, wild type		1.5	0.7
K. pneumoniae 7086042	FQ^r AG^r ESC^r NEM^r (MBL/VIM-1)		3	1.5
K. pneumoniae C8-27	FQ^r AG^r ESC^r ETP^r (ESBL/CTX-M-15)		1.5	0.7
K. pneumoniae FIPP-1	FQ^r AG^r ESC^r NEM^r (MBL/KPC-3)		3	1.5
Escherichia coli ATCC 25922	Reference strain, wild type		1.5	0.7
E. coli W03BG0025	FQ^r AG^r ESC^r (ESBL/CTX-M-15)		0.7	0.7
Enterobacter aerogenes W03BG0067	AG^r ESC^r (ESBL/SHV-5)		1.5	0.7
Enterobacter cloacae W03AN0041	ESC^r (ESBL/SHV-12)		1.5	0.7
Acinetobacter baumannii RUH 134	Reference strain, European clone II		1.5	1.5
A. baumannii RUH 875	Reference strain, European clone I		3	1.5
A. baumannii MR157	FQ^r AG^r ESC^r NEM^r (OXA/OXA-58)		3	1.5
Staphylococcus aureus ATCC 29213	Reference strain, PEN^r		6	96
S. aureus 3851	MR VAN^i		6	96

Figure 8. Comparison of MIC values between SET-M33 and colistin against several clinical isolates; legend: FQ^r, resistant to fluoroquinolones; AG^r, resistant to aminoglycosides (gentamicin, amikacin, and/or tobramycin); ESC^r, resistant to expanded-spectrum cephalosporins; NEM^r, resistance to carbapenems (imipenem and/or meropenem), ETP^r resistance to ertapenem; ESBL, extended spectrum β-lactamase; MBL, metallo-β-lactamase; OXA, oxacillinase; MR methicillin-resistant; PEN^r resistance to penicillin; VAN^i, vancomycin-intermediate [145-146, 151].

SET-M33 showed also a high anti-biofilm activity against *E. coli ATCC 25922*, *P. aeruginosa ATCC 27853* Gram negative strains and a less activity against *S. aureus ATCC 25923* Gram-positive strain (Table 1) [152].

Minimum biofilm eradication concentration (MBEC1, µM) of SET-M33 peptide		
E. coli ATCC 25922	*P. aeruginosa ATCC 27853*	*S. aureus ATCC 25923*
3	1,5	12

Table 1. Anti-biofilm activity of SET-M33 against several bacterial strains [152].

Structural analysis and mechanism of action

Preliminary studies in order to provide information on the structure and the peptide's mechanism of action were carried out. Structural two-dimensional NMR studies of free SET-M33 revealed that the peptide explored a large conformational space, assuming a random coil structure. In addition of sodium dodecyl sulfate (SDS) micelles, used for mimic a membrane environment, NMR analysis was precluded due to the formation of SET-M33-SDS aggregates, promoted by the multimericity of the peptide [153]. An analogue peptide, Q-33, in linear form, was synthetized in order to generate a model of the peptide that could be studied in the presence of SDS. Q-33 did not show any stable conformation in water but with the addition of SDS micelles the electrostatic interaction of its positively charged amino acid residues with the negatively charged sulfate groups of the SDS micelles led to the formation of an amphipathic α-helix conformation. The resulting structure showed the cationic side chains (K and R) arranged parallel to the sulfate groups while the hydrophobic sidechains (I and L) inserted into the micelles [153]. The amphipathic helix structure caused the loss of the membrane functionality leading to the disruption of the bacterial membrane as showed by scanning electron microscopy micrographs (Figure 9) [153]. Circular dichroism (CD) spectra of SET-M33 and Q-33 showed a transition from a non-structured conformation in water to a stable α-helix formation in the presence of SDS micelles, in according with the NMR experiments on the linear analogue [153].

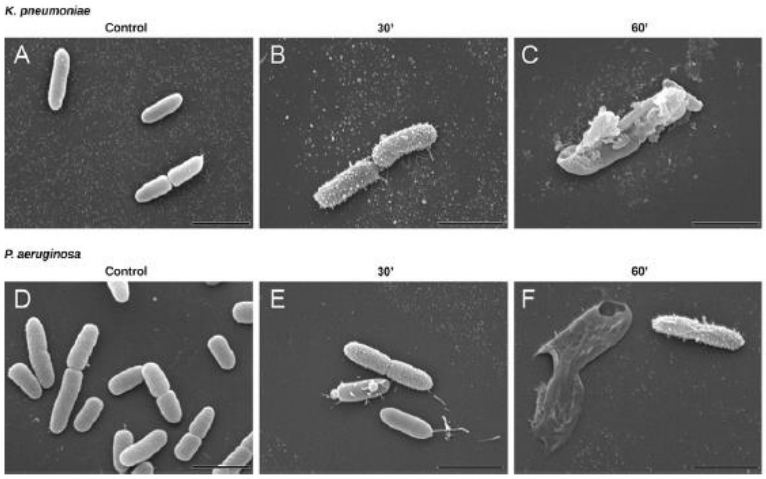

Figure 9. Scanning electron micrographs (SEM) of *K. pneumoniae* ATCC 13833 and *P. aeruginosa* PAO-1. SEM micrographs of A) untreated *K. pneumoniae*; B) *K. pneumoniae* after 30 min incubation with SET-M33 at MIC; C) *K. pneumoniae* after 60 min incubation with SET-M33 at MIC; D) untreated *P. aeruginosa*; E) *P. aeruginosa* after 30 min incubation with SET-M33 at MIC; F) *P. aeruginosa* after 60 min incubation with SET-M33 at MIC. Scale bar 2 μm [153].

Therefore, based on these results, the mechanism of antimicrobial action of SET-M33 peptide could be divided in two steps: the first comprised the high affinity binding of the peptide positive charged K and R with negatively charged phosphate groups of LPS or LTA, which are on the outer surface of Gram-negative and Gram-positive bacteria [67-68] respectively, and the second one comprised the disruption of the bacterial membranes as a result of the amphipathic helix formation (Figure 10).

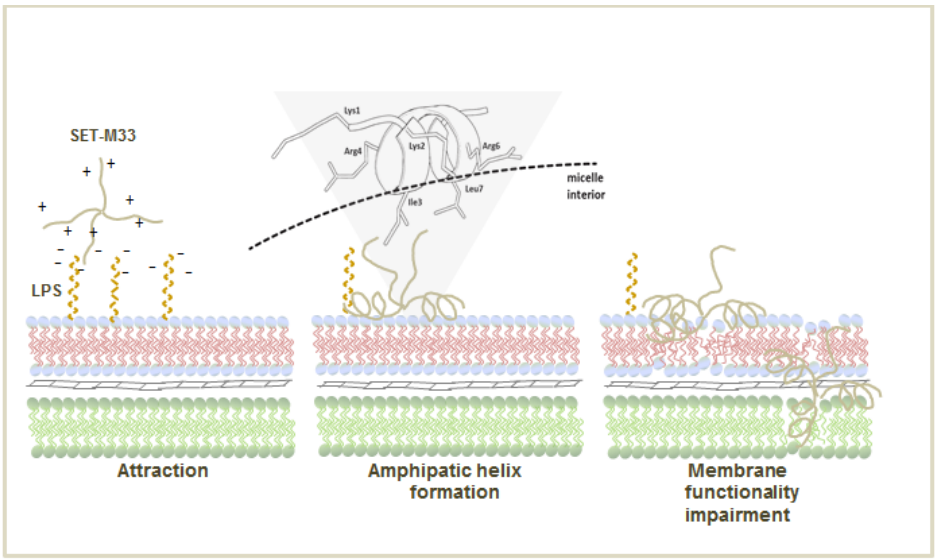

Figure 10. Mechanism of antimicrobial action of SET-M33 peptide against Gram-negative bacteria, based on NMR and CD results [153].

In vivo antimicrobial activity and toxicity

The antimicrobial activity of SET-M33 peptide was also demonstrated in *vivo* in models of sepsis, pneumoniae and skin infections [145]; in the sepsis and pneumoniae models neutropenic mice were injected intra-peritoneally (i.p.) or intra-tracheally (i.t.), respectively, with a lethal amount of *P. aeruginosa* PAO-1. Mice were then treated twice intravenously (i.v.) with SET-M33 at doses compatible for clinical use. In both models the therapeutic activity was demonstrated obtaining 60% survival (sepsis) and 40% (pneumoniae) after treatment with the peptide (Figures 11-12).

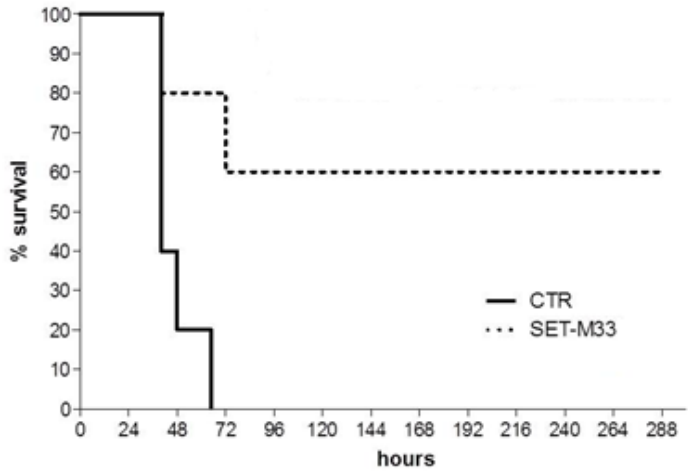

Figure 11. *In vivo* antibacterial activity of SET-M33 peptide in **sepsis** animal model [145]. 10 BALB/c neutropenic mice/group were injected i.p. with a lethal amount of *P. aeruginosa PAO1* and then treated twice i.v. with SET-M33 (5 mg/Kg), 24 and 72 hours post-infection. Percentage survival (y-axis) is plotted as a function of time (x-axis); $p<0.02$.

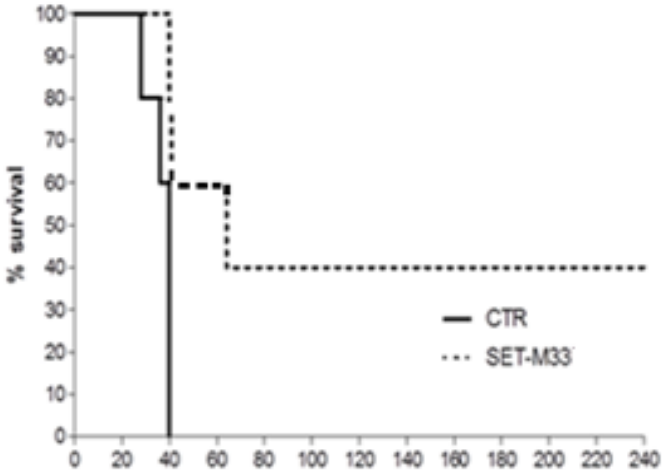

Figure 12. *In vivo* antibacterial activity of SET-M33 peptide in **pneumoniae** model [145]. BALB/c neutropenic mice were injected i.t. with a lethal amount of *P. aeruginosa PAO-1* and then treated twice i.v. with SET-M33 (5 mg/Kg) 1 and 16 hours post-infection. Percentage survival (y-axis) is plotted as a function of time (x-axis); $p<0.05$.

In the model of skin infection neutropenic mice were infected on abraded skin with *P. aeruginosa P1242*, an engineered strain expressing the luciferase gene and its substrate. The treatment with the peptide caused a significant reduction of the luciferase expression that was especially evident 2 days after the challenge [Figure 13].

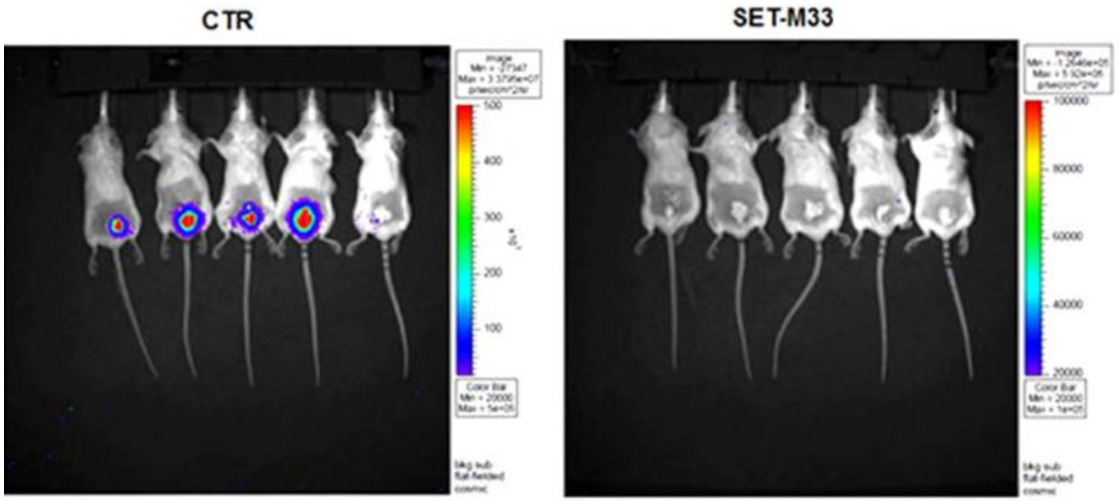

Figure 13. In vivo antibacterial activity of SET-M33 peptide in skin infection. [145] 15 neutropenic mice per group (BALB/c) were infected on abraded skin with *P. aeruginosa P1242* and then treated every day with 10 mg/ml SET-M33-lotion (SET-M33) or with SET-M33 free-lotion (CTR). Example of images of five animals at day 2. Total photon emission from defined areas of the images of each mouse was quantified with the Living Image software package.

Moreover, in *vivo* experiments were also carried out in order to evaluated the acute toxicity of the peptide compared with that of colistin, current antibiotic used in clinical practice; briefly, animals were injected with different amounts of SET-M33 and colistin, in single dose, at different ranges (5-40 mg/Kg). No signs of toxicity were observed up to 20 mg/Kg of SET-M33, while 100% mortality was induced by colistin at the same concentration (Figure 14) [145].

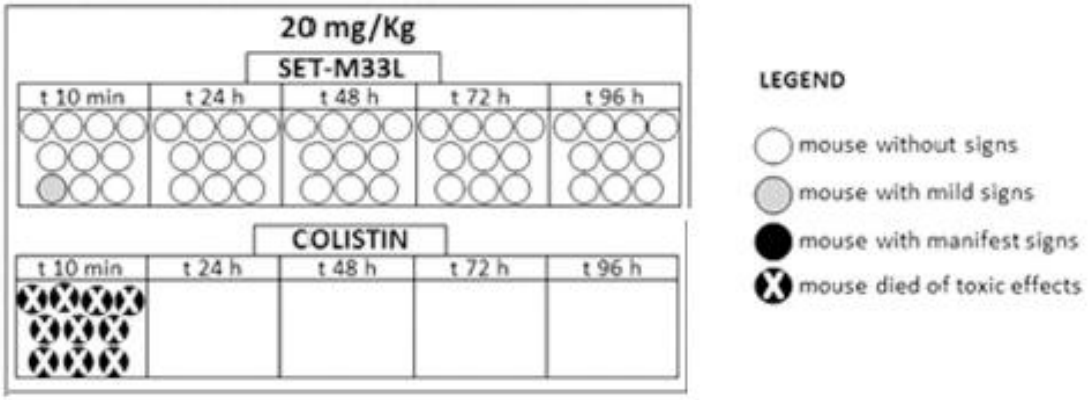

Figure 14. Acute in *vivo* toxicity of SET-M33L and colistin at 20 mg/Kg and given in a single dose [145]. Ten mice/group (each circle represents one mouse) were inoculated i.v. with SET-M33 or colistin and were monitored for 96 hours. Different scales of grey indicate severity of signs as described in the legend.

Unlike colistin, which was 500 times more prone to select resistant mutants [154], SET-M33 showed a lower propensity for bacterial resistance selection after 24h of continuous exposure in extensively resistant isolates of *P. aeruginosa* and *K. pneumoniae*. Therefore, the use of SET-M33 in the clinical application may have advantages over the use of colistin [153].

Moreover, the toxicity of SET-M33 peptide was in *vitro* tested against different human cellular lines as human bronchial epithelial cells (16HBE14o-) from healthy patients and CFBE41o- from CF patients; the results revealed that the synthetic peptide showed an acceptable toxicity unlike many natural antimicrobial peptides that showed a certain degree of toxicity against eukaryotic cells due to their poor selectivity for bacteria [151, 152].

Pharmacokinetic and bio-distribution analyses revealed that the peptide was eliminated mainly via urine [145].

Anti-inflammatory and immunomodulatory activity

Further experiments were performed to evaluate the anti-inflammatory and immunomodulatory activity of SET-M33 peptide. Preliminary studies demonstrated the ability of the synthetic peptide to decrease TNF-α production in vitro in cell stimulated by LPS from *P. aeruginosa* and *K. Pneumoniae* [146]. Indeed, the peptide revealed a strong anti-inflammatory activity in terms of reduced expression in murine macrophages (RAW 264.7) of a number of cytokines, enzymes, and signal transduction factors, including the major NF-KB, involved in inflammation triggered by LPS from *Pseudomonas aeruginosa*, *Klebsiella pneumoniae*, and *Escherichia coli*, according to the RT-PCR results (Figure 15) [155]. The peptide also inhibited the expression of different pro-inflammatory genes in bronchial cells (IB3-1) which were obtained from a CF patient (not shown) trough LPS neutralization [155].

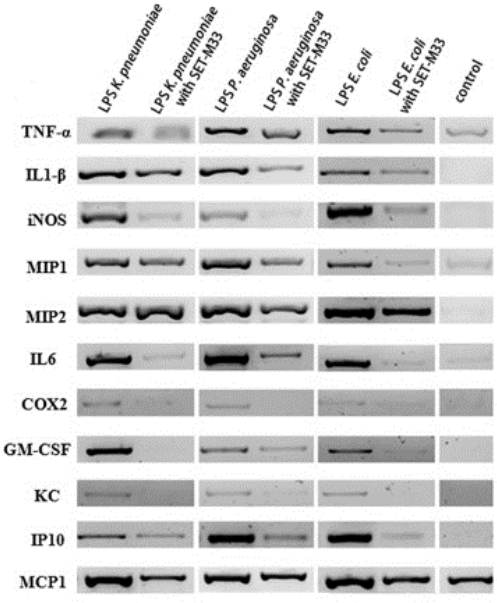

Gene expression percentage			
	LPS *K. pneumoniae* with SET-M33	LPS *P. aeruginosa* with SET-M33	LPS *E. coli* with SET-M33
TNF-α	41.7	4.3	14.6
IL1-β	62.5	22.4	41.2
iNOS	16.7	21.6	18.5
MIP1	60	18.6	15.7
MIP2	100	51.5	68.6
IL-6	3.7	6.3	3.7
COX2	16	18	44.4
GM-CSF	3.5	51.1	18.5
KC	0	44.5	0
IP10	42.9	4.3	0
MCP1	0	24.3	4.9

Figure 15. Gene expression of pro-inflammatory cytokines and enzymes analyzed by RT-PCR before and after treatment with SET-M33 peptide [155].

LPS neutralization was also demonstrated in vivo by challenging bronchoalveolar lavage of SET-M33-treated mice with LPS revealing a sharp reduction in TNF-α with respect to non-SET-M33-treated animals (Figure 16) [155].

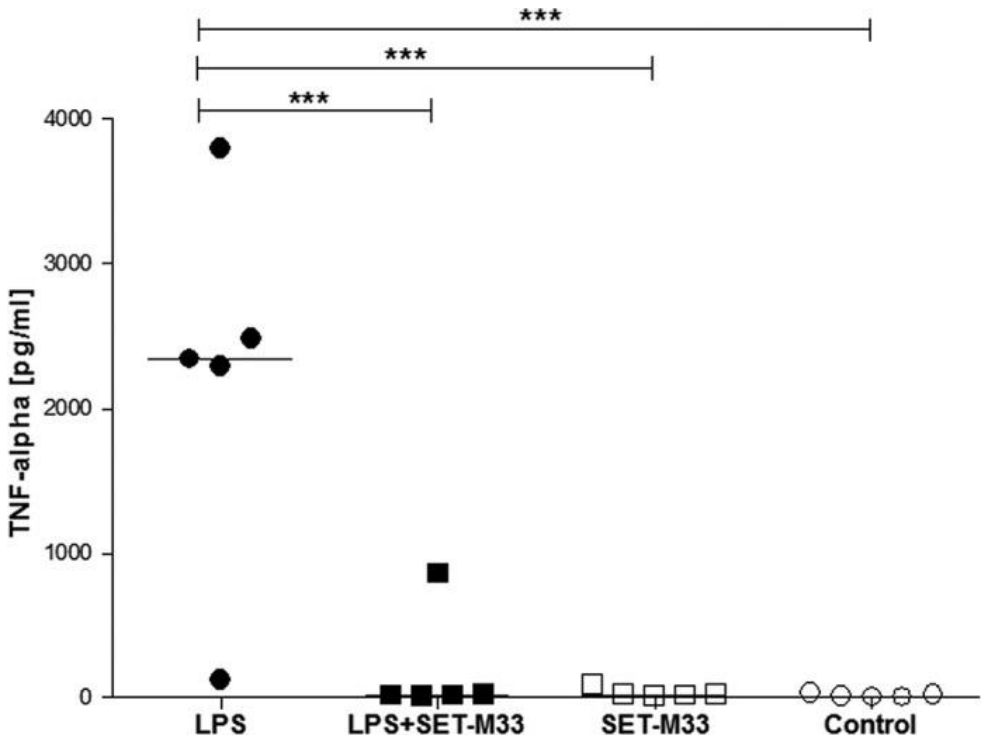

Figure 16. LPS neutralization *in vivo*. TNF-α levels (*y* axis) in BAL of mice (each *square* or *circle* indicates one mouse) challenged with *P. aeruginosa* LPS (*black circles*), LPS with SET-M33 (*black squares*), or SET-M33 alone (*whitsquares*). Controls (*white circles*) show the TNF-α basal level in untreated mice. The horizontal lines in the graph indicate median values. ***, $p < 0.001$ compared with the LPS group [155].

Finally, the synthetic peptide reported a powerful activity in stimulating cell migration of keratinocytes in wound healing experiments in *vitro* demonstrating that the cells treated with SET-M33 promoted wound closure more rapidly than those untreated, revealing an action generally characteristic of molecules taking part in innate immunity [155].

All these powerful characteristics make SET-M33 a promising candidate to face the antimicrobial resistance issue and, especially, to become a new antibacterial agent for the treatment of severe infections due to Gram-negative MDR pathogens. For this reason, the synthetic peptide is currently under preclinical development as a new drug to treat lung infections caused by Gram-negative bacteria.

Although SET-M33 exhibited high antimicrobial, immunomodulatory and anti-inflammatory activities, the peptide showed also a certain level of toxicity towards eukaryotic cells, common characteristic of the most AMPs.

SET-M33 back-up molecules

As previously described, certain drawbacks for the development of AMPs as drugs for bacterial infections are due to toxicity to eukaryotic cells, low stability, costs of production and systemic administration. It was known that the incorporation of non-natural amino acids, like D-amino acids to replace L-amino acids, in the sequence of peptides and the pegylation improved the stability against proteolytic enzymes, increased blood half-life and reduced cell toxicity of the resulting peptide [103-104, 129]. Therefore, in order to improve the biopharmaceutical properties of SET-M33, the respective D (SET-M33D), pegylated (SET-M33-PEG4) and dimeric (SET-M33-DIM) versions of the peptide were produced and characterized.

SET-M33D peptide

SET-M33 peptide, traditionally synthetized with L amino acids, was synthetized using D amino acids (SET-M33D), with the exception of the three lysine residues of the branched core [156]. This change of isomeric peptide version leaded to an improvement of stability against individual proteases and infectious agent proteases dramatically increasing the overall performance of the peptide [152]. Indeed, SET-M33D peptide became also active against Gram-positive pathogens like *Staphilococcus aureus* and *Staphilococcus epidermidis*, including methicillin-resistant (MR) and vancomycin-intermediate (VAN) strains, revealing MICs 4 to 16-fold lower than those of the traditional SET-M33 in L isomeric version; in addition, compared to the traditional peptide version, SET-M33D exhibited the activity against *P. aeruginosa* and the same or a slightly lower activity against Enterobacteriaceae (Table 2).

Species and strains	Relevant features[a]	M33-L (μM)	M33-D (μM)
P.aeruginosa ATCC 27853	Reference strain, wild type	1.5	1.5
P.aeruginosa AV 65	FQ^r AG^r ESC^r NEM^r (MBL/IMP-13)	3	3
K.pneumoniae ATCC 13833	Reference strain, wild type	1.5	3
K.pneumoniae 7086042	FQ^r AG^r ESC^r NEM^r (MBL/VIM-1)	3	6
E.coli ATCC 25922	Reference strain, wild type	3	3
E.coli W03BG0025	FQ^r AG^r ESC^r (ESBL/CTX-M-15)	0.7	3
S.aureus ATCC 29213	Reference strain, wild type	6	1.5
S.aureus USA 300	MR	6	1.5
S.aureus 3851	MR VAN^I	12	0.7
S.epidermidis ATCC 14990	Reference strain, wild type	1.5	0.4
S.epidermidis 6154	MR	3	0.7

[a]M33 antimicrobial activity was evaluated on reference strains and clinical isolates (mostly with an MDR phenotype). Relevant resistance phenotypes and resistance determinants are indicated. Resistance phenotypes: FQ^r, resistant to fluoroquinolones; AG^r, resistant to aminoglycosides (gentamycin, amikacin, and/or tobramycin); ESC^r, resistant to expanded-spectrum cephalosporins; NEM^r, resistant to carbapenems (imipenem and/or meropenem); MR^r, methicillin-resistant; VAN^I, vancomycin-intermediate. Resistance determinants: ESBL, extended spectrum β-lactamase; MBL, metallo-β-lactamase.

Table 2. MICs of SET-M33-L (traditional SET-M33) and SET-M33-D peptides for different bacteria species and strains [152].

The better activity shown by SET-M33D against *S. aureus* compared to the original SET-M33 was confirmed in biofilm eradication experiments where SET-M33 exhibited 12% activity with respect to SET-M33D [152]. The strong antimicrobial activity of SET-M33D peptide was demonstrated, also, in *vivo* models where Balb-c mice were infected i.p. with the LD100 of methicillin–resistant *S. aureus* (MRSA) USA 300. 100% survival, after 7 days, was obtained with mice treated i.p. with SET-M33D 30 minutes after infection; in contrast mice treated with SET-M33 showed complete mortality within 20 hours (Figure 17).

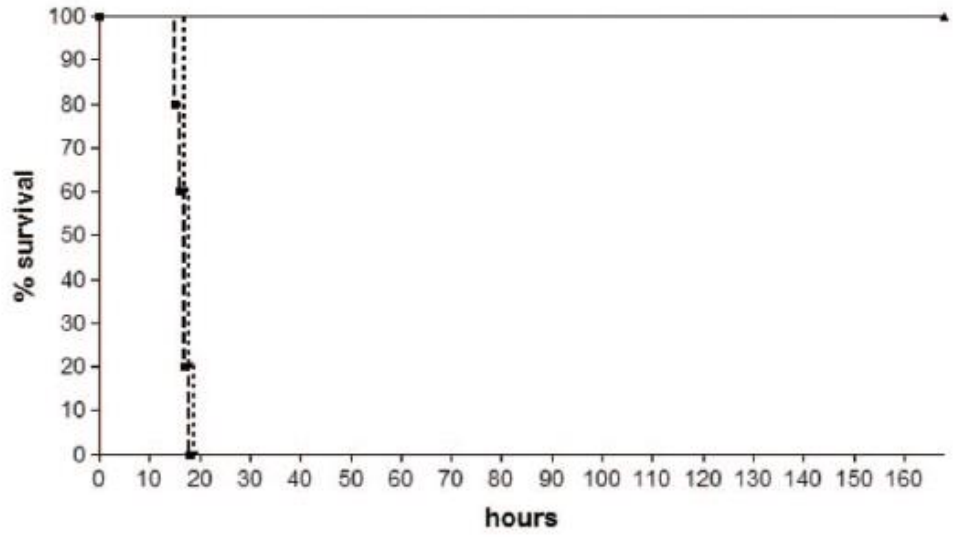

Figure 17. *In vivo* antibacterial activity of SET-M33 and SET-M33D peptides [152]. Balb-c mice (20 g) were injected i.p. with a lethal amount of *S. aureus USA300* cells. Dashed line (Ctr), injection with bacteria and no peptides; dotted line, injection with bacteria and a single injection of SET-M33-L peptide (25 mg/kg) 30 min later; continuous line, injection with bacteria and a single injection of SET-M33-D peptide (25 mg/kg) 30 min later.

The interactions of both peptides with LPS (from *E. coli*, *P. aeruginosa* and *K. pneumoniae*) and with LTA (from *S. aureus* and *S. faecalis*) were analized by surface plasmon resonance. The results showed that the different antimicrobial activity of the peptides was not influenced by the molecular interactions; no significant difference in binding or kinetic rates was observed between the two peptides (Figure 18). SET-M33 and SET-M33D showed, also, similar behaviour in terms of perturbation of membranes prepared with different phospholipid composition; for this experiment two vesicles for mimic membranes of *S. aureus* and *E. coli* were used and the membrane permeability was revealed by measuring the fluorescence increase due to the calcein leakage from the vehicles. The results showed a dose-dependent effect after treating the vehicles with increasing peptide concentrations (0.5 to 1.5 μM). No significant differences in the effects induced by the two peptides were observed, although SET-M33D seemed slightly more efficient toward Gram-positive liposomes at doses above 8 μM (Figure 19).

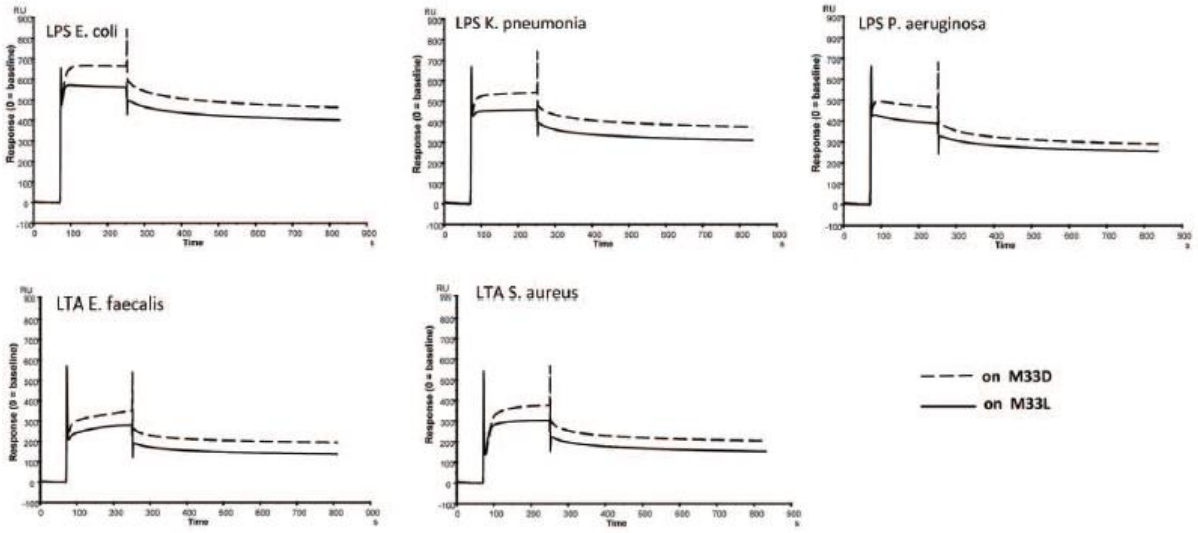

Figure 18. Binding of LTA and LPS on SET-M33 or SET-M33D measured by surface plasmon resonance [152].

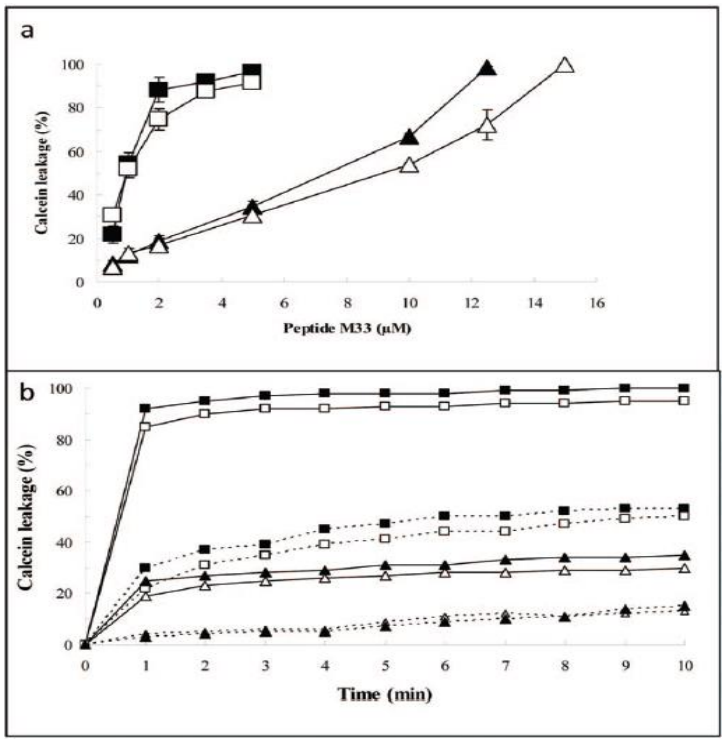

Figure 19. Release of calcein from bacterial-surface-mimicking liposomes. a) dose-response of SET-M33-induced calcein release. The vesicles were incubated with different concentration of M33 peptide for 10 min at 20°C. Gram-positive liposomes (triangles); Gram-negative liposomes (squares); SET-M33-D (full symbols); SET-M33(empty symbols). b) time course of calcein release. Continuous line 5 μM, dotted line 1 μM [152].

The reason of the different antimicrobial activity between the two peptides could be explained by their differential sensitivity to bacterial proteases, as showed by the peptide stability studies to bacterial proteases using purified aureolysin and elastase enzymes derived from *S. aureus* and *P. aeruginosa*, respectively. These enzymes, members of the family of M4 metallo-peptidase, hydrolyzed peptide bonds preferentially on the amino-terminal side of hydrophobic residues. In this case the HPLC and MS analyses revealed that traditional SET-M33 was degraded by aureolysin within 1 hour through hydrolysis at R6-L7 and S8-A9 peptide bonds, while showing moderate stability after 5 hours of incubation with elastase; conversely, SET-M33D was completely stable to proteolysis by these enzymes, remaining unaltered after 24 hours of incubation.

Altogether, these results suggested that the mechanism used by the two peptides for the interaction with bacterial surfaces and disruption of bacterial membranes was basically the same, although SET-M33D, unlike of the original version, persisting on the Gram-positive bacterial membrane by virtue of its resistance to bacterial proteases, showed a strong antimicrobial activity also against Gram-positive bacteria.

Concluding, the peptide SET-M33D was identified as an interesting candidate for the development of active novel broad-spectrum antimicrobials against bacterial pathogens of clinical importance.

SET-M33-PEG4

The pegylated version of SET-M33 peptide, SET-M33-PEG4 was obtained adding a polyethylene glycol 4 molecule (PEG4) at the C-terminus of the three lysine-branching core. It was known that the method of covalent attachment of PEG prevented immunogenicity, reduced protein aggregation and increased protease stability of AMPs [156]. This modification led the peptide to have a longer persistence in plasma than the traditional peptide form [145]; this property could partially explain the better performance of the pegylated molecule in eradicating infections *in vivo* models of *P. aeruginosa* infections. SET-M33-PEG4 enabled a survival percentage of 80% and 60% in sepsis and lung infections, respectively, when injected twice i.v. at 5 mg/Kg after mice infection with a lethal amount of *P. aeruginosa PAO-1.* Conversely, the traditional version of the peptide showed a survival percentage of 60% and 40%, in sepsis and lung infections, respectively (Figures 20-21).

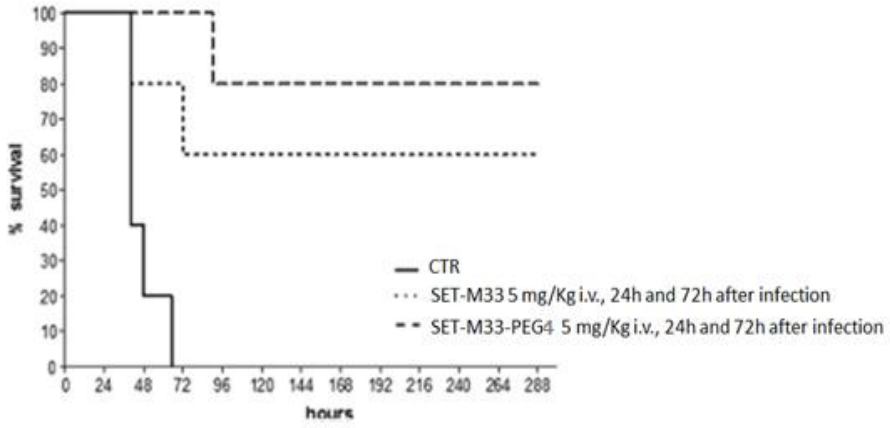

Figure 20. *In vivo* antibacterial activity of SET-M33 and SET-M33-PEG4 peptides in sepsis animal model induced by *P. aeruginosa PAO-1* [145].

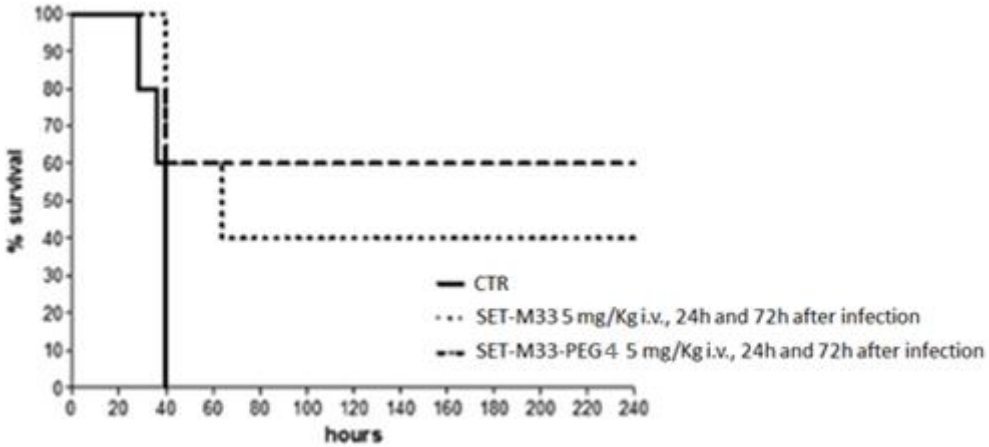

Figure 21. *In vivo* antibacterial activity of SET-M33 and SET-M33-PEG4 peptides in lung infections induced by *P. aeruginosa PAO-1* [145].

The peptide SET-M33-PEG4 produced similar toxicity profile to that of SET-M33 peptide revealing in animals no signs of toxicity up to 20 mg/Kg [145].

The strategies of the incorporation of D amino acids and the pegylation have been examined to overcome the principal drawbacks of AMPs in clinical applications. Despite it was demonstrated that both strategies led to an improvement of the performance of SET-M33 peptide, some issues had to be considered; for instance, although the incorporation of D-amino acids improved the stability and retained the antimicrobial activity of the peptide, the synthesis with D-amino acids is very costly, especially for the use of D-Isoleucine residues [98] and, for the pegylated version, the site and the nature of the conjugation chemistry could affect the antimicrobial activity of the peptide [105]. Therefore, alternatives strategies have to be found for reducing the synthetic manufacturing costs of SET-M33 without affecting its strong antimicrobial activity.

SET-M33-DIM

The amino acid sequence (KKIRVRLSA) of the original peptide was synthetized in two-branched dimeric form to obtain SET-M33-DIM peptide. This peptide showed a toxicity more than 20 times lower than that of the original tetra-branched SET-M33 in cytotoxicity tests toward bronchial cells [157]. Experiments *in vivo* demonstrated a sharp improvement in toxicity with less morbidity and mortality for SET-M33-DIM respect to the original peptide [157]. In addition, SET-M33-DIM revealed strong anti-inflammatory activity, inhibiting expression of 14 cytokines, growth factors and enzymes involved in inflammation, triggered in cells or tissues by incubation with soluble LPS from *P. aeruginosa, K. Pneumoniae* and *E. coli,* (Figure 22) or by infection with living *P. aeruginosa* cells [157].

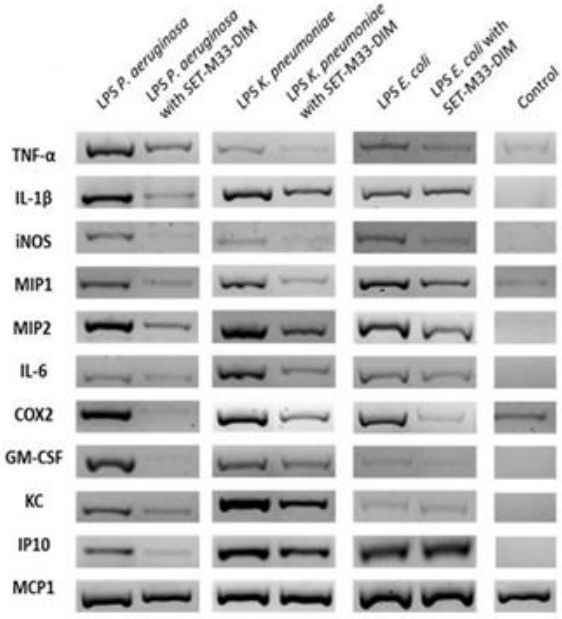

Gene expression percentage			
	LPS *P. aeruginosa* with SET-M33-DIM	LPS *K. pneumoniae* with SET-M33-DIM	LPS *E. coli* with SET-M33-DIM
TNF-α	25	21	8
IL-1β	30	69	91
iNOS	13	57	55
MIP1	0	15	37
MIP2	27	56	57
IL-6	21	46	52
COX-2	0	4	0
GM-CSF	15	73	15
KC	58	53	100
IP10	10	66	100
MCP1	100	100	91

Figure 22. Gene expression of pro-inflammatory cytokines and enzymes analyzed by RT-PCR [157]

AIM OF THE RESEARCH

The increasing frequency of multidrug-resistant (MDR) pathogens leads to an urgent need for the development of new antimicrobial drugs and new strategies for the treatment of infectious diseases. AMPs are described as a promising alternative to traditional antibiotics, powerful to address the increasing problem of antibiotic resistance and hold promise to be developed as novel antibiotics [16]. Although many eukaryotic AMPs have been discovered and characterized, only a few have been approved by US Food and Drug Administration for clinical use [41]. The principal drawbacks of AMPs in clinical applications are due to systemic toxicity, low stability, manufacturing costs and systemic administration [36, 73, 95].
This PhD thesis is divided in two sections focused to improve the biopharmaceutical development and manufacturing procedures of the peptide SET-M33.

1) **NMR study of the secondary structure and biopharmaceutical formulation of SET-M33 peptide**

   The presence of helixes or β-sheets in the structure of SET-M33 had to be explored to fully characterize the product in the framework of preclinical studies with a view to designing a formulation for parental administration. NMR studies of multiple branched peptides are extremely uncommon because their spectra are complex due to non-equivalent branches carrying the same amino acid sequence. Therefore, the secondary structure of branched peptides in solution is deducted from analogue linear peptides or studied using CD technique [153]. Previous CD studies on the peptide and NMR analysis on the linear analogue showed a transition from an unstructured state to a α-helix only in presence of micelle-like-structures [153]. Thus, the secondary structure of SET-M33 was investigated by $^{1}H/^{13}C/^{15}N$ NMR spectroscopy to completely confirm the results obtained with the monomeric analogue [153]. Salt formation is important in biopharmaceutical drug development as it modulates drug solubility, stability and bioavailability. Since the final formulation of SET-M33 had to be strictly defined in terms of counter-ions, a novel salt form, SET-M33 chloride was synthetized and characterized.

   This research is reported in the article published on *Molecules*.
   Castiglia, F.; Zevolini, F.; Riolo, G.; Brunetti, J.; De Lazzari, A.; Moretto, A.; Manetto, G.; Fragai, M.; Algotsson, J.; Evenäs, J.;Bracci, L.; Pini, A.; Falciani, C. NMR Study of the Secondary Structure and Biopharmaceutical Formulation of an Active Branched Antimicrobial Peptide. *Mol.* **2019**, 24(23):4290.

2) **Production and analysis of SET-M33 back-up molecules: SET-M33D-L-Ile, SET-M33D-Leu/Ile and SET-M33-Gly/Ala.**

   To identify back-up molecules, a panel of modified versions of SET-M33 was tested in order to produce new molecules with better performance in terms of pharmaceutical profile and manufacturing costs. Amongst them, the peptides SET-M33D-L-Ile and SET-M33D-Leu/Ile, proposed for replacing D-Isoleucine, D-Ile, which is the most expensive amino acid in the

sequence of the peptide, and SET-M33-Gly/Ala, attempted to eliminate the degradation site for bacterial proteases [152], replacing alanine with glycine, were synthetized, tested for the antimicrobial activity, by means of MIC assays, and subjected to stability study upon the time. In addition, SET-M33-PEG4 and SET-M33-DIM, due to their very promising profiles [145,157], were synthetized again and included in these analyses.

RESULTS

1

NMR study of the secondary structure and biopharmaceutical formulation of SET-M33 peptide

NMR study of the secondary structure of SET-M33 peptide

The upstream and downstream processes of SET-M33 are currently being developed together with full characterization of the product. Like most peptides, SET-M33 is routinely characterized by HPLC and mass spectrometry (MS) for its purity and chemical structure. Here are reported its $^{1}H/^{13}C/^{15}N$ NMR spectroscopy characterization for full atom-specific assignment and the primary and secondary structure of the peptide in solution based on observed chemical shifts. Assessment of SET-M33 secondary structure in water allows predicting aggregation potential, which can affect drug product design and formulation strategy. Aqueous environments are involved in most typical peptide drug manufacturing processes, that can be crucial for successful development, such as the lyophilization process and the preparation of injectable pharmaceutical forms.

NMR characterization of SET-M33 peptide

The 40 amino acid long peptide SET-M33 was characterized using ^{1}H-/^{13}C-/^{15}N-NMR spectroscopy to perform complete atom-specific assignment, to verify the primary peptide structure and to evaluate possible secondary or other ordered structures based on observed chemical shift values and possible medium- and long-range NOEs.
To allow a faster NMR data collection, a 12.5 mg/mL peptide solution was used. The pH was adjusted to pH 4.9 by a small addition of TFA-*d* in order to minimize the rate of proton exchange between amide groups of the peptide and water molecules resulting in clear observation of the backbone amide proton signals critical to effectively obtain the atom-specific chemical shift assignments. The resulting 1D ^{1}H-NMR spectrum is shown in Figure 23.

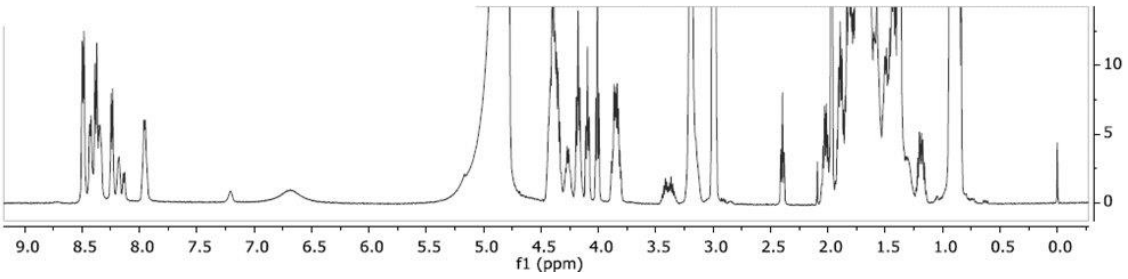

Figure 23. 1D ^{1}H-NMR spectrum of 12.5 mg/Ml SET-M33 in H_2O/D_2O (9:1) and TFA-*d* (12.5 mg/mL) at 298 K [158].

The spectral quality and resolution were good although the amide region contained some broadened signals, presumably due to fast proton exchange with the solvent. All observed signals originated from SET-M33, except those that originate from residual NMR solvents and sodium trimethylsilylpropanesulfonate, DSS. In addition, a singlet ^{1}H signal was observed at 1.97 ppm (proton(s) bound to carbon with a ^{13}C chemical shift of 25.0 ppm), tentatively assigned to acetate. The broad ^{1}H signal at 6.68 ppm sharpened further at pH values lower than 4.9, and an additional broad peak also appeared at 7.54 ppm at these more acidic conditions (data not shown). These two broad signals presumably originated from the guanidine- and amino side chain groups of arginine and lysine residues. The first step in the NMR study was to assign the ^{1}H, ^{13}C and ^{15}N chemical shifts of SET-M33 applying the conventional backbone amide proton strategy developed for non-isotope-enriched proteins [159]. Figure 24 (panel **A**) shows the amino acid numbering and atom labelling of SET-M33. The four identical segments of nine amino acids are indicated A, B, C and D. The three linking lysine residues are indicated Lys'10, Lys'11 and Lys'12, respectively and the C-terminal βAla, as βAla 13.

The ^{1}HN-$^{1}H\alpha$ fingerprint region of the 2D ^{1}H COSY spectrum and the ^{1}HN-^{15}N fingerprint region of the ^{1}H-^{15}N HSQC spectrum are shown in Figure 24 (panels **B** and **C**, respectively), with each peak labelled with the assigned amino acid. The amino group of Lys1 was not detectable due to fast proton exchange with the solvent and also the backbone amide proton signal of Lys2 was significantly weaker presumably for the same reason. The assignment procedure readily revealed virtually identical chemical shifts of the four 9-amino acid chains, strongly indicating the same conformation(s) of all the branches of SET-M33. There were, however, small chemical shift changes clearly observed between Ala9 of A, D and Ala9 of B, C, consistent with the asymmetric coupling to the branched core, i.e., A, D are connected via the sidechain amino group of Lys'10 and Lys'12 while B, C are connected via the backbone amino groups of Lys'10 and Lys'12.

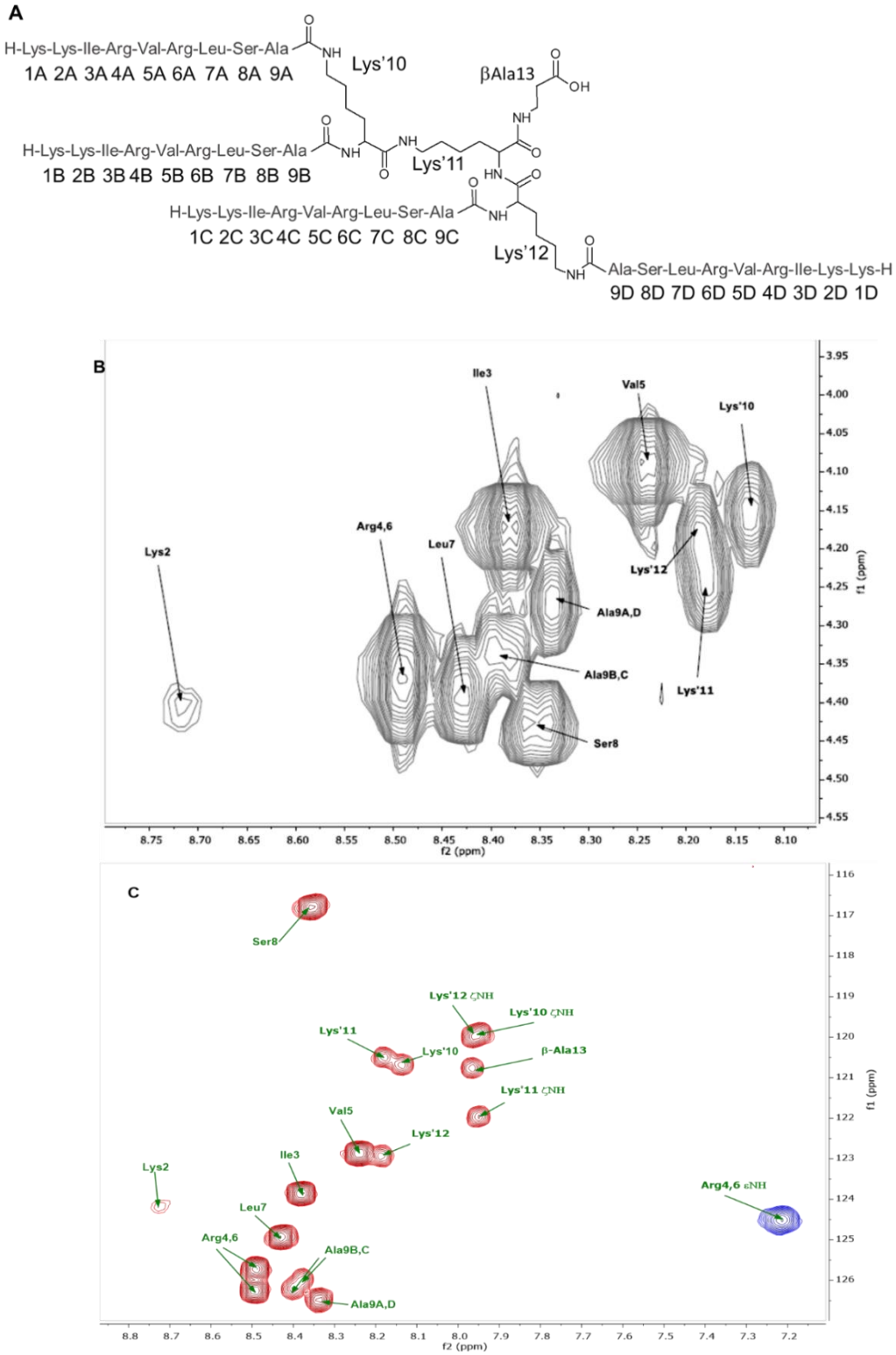

Figure 24. A) The primary structure of SET-M33 with amino acid numbering. Amino acids are labeled with a three-letter code and sequence number as reported above. **B**) The ^{1}HN-^{1}Hα fingerprint region of the 2D ^{1}H COSY spectrum of SET-M33 in H_2O/D_2O (9:1) with addition of TFA-*d*, pH 4.9 at 298 K. The assignment of each cross-peak is shown using the three-letter amino acid code followed by the sequence number. **C**) The 2D ^{1}H-^{15}N HSQC spectrum of SET-M33 in H_2O/D_2O (9:1) with addition of TFA-*d* at 298 K. The peaks for the sidechain εNH groups of Arg4,6 are folded into the spectrum with opposite sign (blue color). The assignment of each cross-peak is indicated using the three-letter amino acid code followed by the sequence number [158].

The primary structure was confirmed by the "sequential walk" in the ^{1}HN(i)-^{1}Hα fingerprint region of the 2D ^{1}H NOESY spectrum connecting sequential amino acids (Figure 25). This plot showed the "walk" between alternating sequential and intra-residue NOE (^{1}HN-^{1}Hα) from Lys1 to Lys'10, Lys'11 and Lys'12 – a key step to confirm the amino acid sequence. All assigned ^{1}H-, ^{13}C-, and ^{15}N-NMR chemical shifts were reported in Table 3 and fully confirmed the anticipated amino acid sequence and chemical structure of SET-M33.

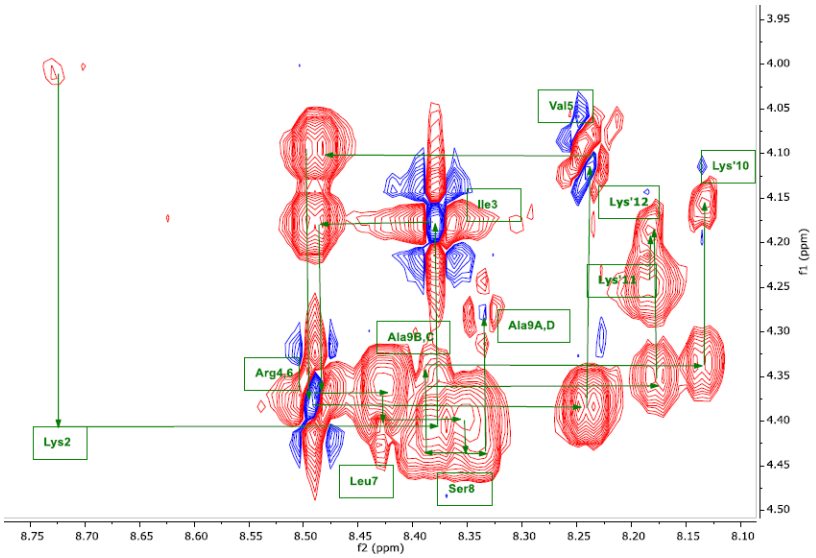

Figure 25. Sequential walk through the amide backbone fingerprint region of 2D ^{1}H NOESY spectrum of SET-M33 in H_2O/D_2O (9:1) with addition of TFA-*d*, pH 4.9 298 K is shown. The assignment of each cross-peak is shown using the three-letter amino acid code followed by the sequence number. The sequential walk follows the arrows between alternating sequential inter-residue HN(i)-Hα(i-1) and intra-residue HN(i)-Hα(i) NOEs [158].

Residue	^{1}HN	^{15}N	^{1}Hα	^{13}Cα	^{1}Hβ	^{13}Cβ	Others
Lys1A-D	*NO*	*NO*	4.01	55.5	1.89	33.2	γ: 1.43/23.8; δ: 1.69/29.1; ε: 2.99/41.9
Lys2A-D	8.72	124.2	4.40	56.1	1.76	33.1	γ: 1.40/24.7; δ: 1.40/24.7; ε: 2.99/41.9
Ile3A-D	8.38	123.9	4.18	60.7	1.83	38.9	γ1: 1.19, 1.47/27.1; γ2: 0.89/17.3; δ1: 0.86/12.6
Arg4A-D	8.49	125.7[1]	4.37	55.8	1.75, 1.82	30.8	γ:1.58, 1.64/27.0; δ: 3.20/43.3; ε: 7.21/84.5 (^{15}N)
Val5A-D	8.24	122.9	4.10	62.0	2.03	33.0	γ1: 0.92/20.8; γ2:0.94/20.5
Arg6A-D	8.49	126.3[1]	4.37	55.8	1.75, 1.82	30.8	γ:1.58, 1.64/27.0; δ: 3.20/43.3; ε: 7.21/84.5 (^{15}N)
Leu7A-D	8.43	124.9	4.40	55.1	1.59, 1.64	42.4	γ: 1.64/26.8; δ1: 0.93/24.8; δ2: 0.87/23.3
Ser8A-D	8.35	116.8	4.44	57.9	3.85	63.8	
Ala9A,D	8.34	126.5	4.27	52.6	1.38	19.4	
Ala9B,C	8.40, 8.38	126.2, 126.0	4.34	52.4	1.38	19.4	
Lys'10	8.13	120.7	4.15	56.7	1.76	33.1	γ: 1.32/25.0; δ: 1.50/30.5; ε: 3.18/41.8; ζ: 7.95/119.9 (^{15}N)
Lys'11	8.18	120.5	4.25	56.4	1.76	33.1	γ: 1.32/25.0; δ: 1.50/30.5; ε: 3.18/41.8; ζ: 7.95/122.0 (^{15}N)
Lys'12	8.19	122.9	4.17	56.7	1.76	33.1	γ: 1.32, 1.40/25.0; δ: 1.50/30.5; ε: 3.18/41.8; ζ: 7.95/119.9 (^{15}N)
β-Ala13	7.96	120.8	3.38	39.3	2.40	39.0	

Table 3. ^{1}H/^{13}C/^{15}N chemical shifts (ppm) of SET-M33 in H_2O/D_2O (9:1) with addition of TFA-d at 298 K [158].

The chemical shifts were determined in the 2D ^{1}H-^{13}C HSQC and 2D ^{1}H-^{15}N HSQC spectra. Referencing for ^{1}H- and ^{13}C- spectra is relative to the ^{1}H- and ^{13}C-NMR chemical shifts of the methyl groups of DSS (set to 0 ppm for both nuclei) while indirect chemical shift referencing is applied for ^{15}N chemical shifts using the gyromagnetic ratio of ^{1}H and ^{15}N. The notation *NO* indicates that the signals of these atoms are not observed. The ^{15}N-NMR chemical shifts of Arg4 and Arg6 may be interchanged, i.e., the ^{15}N chemical shift of Arg4 may belong to Arg6 and vice versa.
Based on the peak integral measured of aliphatic protons in the quantitative 1D ^{1}H-NMR spectrum, the number of amino acids in the peptide was verified.

Assessment of secondary structure elements

The chemical shift index (CSI) method for ^{1}Hα, ^{13}Cα and ^{13}Cβ atoms was used as the primary means to assess the degree of secondary structure and its possible sequence-specific locations [160]. The chemical shifts obtained experimentally were compared with the so-called random coil chemical shifts of the corresponding amino acid residue type (Xxx) measured in Gly-Gly-Xxx-Ala-Gly-Gly peptides in 1M urea [161]. Figure 26 shows the CSI values for ^{1}Hα, ^{13}Cα and ^{13}Cβ atoms, as well as the absolute deviation in ppm from the random coil shifts.

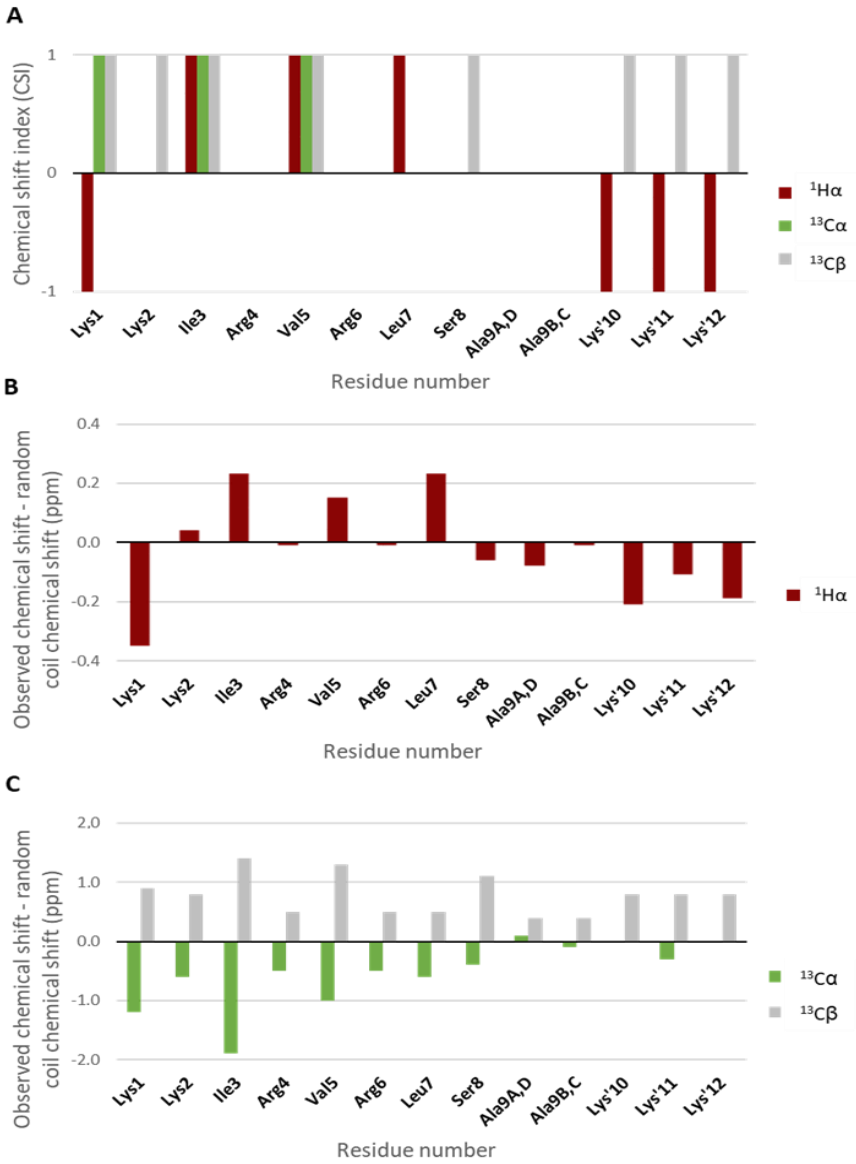

Figure 26. ^{1}Hα, ^{13}Cα and ^{13}Cβ chemical shift data of SET-M33 in H_2O/D_2O (9:1) with addition of TFA-*d*, pH 4.9 at 298 K. **A**) CSI values for ^{1}Hα, ^{13}Cα and ^{13}Cβ atoms. **B**) The absolute difference between observed chemical shift values and random coil chemical shift values for ^{1}Hα atoms. **C**) The absolute difference between observed chemical shift values and random coil chemical shift values for ^{13}Cα and ^{13}Cβ atoms [158].

An index of 1 for more than three residues in a row indicates β-strand while an index of -1 for at least four consecutive residues indicates helical structure. The index is set to 1 if the difference between experimental shift and random coil shift is greater than 0.1 ppm (^{1}Hα), greater than 0.7 ppm (^{13}Cβ) or less than -0.7 ppm for ^{13}Cα, while it is set at -1 if the difference is less than -0.1 ppm (^{1}Hα), less than -0.7 ppm (^{13}Cβ) or greater than 0.7 ppm for ^{13}Cα. If the absolute chemical shift difference is less than 0.1 ppm (^{1}H) or 0.7 ppm (^{13}C), the index is set to 0.

The chemical shift data including the several positive CSI values of the ^{1}Hα, ^{13}Cα and ^{13}Cβ atoms indicate a generally more extended peptide backbone configuration for several amino acids in the Lys1–Ser8 sequence. However, as there are no clear stretches of three such amino acids in a row, the conclusion is that the peptide has no stable β-strand configurations.

In addition to the chemical shift analysis, the NOESY spectra were examined to further investigate the structural properties of SET-M33 in water, pH 4.9. Besides several intra- and sequential NOEs, no resolved medium- or long-range NOEs were observed, strongly indicating the lack of any stable secondary or tertiary structure. Several sequential ^{1}HN-^{1}HN NOEs were observed primarily for the inner core of the peptide.

The finding of virtually identical chemical shifts for all four branches, reported above, prevented most conclusions using inter-branch NOEs as such potential cross peaks would fully overlap with the intra-branch NOE cross peaks. In conclusion, the NMR data were fully consistent with anticipated chemical structure of SET-M33 but no stable secondary or tertiary structure could be shown. Furthermore, the data showed that all four 9-amino acid chains of the branched peptide were in the identical conformation(s). The data suggested that these chains have a propensity to adopt an extended, flexible conformation as compared with the so-called random coil conformation.

Biopharmaceutical formulation of SET-M33 peptide

Salt formation is important during biopharmaceutical drug development as it modulates drug solubility, stability and bioavailability. SET-M33, like almost all synthetic peptides, is obtained as trifluoroacetate salt (SET-M33 TFA), due to the cleavage and purification conditions. Preliminary studies, on the efficacy and toxicity of SET-M33 revealed that the acetate form of the peptide, SET-M33 acetate, was less toxic to human cells and animals than SET-M33 TFA [151]. Thus, the peptide is traditionally converted into the acetate form at the end of the synthesis. However, this counter-ion exchange requires the use of a quaternary ammonium salt resin that is unsuitable for industrial scaling [162]. In order to avoid this step, hydrochloric acid was chosen, as a stronger acid than TFA, so that chloride counter-ion could be replaced TFA [163-165], for producing SET-M33 chloride. Complete replacement of TFA with chloride and stability of SET-M33 to HCl treatment were assessed. Finally, the antimicrobial activity and toxicity of SET-M33 with the three different counter-ions, TFA, acetate and chloride, were assessed in mammalian cells and in mice.

TFA/chloride counter ion exchange

SET-M33 TFA (2 mg/mL) was dissolved in 100 mM HCl solution, frozen and dried. The HPLC and MS analyses revealed that the peptide was intact after the ion exchange procedure; the HPLC profile was unchanged and the MS profile showed a single peak of molecular mass of 4683 Da in line with the calculated mass of $C_{209}H_{399}N_{75}O_{45}$.

Residual TFA counter-ions was determined by comparing the intensity of the fluorine signal in the NMR spectra of the sample before and after the exchange procedure, using the same concentration and volume of SET-M33 TFA and SET-M33 chloride and the same NMR settings. The NMR experiments were recorded at 298 K on a Bruker Avance III spectrometer operating at 800 MHz and equipped with a 5 mm PHTXI 1H-13C/15N probe, tuned on 19F. The intensity of the fluorine signal after exchange decreased by a factor of about 200 with respect to the signal recorded on the sample before exchange. The solubility of SET-M33 chloride in water was much higher (100 mg/mL) than that of the acetate (15 mg/mL) and TFA forms (10 mg/mL).

MIC Determination

Minimum inhibitory concentrations (MICs) of SET-M33 chloride were determined against two Gram-negative pathogens like *E. coli TG-1* and *P. aeruginosa PAO-1* and compared to those of SET-M33 acetate. SET-M33 chloride retained its antimicrobial activity against both species and actually improved from 3.0 µM to 1.5 µM against *P. aeruginosa*, as revealed by MIC results (Table 4).

Bacterial Species	MIC (µM) SET-M33	
	Acetate	Chloride
E. coli TG-1	1.5	1.5
P. aeruginosa PAO-1	3	1.5

Table 4. MICs of SET-M33 acetate and SET-M33 chloride [158].

Cytotoxicity

T24 human bladder epithelial cells, 16HBE14o- human bronchial epithelial cells and RAW264.7 mouse macrophages were used to test the cytotoxicity of SET-M33 chloride and to compare it with that of the TFA and acetate salts. Bladder cells and human bronchial cell lines were selected, with a view to using SET-M33, as local treatment for urinary tract infections and pneumonia, respectively. Being a cationic hydrophilic molecule, SET-M33 peptide is also most probably eliminated in the urine when administered systemically, as observed in previous studies [145]. Hence bladder cells will be the most targeted.

The 3-(4,5-dimethylthiazol-2-yl)2,5-diphenyltetrazolium bromide (MTT) assay results revealed that no SET-M33 form was toxic, except at very high concentrations. 100% cytotoxicity occurred at 100 µM for T24 and 16HBE14o- cells and at 10 µM for RAW264.7. SET-M33 chloride showed slightly lower toxicity for T24 and RAW264.7 cells (Figure 27, Table 5).

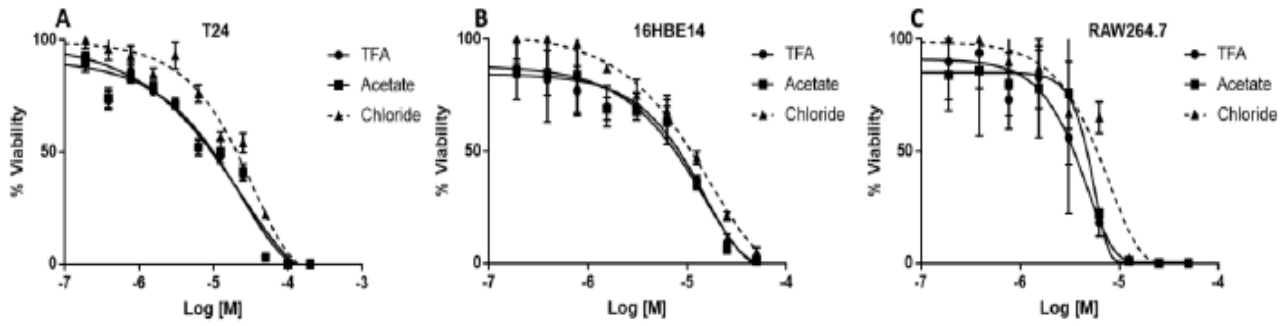

Figure 27. Cytotoxicity of SET-M33 salts for T24 (A), 16HBE14o- (B) and RAW264.7 (C) cells. Circles, incubation with SET-M33 TFA; squares incubation with SET-M33 acetate; triangles, incubation with SET-M33-chloride (dotted line) [158].

SET-M33	EC50 [M]		
Counter ion	T24	16HBE14o-	RAW264.7
TFA	1.363×10^{-5}	1.105×10^{-5}	3.846×10^{-6}
Acetate	1.243×10^{-5}	9.618×10^{-6}	5.104×10^{-6}
Chloride	2.260×10^{-5}	1.034×10^{-5}	6.125×10^{-6}

Table 5. In vitro toxicity of the different SET-M33 salts, measured as inhibition of growth [158].

Acute toxicity

Acute toxicity of SET-M33 chloride was tested in mice and compared with the acetate and TFA counter-ions. Ten animals per group (five males and five females) were injected with two doses of SET-M33 chloride, 20 and 30 mg/kg, known to be below the LD50 [145]. Signs of toxicity were scored as not-observable, mild and severe. SET-M33 chloride and SET-M33 acetate scored 100% not-observable signs of toxicity, unlike, SET-M33 TFA that scored 100% toxicity at 25 mg/kg, described as 33% severe and 66% mild [145] (Table 6).

SET-M33 / Counter ion	20 mg/kg	25 mg/kg	30 mg/kg
TFA	(-)	mild to severe	(-)
Acetate	not-observable [146]	not-observable	not-observable
Chloride	not-observable	(-)	not-observable

(-) not measured.

Table 6. Signs of acute toxicity in vivo of the three SET-M33 salts [158].

2

Production and analysis of SET-M33 back-up molecules: SET-M33D-L-Ile SET-M33D-Leu/Ile and SET-M33-Gly/Ala

To identify back-up molecules, modified versions of SET-M33 were tested in order to produce new molecules with better performance in terms of pharmacological profile and manufacturing costs. Here are reported the synthesis of three novel SET-M33 analogues, SET-M33D-L-Ile, SET-M33D-Leu/Ile and SET-M33-Gly/Ala, obtained as acetate salt, and their activity against many bacterial isolates. In addition, the SET-M33 analogues were subjected to a stability study observing their MIC values, HPLC and MS profiles during the time. Moreover, SET-M33-PEG4 and SET-M33-DIM due to their very promising profile [145,157], were synthetized again and included in these analysis.

Synthesis of SET-M33D-L-Ile

The peptide SET-M33D-L-Ile has the same amino acid sequence of the peptide SET-M33 (KKIRVRLSA) synthesized in tetrameric form using amino-acids in D configuration with the exception of the isoleucine residues in L configuration; the synthesis with D amino-acids was carried out in order to improve the stability of the resulting peptide and to replace D-Ile residues, which are the most expensive amino-acid in the peptide sequence, with L-Ile. This analogue was obtained as acetate salt. According to the conditions described in material and method section, synthesis and purification processes of SET-M33D-L-Ile resulted in more than 98% pure product, as shown by analytical reversed phase chromatography on a Jupiter C18 column (Fig. 28). The retention time of the peptide was 21 minutes. The MS profile showed a single peak at molecular mass of 4686 Da, in according to the calculated $C_{209}H_{399}N_{75}O_{45}$ tetra-branched peptide (Figure 29).

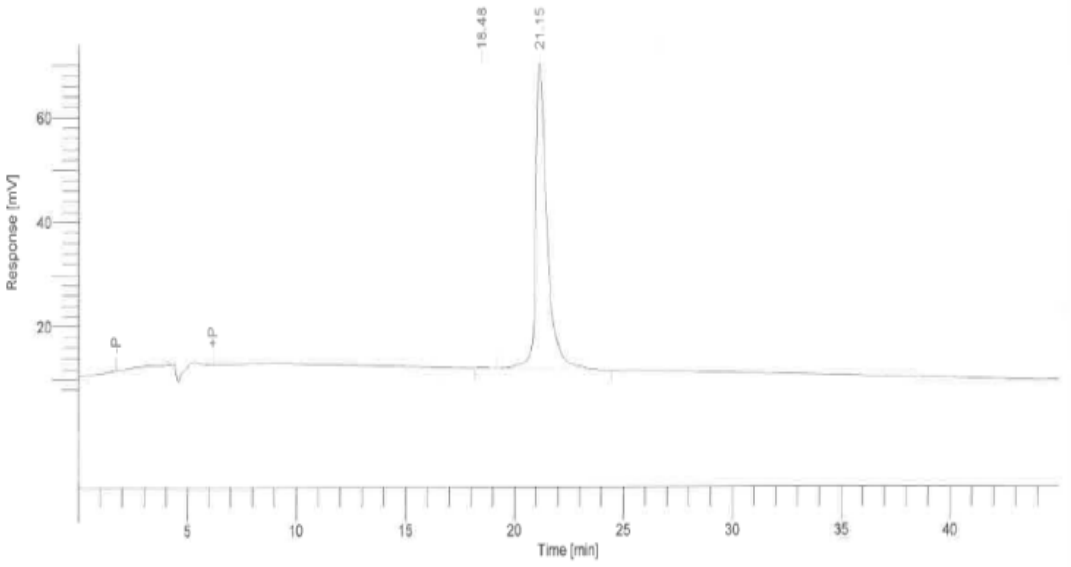

.

Figure 28. HPLC profile of SET-M33D-L-Ile on a Phenomenex analytical Column Jupiter C18 300Å µm 4.6 x 250mm, eluent A: 0.1% TFA / H_2O, eluent B: Acetonitrile, gradient from 83:17 A/B to 70:30 A/B in 40min.

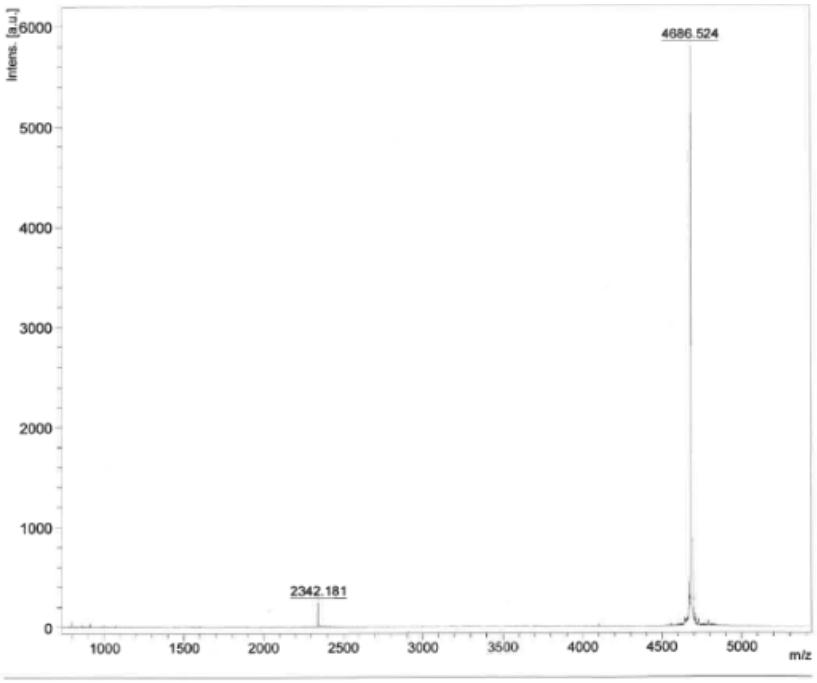

Figure 29. MALDI TOF MS profile of SET-M33D-L-Ile.

Synthesis of SET-M33D-Leu/Ile

The peptide SET-M33D-Leu/Ile has the sequence KKLRVRLSA synthesized in tetrameric form with all amino-acids in D configuration and D-Ile residues replaced with D-Leu residues. The analogue was obtained as acetate salt. According to the conditions described in material and method section, synthesis and purification processes of SET-M33D-Leu/Ile resulted in more than 97% pure product, as shown by analytical reversed phase chromatography on a Jupiter C18 column (Fig. 30), the retention time of the peptide was 22 minutes (Figure 30). The MS profile showed a single peak at molecular mass of 4686 Da, in according to the calculated $C_{209}H_{399}N_{75}O_{45}$ tetra-branched peptide (Figure 31).

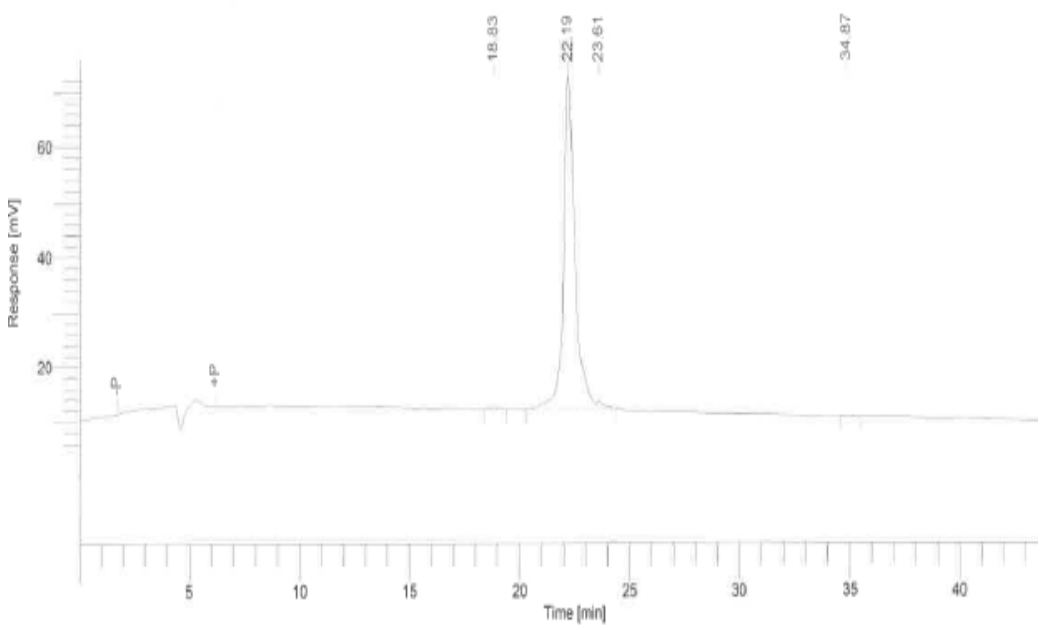

Figure 30. HPLC profile of SET-M33D-Leu/Ile on a Phenomenex analytical Column Jupiter C18 300Å 5µm 4.6 x 250mm, eluent A: 0.1%TFA / H_2O, eluent B: Acetonitrile, gradient from 83:17 A/B to 70:30 A/B in 40min.

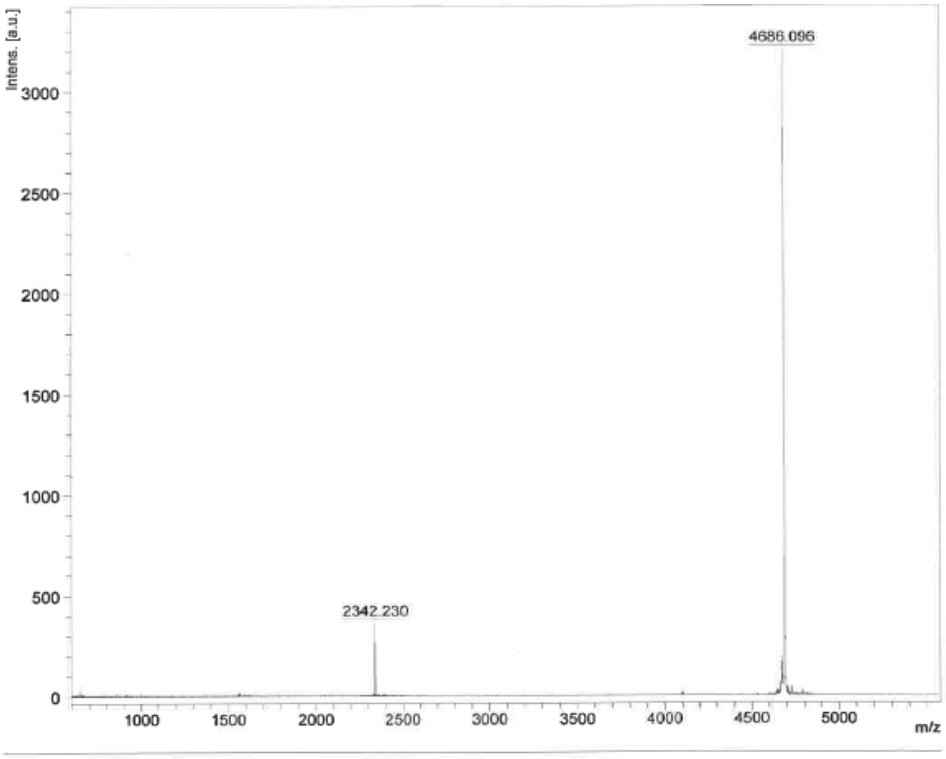

Figure 31. MALDI TOF MS profile of SET-M33D-Leu/Ile.

Synthesis of SET-M33-Gly/Ala

The peptide SET-M33-Gly/Ala has the sequence KKIRVRLSG synthetized in tetrameric form using all amino acids in L configuration; the replacement of the alanine residues, originally presents in the traditional SET-M33 sequence, with glycine residues was attempted to eliminate the degradation site for bacterial proteases [152]. The peptide was obtained as acetate salt. According to the conditions described in material and method section, synthesis and purification processes of SET-M33-Gly/Ala resulted in more than 95% pure product, as shown by analytical reversed phase chromatography on a Jupiter C18 column (Fig. 32). The retention time of the peptide was 19 minutes (Figure 32).

The MS profile showed a single peak at molecular mass of 4629 Da, in according to the calculated $C_{205}H_{391}N_{75}O_{45}$ tetra-branched peptide (Figure 33).

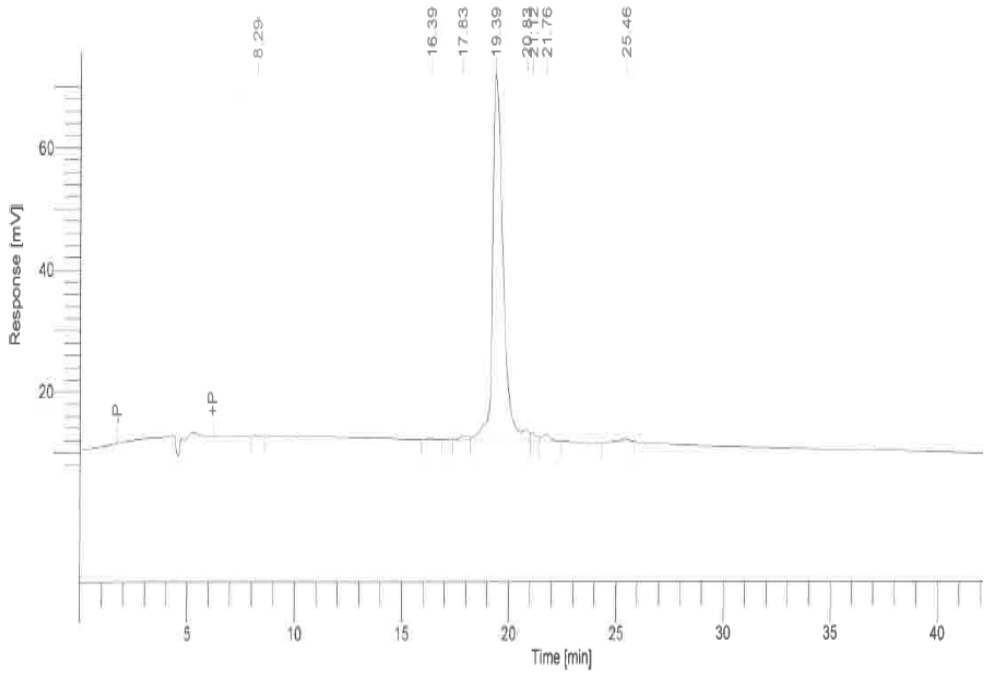

Figure 32. HPLC profile of SET-M33-Gly/Ala on a Phenomenex analytical Column Jupiter C18 300Å 5µm 4.6 x 250mm, eluent A: 0.1%TFA / H_2O, eluent B: Acetonitrile, gradient from 83:17 A/B to 70:30 A/B in 40min.

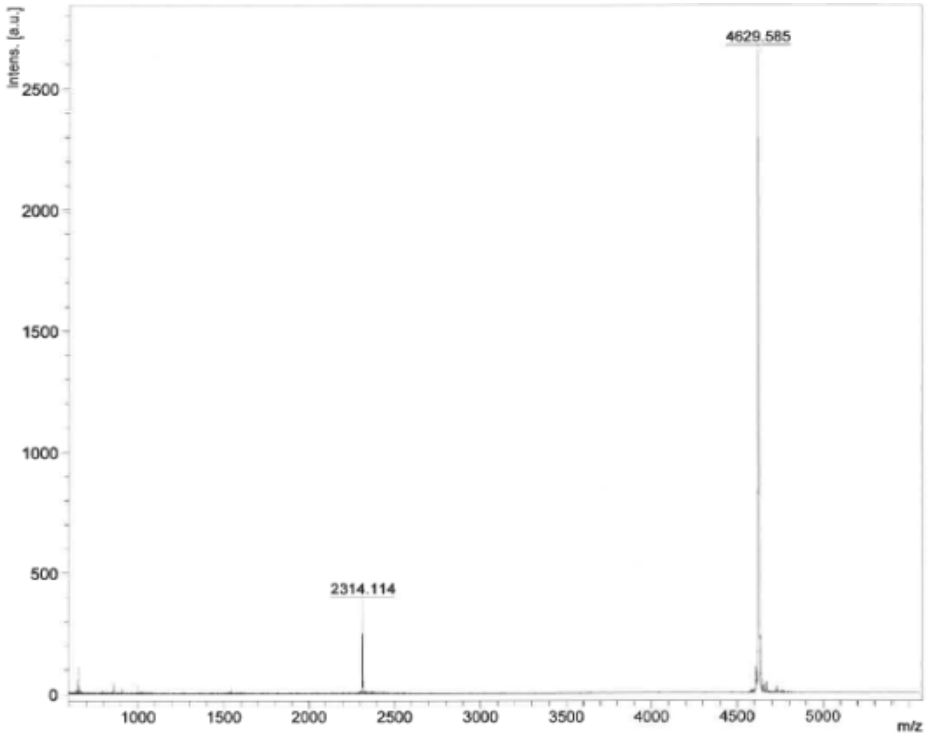

Figure 33. MALDI TOF MS profile of SET-M33-Gly/Ala.

Synthesis of SET-M33-PEG4

The peptide SET-M33-PEG4 has the same sequence of the peptide SET-M33 synthesized in tetrameric form with all amino acids in L configuration with the insertion of polyethylene glycol 4 molecule (PEG4) at the C terminus of the three lysine-branching core; this modification led the peptide to have a longer persistence in plasma than the traditional peptide [145]. The peptide was obtained in acetate salt. According to the conditions described in material and method section, synthesis and purification processes of SET-M33-PEG4 resulted in more than 95% pure product, as shown by analytical reversed phase chromatography on a Jupiter C18 column (Fig. 34); the retention time of the peptide was 21 minutes (Figure 34); The MS profile showed a single peak at molecular mass of 4861 Da, in according to the calculated $C_{217}H_{416}N_{76}O_{48}$ tetra-branched peptide (Figure 35).

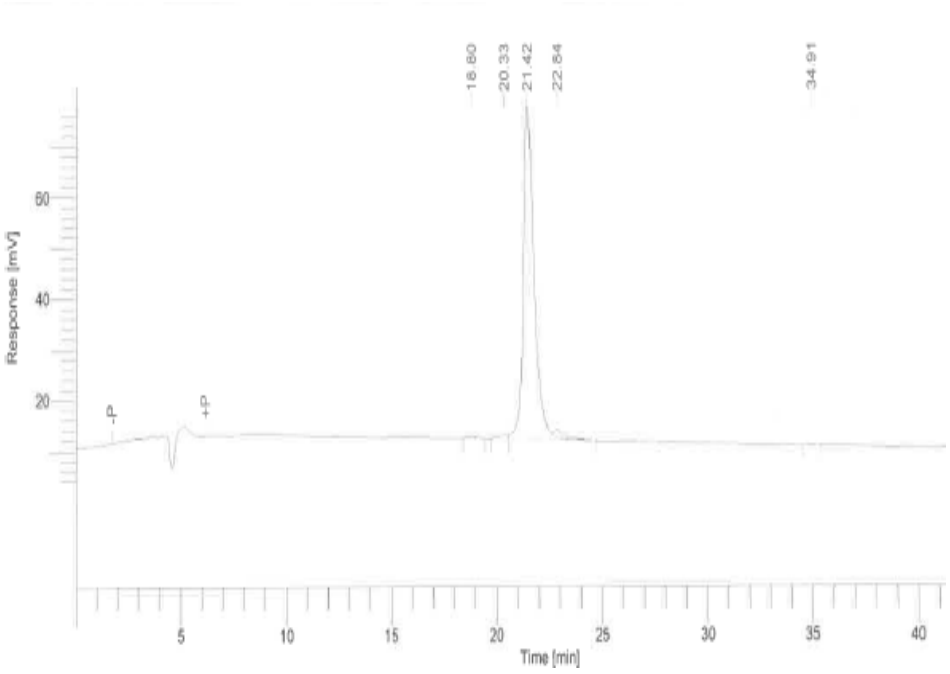

Figure 34. HPLC profile of SET-M33-PEG4 on a Phenomenex analytical Column Jupiter C18 300Å 5µm 4.6 x 250mm, eluent A: 0.1%TFA / H_2O, eluent B: Acetonitrile, gradient from 83:17 A/B to 70:30 A/B in 40min.

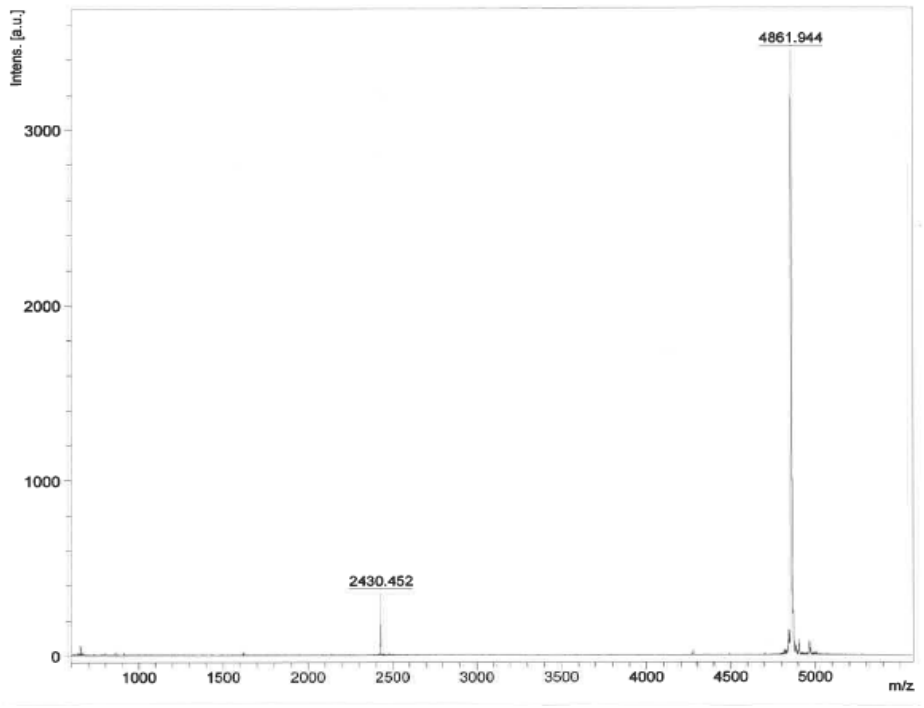

Figure 35. MALDI TOF MS profile of SET-M33-PEG4.

Synthesis of SET-M33-DIM

The SET-M33-DIM peptide has the same sequence of SET-M33 synthetized in L configuration in two-branched form, instead of the traditional tetra-branched form. This peptide was more than 20 fold less toxic for eukaryotic bronchial cells respect of the traditional peptide SET-M33 [157]. The analogue was obtained as acetate salt. According to the conditions described in material and method section, synthesis and purification processes of SET-M33-DIM resulted in more than 96% pure product, as shown by analytical reversed phase chromatography on a Jupiter C18 column (Fig. 36); the retention time of the peptide was around 20 minutes (Figure 36). The MS profile showed a single peak at molecular mass of 2321 Da, in according to the calculated $C_{103}H_{198}N_{38}O_{22}$ two-branched peptide (Figure 37).

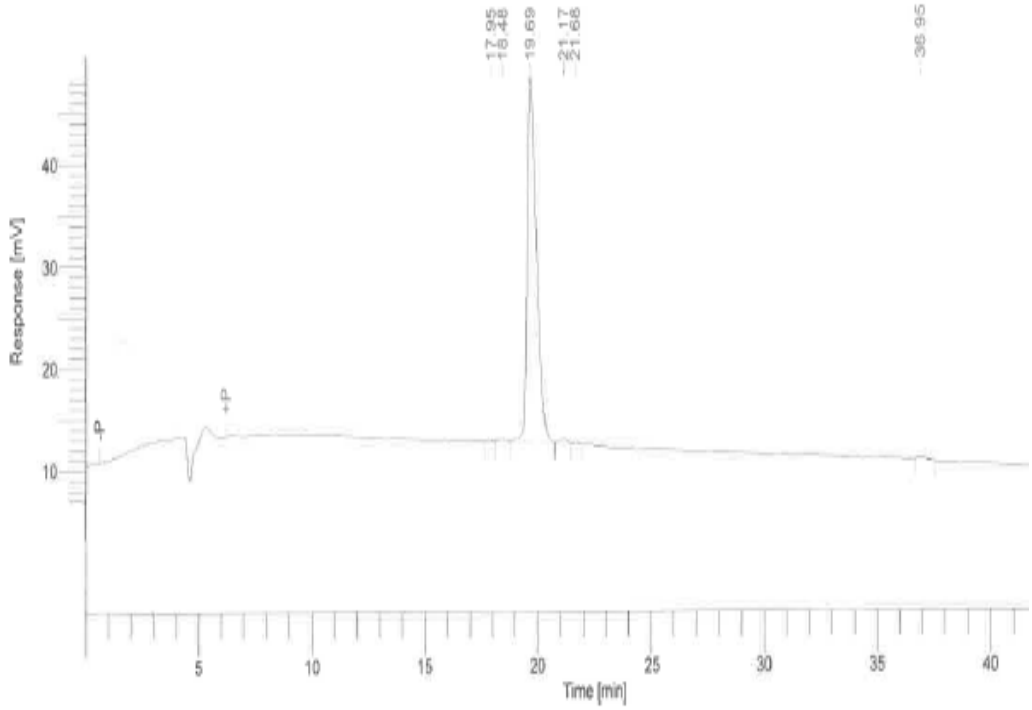

Figure 36. HPLC profile of SET-M33-DIM on a Phenomenex analytical Column Jupiter C18 300Å 5µm 4.6 x 250mm, eluent A: 0.1%TFA / H_2O, eluent B: Acetonitrile, gradient from 85:17 A/B to 70:30 A/B in 40min.

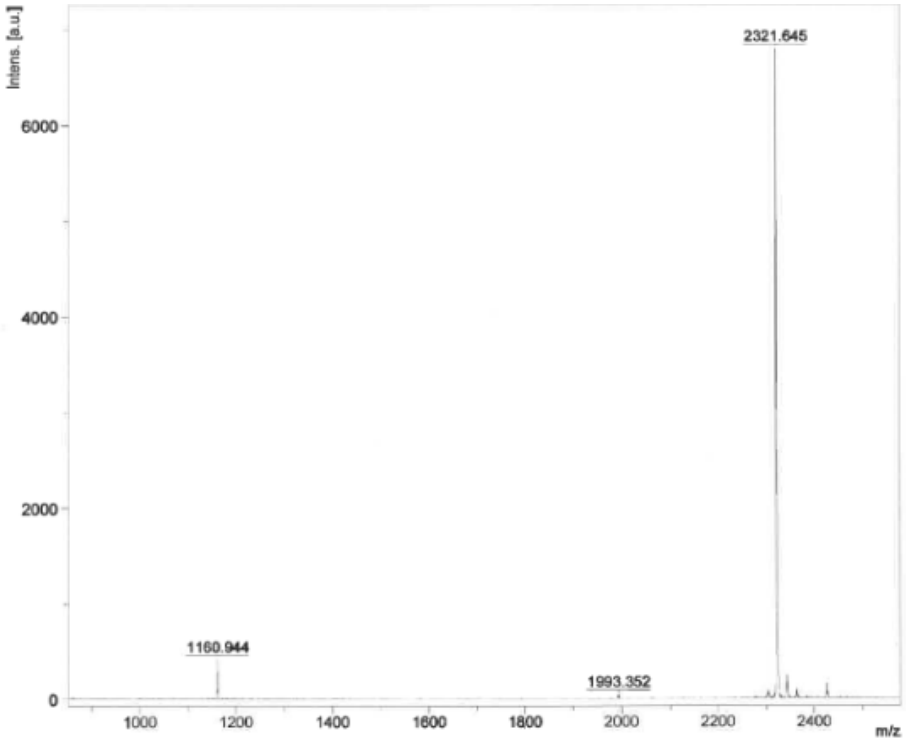

Figure 37. MALDI TOF MS profile of SET-M33-DIM.

MIC determination of SET-M33 analogues

MIC values of the SET-M33 analogues were determined against a collection of clinical isolates of Gram-negative and Gram-positive pathogens and compared to the original SET-M33 (in L configuration) and SET-M33D peptides, in collaboration with Professor Rossolini from Department of Experimental and Clinical Medicine at the University of Florence. Isolates were selected according to their phenotype or genotype. Overall, 34 representative isolates were tested, including 18 Gram-negatives and 16 Gram-positives (Tables 7a-b).

The tetra-branched SET-M33 analogues showed MIC values against Gram-negative strains comparable to those of SET-M33 and SET-M33D with MICs mostly in the range between 0.7- 1.5 μM. Among the peptide tested, SET-M33D-Leu/Ile and SET-M33-PEG4 showed a higher antimicrobial activity than those of SET-M33 and SET-M33D against *K. pneumoniae* (Table 7a). In particular, SET-M33D-Leu/Ile showed MIC values of 0.7 μM versus 3 μM of SET-M33 against *K. pneumoniae* 7086042 and of 1.5 μM versus 6 μM of SET-M33D against *K. pneumoniae* FI-20. SET-M33-PEG4 observed MIC values of 0.7 μM versus 3 μM of SET-M33 against *K. pneumoniae 7086042* and of 0.7 μM versus 3 μM of SET-M33 against *K. pneumoniae* FI-20. In addition SET-M33D-Leu/Ile resulted also more efficient against *E.coli W03BG0025,* compared to SET-M33D, with lower MIC values (0.3 vs 1.5 μM) and SET-M33-PEG4 more efficient than SET-M33 against Enterobacter cloacae W03AN0041 (0.3 vs 1.5 μM). No obvious correlation of the MICs with the different resistance phenotypes and resistance mechanisms could be observed except for MICs of those species that are naturally resistant to colistin (e.g *Proteus mirabilis, Serratia marcescens, Bulkholderia cepacia*), that were in general higher than those observed for colistin-susceptible strains.

The SET-M33 analogues were less active against Gram-positive strains showing MIC values higher than those observed for Gram-negatives, mostly in the range 1.5-12 μM (Table 7b) with relatively lower MIC values (range 0.15-0.3 μM) observed for *S. saprophyticus* strains than SET-M33 (1.5 μM). SET-M33D-Leu/Ile peptide resulted the more efficient against gram-positive bacteria, compared to the other analogues.

Among the tested peptides, SET-M33D-Leu/Ile was apparently the most active against Gram-negative and Gram-positive bacteria and SET-M33-DIM was the less active, according to the highest MIC values obtained in these experiments.

a

Strain	Strain Features	SET-M33D-L-Ile	SET-M33D-Leu/Ile	SET-M33-Gly/Ala	SET-M33-PEG4	SET-M33-DIM	SET-M33	SET-M33D
		µM	µM	µM	µM	µM	µM	µM
Pseudomonas aeruginosa ATCC 27853	Reference strain, wild type	0,7	0,7	0,7	0,7	11	1,5	0,7
Pseudomonas aeruginosa PAO-1	Reference strain, wild type	0,7	0,7	0,7	0,7	11	1,5	0,3
Pseudomonas aeruginosa VR-143/97	FQr AGr ESCr NEMr (MBL/VIM-1)	0,7	0,7	1,5	1,5	>22	1,5	1,5
Pseudomonas aeruginosa CEFTO49	FQr AGr ESCr NEMr (CARB/GES-5)	0,7	0,7	1,5	1,5	>22		
Klebsiella pneumoniae ATCC 13833	Reference strain, wild type	1,5	0,7	0,7	0,7	11	1,5	1,5
Klebsiella pneumoniae 7086042	FQr AGr ESCr NEMr (MBL/VIM-1)	1,5	0,7	1,5	0,7	3	3	3
Klebsiella pneumoniae FIPP-1	FQr AGr ESCr NEMr (CARB/KPC-3)	6	1,5	1,5	1,5	22	3	1,5
Klebsiella pneumoniae FI-47	FQr, AGr, ESCr, NEMr, COLr (CARB/KPC)	>12	1,5	3	1,5	>22	3	
Klebsiella pneumoniae FI-20	FQr, AGr, ESCr, NEMr, COLr (CARB/KPC, mcr 1.2)	12	1,5	1,5	0,7	22	3	6
Escherichia coli ATCC 25922	Reference strain, wild type	1,5	1,5	1,5	0,7	5,5	1,5	0,7
Escherichia coli W03BG0025	FQr AGr ESCr (ESBL/CTX-M-15)	0,7	0,3	1,5	0,3	5,5	0,7	1,5
Proteus mirabilis W03VA1017	FQr ESCr (AmpC/CMY-16)	>12	>12	>12	>12	>22	>24	>12
Enterobacter aerogenes W03BG0067	AGr ESCr (ESBL/SHV-5)	1,5	1,5	0,7	0,3	11	1,5	
Enterobacter cloacae W03AN0041	ESCr (ESBL/SHV-12)	1,5	1,5	0,7	0,3	5,5	1,5	1,5
Acinetobacter baumannii RUH 134	Reference strain, European clone II	1,5	1,5	1,5	0,7	3	1,5	1,5
Acinetobacter baumannii N50-ColR	NEMr COLr (OXA/OXA-24)	1,5	0,7	0,7	0,7	22	3	
Burkholderia cepacia FI-65	none	>12	>12	>12	>12	>22		
Serratia marcescens W03BG0003	FQr AGr ESCr (ESBL/SHV-12)	>12	>12	>12	>12	>22	>24	

b

Strain	Strain Features	SET-M33D-L-Ile	SET-M33D-Leu/Ile	SET-M33-Gly/Ala	SET-M33-PEG4	SET-M33-DIM	SET-M33	SET-M33D
		µM	µM	µM	µM	µM	µM	µM
Streptococcus pneumoniae ATCC 49619	Reference strain, wild type	>12	>12	>12	>12	>22	12	3
Streptococcus pneumoniae FI-61	none	>12	>12	>12	>12	>22		
Streptococcus agalactiae ATCC 13813	Reference strain, wild type	12	>12	6	6	>22	1,5	0,7
Staphylococcus aureus ATCC 29213	Reference strain, PENr	12	0,3	3	6	>22	6	0,3
Staphylococcus aureus 3851	MR, VANi	12	0,7	6	12	>22	6	0,3
Staphylococcus aureus FI-9LNZ	LNZr	1,5	<=0,15	0,3	0,7	5,5		
Staphylococcus epidermidis ATCC 14990	Reference strain, wild type	1,5	0,3	1,5	1,5	11	0,7	0,15
Staphylococcus epidermidis FI-62	none	0,7	0,3	0,3	0,7	5,5		
Staphylococcus epidermidis 6154	MR	1,5	0,3	0,7	1,5	5,5	1,5	0,15
Staphylococcus capitis ATCC 27840	Reference strain, wild type	0,3	<=0,15	<=0,15	<=0,15	0,7	0,3	0,15
Staphylococcus saprophyticus FI-1	none	0,3	<=0,15	0,3	0,3	<=0,3	1,5	0,7
Straphylococcus saprophyticus FI-2	none	0,3	<=0,15	<=0,15	0,3	<=0,3	1,5	1,5
Enterococcus faecalis ATCC 29212	Reference strain, wild type	>12	1,5	3	3	>22	3	0,3
Enterococcus faecalis FI-4	FQr, GLYr	>12	0,7	3	3	22	3	1,5
Enterococcus faecium FI-63	none	1,5	0,7	3	3	>22		
Enterococcus faecium FI-64	none	3	0,3	1,5	1,5	11		

Table 7. MIC values of SET-M33 analogues on a collection of major clinical Gram-negative (**a**) and Gram-positive (**b**) strains compared to SET-M33 and SET-M33D. Tested strains included either reference strains (indicated) or clinical isolates mostly with an MDR phenotype. Relevant resistance traits and resistance mechanisms are indicated. FQr, resistant to fluoroquinolones; AGr, resistant to aminoglycosides (gentamicin, amikacin and/or tobramycin); ESCr, resistant to expanded-spectrum cephalosporins; NEMr, resistance to carbapenems (imipenem and/or meropenem); COLr, resistance to colistin; ESBL, extended spectrum-lactamase; MBL, metallo-ß-lactamase; CARB, class A carbapenemase; AmpC, class C ß-lactamase; OXA, oxacillinase; PENr, resistant to penicillin; MR, methicillin-resistant; VANi, vancomycin-intermediate; GLYr, resistant to glycopetides; LNZr, resistant to linezolid.

Stability studies of SET-M33 analogues

Stability studies of pharmaceutical products may be expressed as the time during which the pharmaceutical products retain their physical, chemical, microbiological, pharmacokinetic properties and characteristics throughout the shelf life, defined as the reduction of the compound to 90% of its original concentration, from the time of manufacture [166]. The shelf-life prediction has an important role for the pharmaceutical product development of all the dosage forms and, also, it is utilized to determine the particular storage conditions. Thus, stability studies of pharmaceutical products are considered as pre-requisite for the acceptance and approval of any pharmaceutical products.

Therefore, a stability study of the SET-M33 analogues, stored at -20 and 25 °C in lyophilized form, was evaluated by means of MIC assays by analytical HPLC profile, observing area (%), defined as the area under the peak corresponding to the respective peptide obtained by the normalization of all areas in the chromatogram including those associated to impurities, and by MS profile. The experiments of stability were carried out at the following times: after synthesis (**T_0**) (peptides not stored at any temperature), 1 week (**T_1**), 2 weeks (**T_2**),1 month (**T_3**), 2 months (**T_4**), 4 months (**T_5**), and 6 months (**T_6**). The antimicrobial activity of the SET-M33 analogues was tested against the Gram-negative *E. coli TG-1* strain and compared to that of traditional SET-M33 peptide. The antimicrobial activity of each peptide, at the tested times, expressed as MIC values, is reported in Tables 8 and 9.

-20 °C	MIC (μM) vs *E.coli TG-1*						
Peptide	**T_0**	**T_1**	**T_2**	**T_3**	**T_4**	**T_5**	**T_6**
SET-M33D-L-Ile	0,7	0,7	0,7	0,7	0,7	0,7	0,7
SET-M33D-Leu/Ile	0,7	1,5	1,5	1,5	1,5	1,5	1,5
SET-M33-Gly/Ala	1,5	0,7	0,7	0,7	0,7	0,7	0,7
SET-M33-PEG4	0,7	0,7	0,7	0,7	0,7	1,5	1,5
SET-M33-DIM	1,5	1,5	1,5	3	1,5	3	3
SET-M33	0,7	0,7	0,7	0,7	0,7	0,7	1,5

Table 8. MIC of SET-M33 analogues against *E. coli TG-1* at -20 °C from T_0 to T_6.

25 °C	MIC (μM) vs *E.coli TG-1*						
Peptide	**T_0**	**T_1**	**T_2**	**T_3**	**T_4**	**T_5**	**T_6**
SET-M33D-L-Ile	0,7	0,7	0,7	0,7	0,7	0,7	0,7
SET-M33D-Leu/Ile	1,5	0,7	1,5	0,7	3	3	3
SET-M33-Gly/Ala	1,5	0,7	1,5	0,7	1,5	0,7	0,7
SET-M33-PEG4	0,7	0,7	1,5	0,7	1,5	1,5	1,5
SET-M33-DIM	1,5	1,5	1,5	1,5	3	3	3
SET-M33	1,5	1,5	1,5	1,5	1,5	1,5	1,5

Table 9. MIC of SET-M33 analogues against *E. coli TG-1* at 25 °C from T_0 to T_6.

Stability of SET-M33D-L-Ile

The peptide SET-M33D-L-Ile, stored at -20 °C, was stable during the time as revealed by HPLC profiles that showed a single pure peak of the peptide that retained an area (%) of 99% up to 6 months (Figures 38a-b). The HPLC profile of the peptide stored at 25 °C revealed small peaks only at 6 months (T_6) (Figure 38d) reporting an area (%) of SET-M33D-L-Ile's peak of 90%. The MS profiles at T_6 of the peptide stored at -20 °C and 25 °C showed both the peak of molecular mass of 4682.1 Da, associated to the peptide, and some small peaks of unidentified impurities (Figure 38 c, e).
The antimicrobial activity did not result altered, in both temperatures, as shown in Tables 8 and 9.

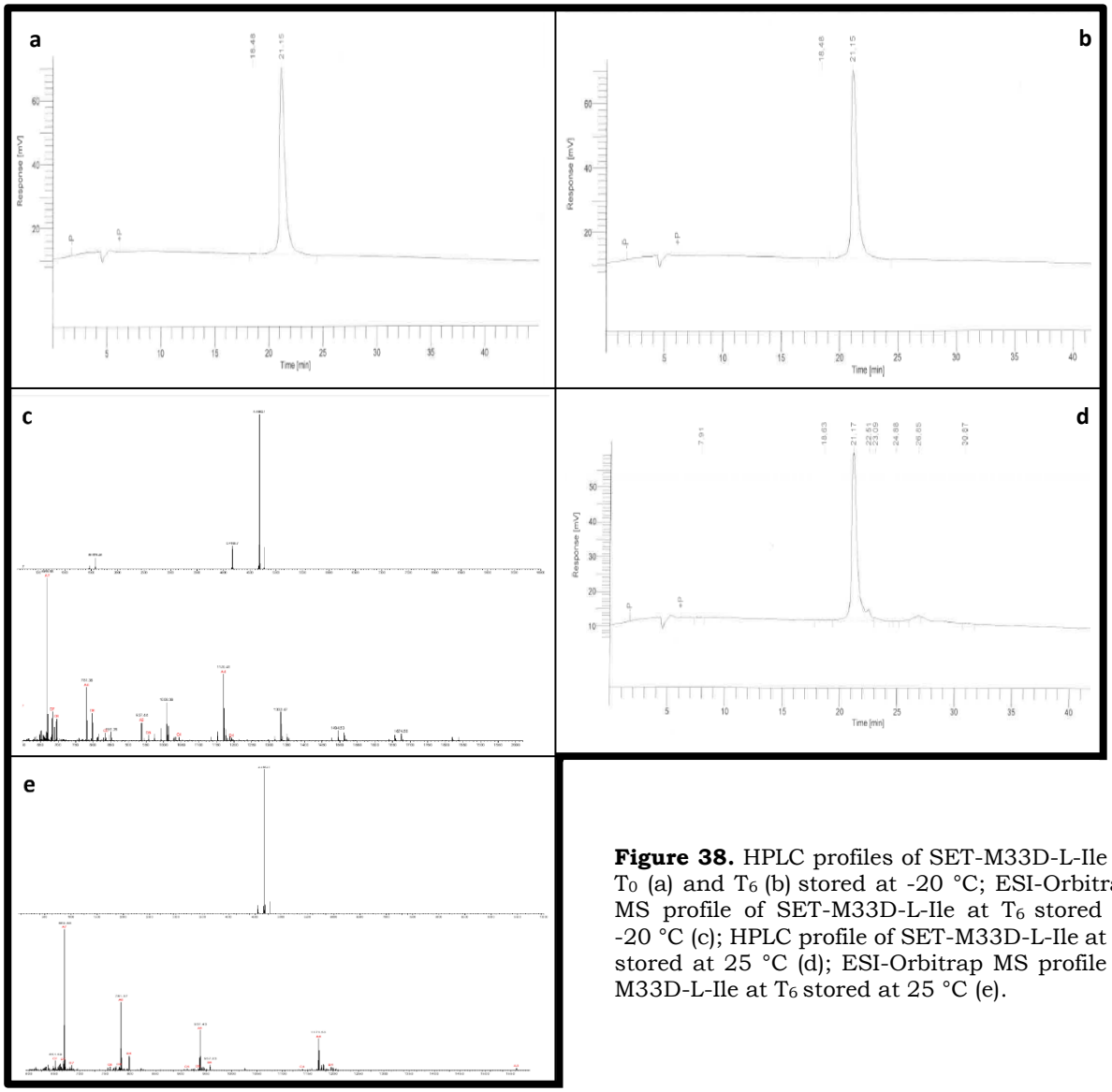

Figure 38. HPLC profiles of SET-M33D-L-Ile at T_0 (a) and T_6 (b) stored at -20 °C; ESI-Orbitrap MS profile of SET-M33D-L-Ile at T_6 stored at -20 °C (c); HPLC profile of SET-M33D-L-Ile at T_6 stored at 25 °C (d); ESI-Orbitrap MS profile of M33D-L-Ile at T_6 stored at 25 °C (e).

Stability of SET-M33D-Leu/Ile

The peptide SET-M33D-Leu/Ile stored at -20 °C was stable over time as revealed by HPLC profile that showed a single pure peak of the peptide with an area (%) of 98% up to 6 months (Figures 39a-b); the antimicrobial activity did not result altered toward T_6. The results for the peptide stored at 25 °C showed HPLC profile with small peaks already at 1 month (not shown) and more evident at 6 months reporting an area (%) of SET-M33D-Leu/Ile's peak of 75% respect to 98% at T_0, suggesting a possible degradation of the peptide upon the time (Figure 39d). This tendency was in accordance with the propensity of the peptide to loss antimicrobial activity during the time (Table 9). The MS profile at T_6 of the peptide stored at the defined temperatures showed both the peak at molecular mass of 4682.2 Da, associated to the peptide, and some small peaks of unidentified impurities (Figures 39 c, e).

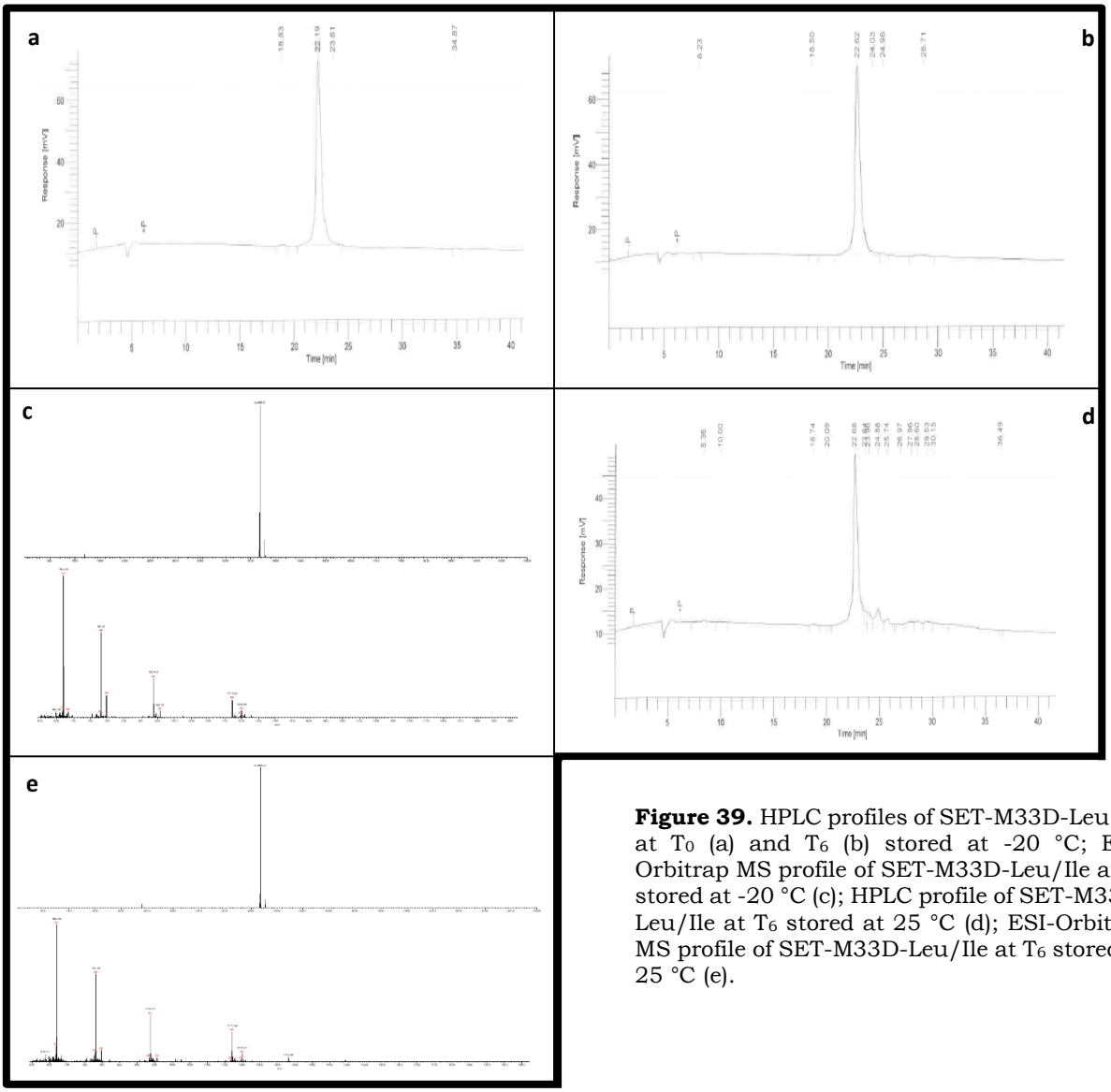

Figure 39. HPLC profiles of SET-M33D-Leu/Ile at T_0 (a) and T_6 (b) stored at -20 °C; ESI-Orbitrap MS profile of SET-M33D-Leu/Ile at T_6 stored at -20 °C (c); HPLC profile of SET-M33D-Leu/Ile at T_6 stored at 25 °C (d); ESI-Orbitrap MS profile of SET-M33D-Leu/Ile at T_6 stored at 25 °C (e).

Stability of SET-M33-Gly/Ala

The peptide SET-M33-Gly/Ala, stored at -20° C, was stable during the time as revealed by HPLC profiles showing a clear single pure peak of the peptide with an area (%) of 96% up to 6 months (Figures 40a-b), accordingly to the MIC assay results. The peptide stored at 25 °C evidenced small peaks in its HPLC profile already at 2 weeks (not shown) and more marked at 6 months decreasing the area (%) of its peak of 74% respect to 96% at T_0 (Figure 40d). This tendency did not show significant difference of the antimicrobial activity of the peptide (Table 9). The MS profiles at T_6 of the peptide stored at the two temperatures showed both the peak at molecular mass of 4626.1 Da, associated to the peptide, and some small peaks of unidentified impurities (Figures 40 c, e).

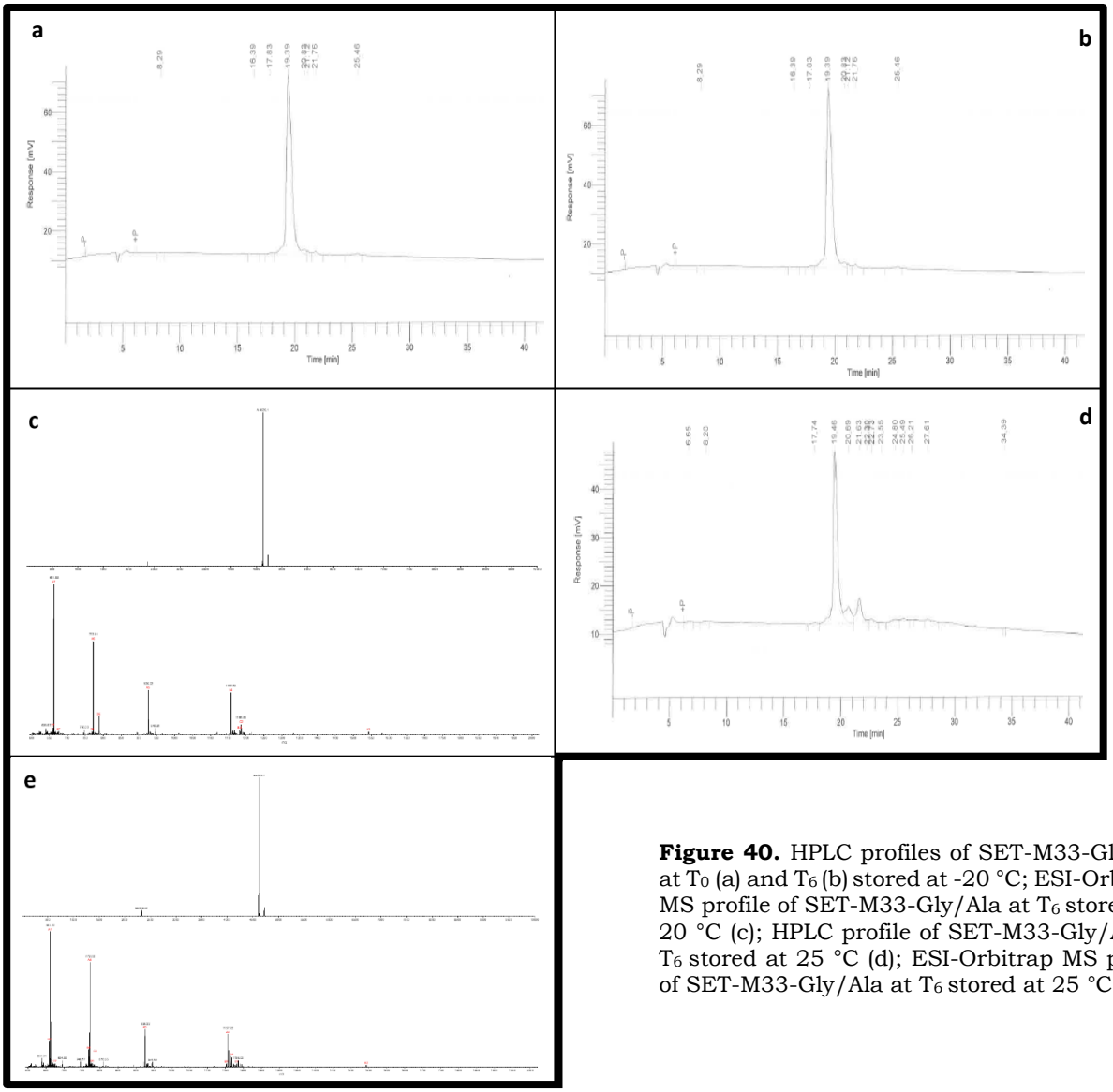

Figure 40. HPLC profiles of SET-M33-Gly/Ala at T_0 (a) and T_6 (b) stored at -20 °C; ESI-Orbitrap MS profile of SET-M33-Gly/Ala at T_6 stored at -20 °C (c); HPLC profile of SET-M33-Gly/Ala at T_6 stored at 25 °C (d); ESI-Orbitrap MS profile of SET-M33-Gly/Ala at T_6 stored at 25 °C (e).

Stability of SET-M33-PEG4

SET-M33-PEG4 peptide, stored at -20 °C, was stable during the time as revealed by HPLC profile that showed a single pure peak of the peptide with an area (%) of 95% up to 6 months (Figures 41a-b). The antimicrobial activity was slightly influenced as revealed by MIC results obtained towards T_6 from 0.7 to 1.5 μM (Table 8). The storage of the peptide at 25 °C determined small peaks in its HPLC profile at 2 months (not shown) becoming more prominent at 6 months and leading the area (%) of SET-M33-PEG4's peak to 71% respect to 95% at T_0 (Figure 41d). This tendency suggested a possible degradation of the peptide stored at 25 °C. These results were in accordance with a slight increase of obtained MIC values (Table 9). The MS profiles at T_6 of the peptide stored at the respective temperatures showed both the peak of molecular mass of 4857.3 Da, associated to the peptide, and some small peaks of unidentified impurities. (Figures 41 c, e).

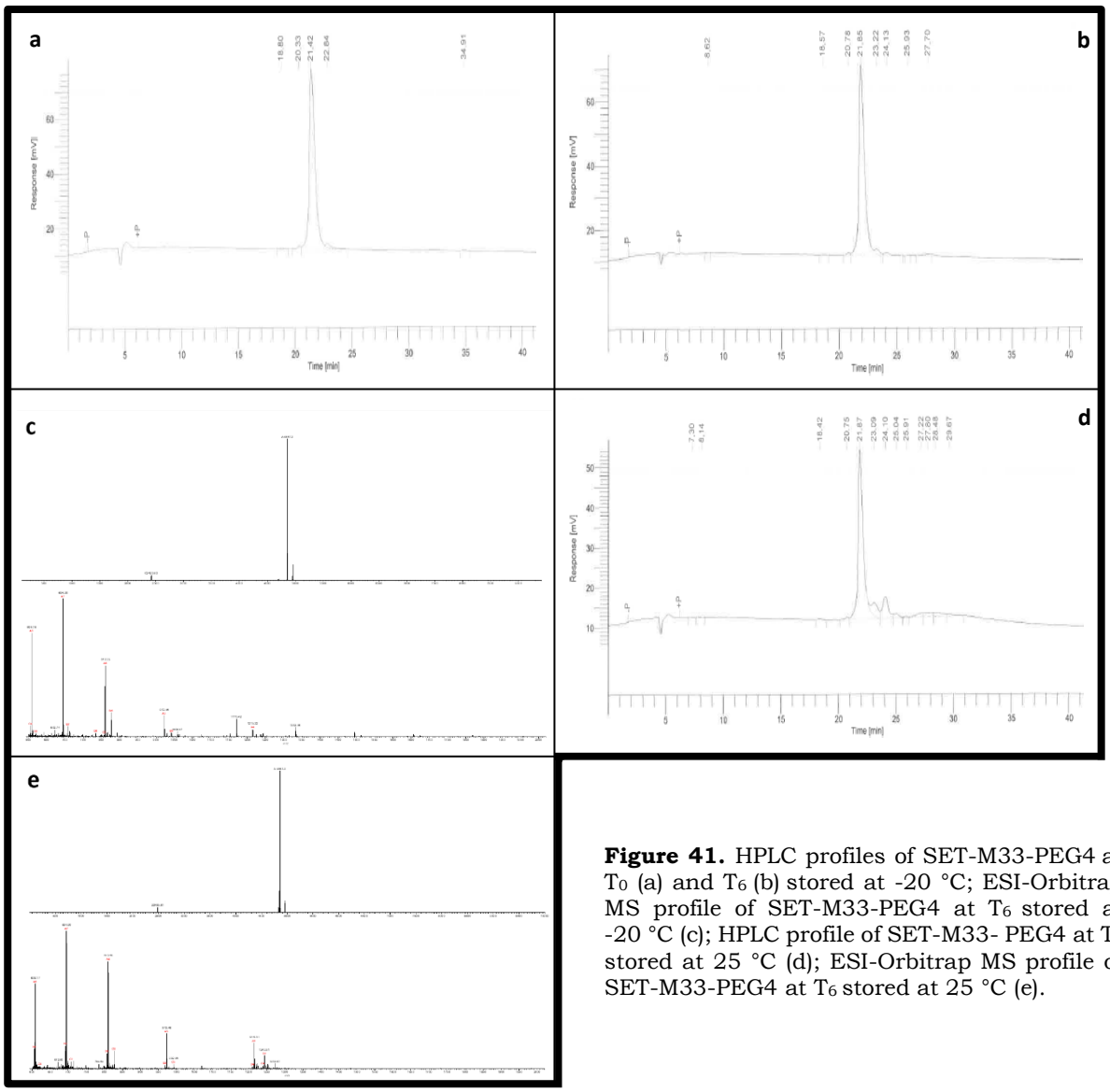

Figure 41. HPLC profiles of SET-M33-PEG4 at T_0 (a) and T_6 (b) stored at -20 °C; ESI-Orbitrap MS profile of SET-M33-PEG4 at T_6 stored at -20 °C (c); HPLC profile of SET-M33- PEG4 at T_6 stored at 25 °C (d); ESI-Orbitrap MS profile of SET-M33-PEG4 at T_6 stored at 25 °C (e).

Stability of SET-M33-DIM

The peptide SET-M33-DIM, stored at -20 °C, was stable during the time as revealed by HPLC profile that showed a clear pure peak of the peptide with an area (%) of 97% up to 6 months (Figures 42a-b); The HPLC profile of the peptide stored at 25 °C showed two small peaks at 2 months (not shown) due a possible poor fragmentation of the peptide; these peaks were more evident at 6 months revealing an area (%) of SET-M33-DIM's peak of 72% respect to 97% at T_0 (Figure 42d). The obtained MIC values, in both temperatures, ranged between 1.5 µM and 3 µM (Tables 8-9). The MS profiles at T_6 of the peptide stored at the defined temperatures, showed both the peak at molecular mass of 2320.55 Da, associated to the peptide, and some small peaks of unidentified impurities (Figures 42 c, e).

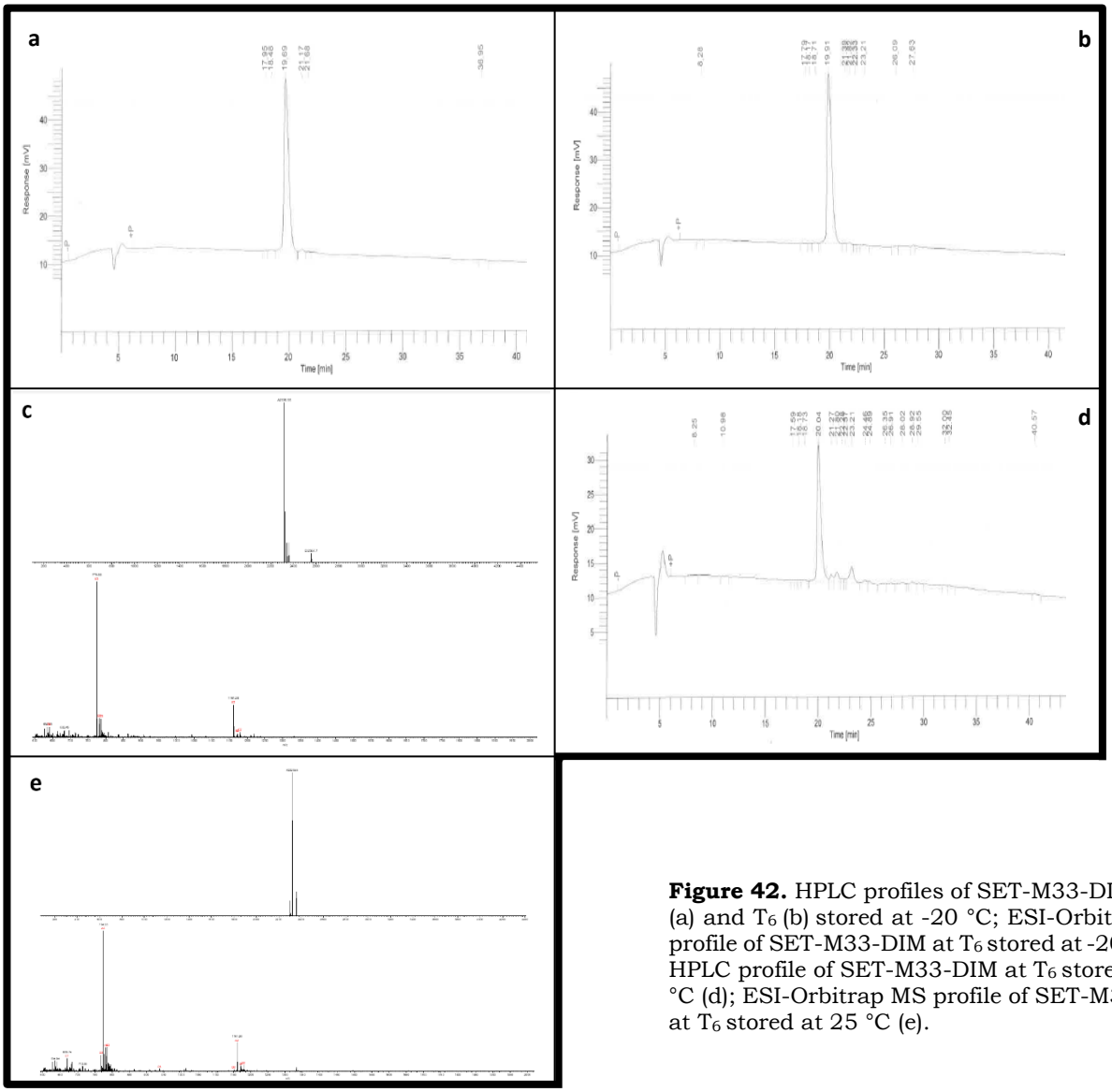

Figure 42. HPLC profiles of SET-M33-DIM at T_0 (a) and T_6 (b) stored at -20 °C; ESI-Orbitrap MS profile of SET-M33-DIM at T_6 stored at -20 °C (c); HPLC profile of SET-M33-DIM at T_6 stored at 25 °C (d); ESI-Orbitrap MS profile of SET-M33-DIM at T_6 stored at 25 °C (e).

The areas (%) of the SET-M33 analogues, obtained at the defined storage temperatures, were reported as a function of the time. SET-M33 analogues appeared more stable when stored at -20 °C than 25 °C as revealed by the higher areas (%) than those reported at 25 °C (Figures 43-44).

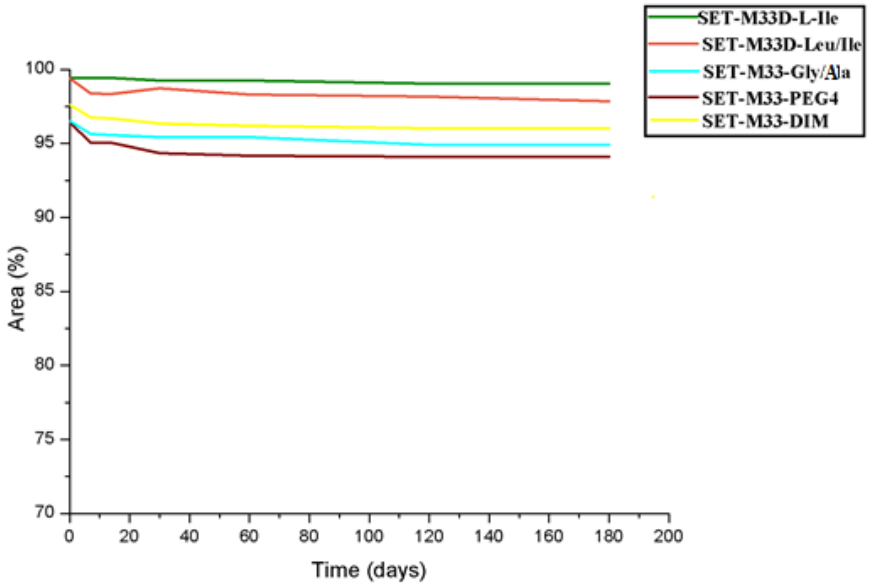

Figure 43. Stability of the SET-M33 analogues at -20 °C expressed as area (%) as a function of the time.

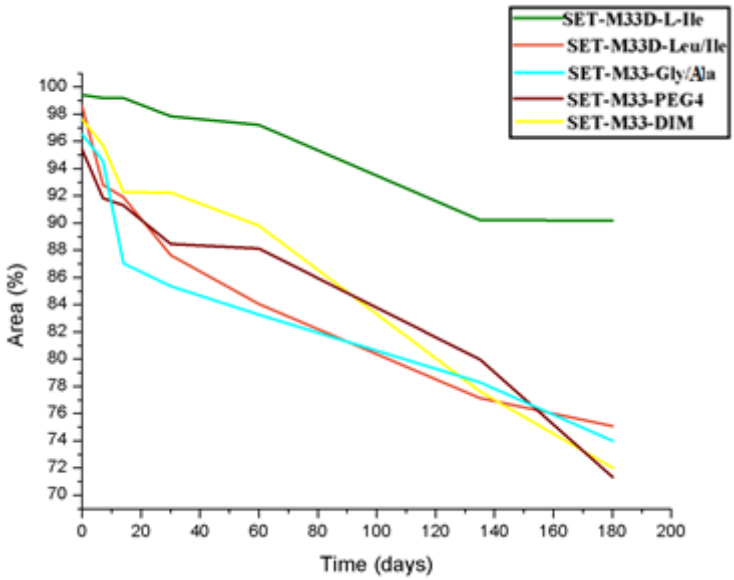

Figure 44. Stability of the SET-M33 analogues at 25 °C expressed as area (%) as a function of the time.

Further experiments must be performed in order to identify the small peaks, presumably associated to impurities in the MS profiles of the peptides at all tested times and at the defined temperatures.

MATERIAL AND METHODS

SET-M33 peptide synthesis

SET-M33 peptide was synthesized by solid phase synthesis in an automated Syro multiple peptide synthesizer (MultiSynTech, Witten, Germany), using standard 9-fluorenylmethyl-oxycarbonyl (Fmoc) strategy. The amino acid sequences were build up stepwise on TentaGel 4 branch β-Ala resin (loading 0.45 mmol/g) (Rapp Polymere, Tübingen, Germany) by successive cycles of Fmoc deprotection with piperidine 40%/dimethylformamide and coupling of the subsequent amino acids by activation of the respective carboxylic groups with *O*-(benzotriazol-1-yl)-*N*,*N*,*N*,*N*-tetramethyl-uronium hexafluorophosphate (HBTU)/1,3-isopropylethylamine (DIPEA). Amino acids were coupled in dimethylformamide (DMF), using the molar ratio of amino acids/HBTU/DIPEA on the resin of 5 eq/5 eq/10 eq., until completing the nine sequential additions KKIRVRLSA of the peptide. Side chain-protecting groups were 2,2,4,6,7-pentamethyldihydrobenzofuran-5-sulfonyl for R, t-butoxycarbonyl for K and t-butyl for S (Iris Biotech, Marktredwitz, Germany). The peptide was cleaved from the solid support, deprotected in a single step by treatment with TFA containing triisopropylsilane and water (95/2.5/2.5), and precipitated with diethyl ether. Crude peptide was purified by reversed-phase HPLC chromatography on a Waters XBridge® Peptide BEH C18 OBD Prep column (Waters, Milford, MA, USA, 300 Å, 10 µm, 19 × 250 mm), using 0.1% TFA/water as eluent A and acetonitrile as eluent B, performing a linear gradient from 83:17 A/B to 70:30 A/B in 40 min. The peptide was obtained as TFA salt. Final peptide purity was confirmed by reversed-phase chromatography on a Jupiter C18 analytical column (Phenomenex, Torrance, CA, USA, 300 Å, 5 µm, 4.6 × 250 mm), under the same conditions as for the HPLC purification. The identity of the peptide was checked by MALDI ToF/ToF mass spectrometry (Ultraflex III, Brucker Daltonics, Bremen, Germany).

The traditional ion exchange from TFA to acetate of the peptide was carried out using a quaternary ammonium resin in acetate form (AG1-X8, 100-200 mesh, 1.2 meq/mL capacity, BioRad, Hercules, CA, USA), with a resin: peptide ratio of 2000:1. Resin and peptide were stirred for 1 h, the resin was then filtered off and washed thoroughly.

TFA/chloride counter-ion exchange

SET-M33 TFA was dissolved in double distilled H_2O at a concentration of 2 mg/ml (3.4×10^{-4} M) and mixed 1:1 with an HCl solution to yield a final HCl concentration of 50 mM. The sample was freeze dried overnight and then weighted to evaluate no loss of product (<95% of the calculated yield). TFA/Chloride exchange was followed by quantitative ^{19}F-NMR and ^{1}H-NMR to determine the exact amount of counter-ion [167-168]. The NMR experiments were recorded at 298 K on an Avance III spectrometer (Bruker, Billerica, MA, USA) operating at 800 MHz (proton Larmor frequency) equipped with a 5 mm PHTXI ^{1}H-^{13}C/^{15}N probe, tuned to ^{19}F. SET-M33 TFA and SET-M33 chloride samples were prepared at the same concentration (1 mM) in 600 µL of D_2O; spectra were acquired with 512 scans, with receiver gain factor of 64 and a relaxation delay of 6.5 s.

NMR characterizations

A 500 MHz Inova spectrometer (Varian, Palo Alto, CA, USA) equipped with a 5 mm $^{1}H/^{13}C/^{15}N$ triple resonance probe was used for the NMR experiments. A ^{1}H 90° pulse length of 10.9 µs was determined. Suppression of the intense water signal in the performed 1D and 2D NMR experiments was achieved using pre-saturation or watergate pulse sequences. A relaxation delay of 57 *s* was applied for the acquired quantitative 1D ^{1}H experiments.

The following NMR spectra were recorded: 1D ^{1}H; 2D ^{1}H gradient-COSY (pulsed field gradient COSY acquired in magnitude mode, standard version in VNMRJ 2.3); 2D ^{1}H TOCSY (standard version in VNMRJ 2.3; mixing time = 80 ms); 2D ^{1}H NOESY (standard version in VNMRJ 2.3; mixing times: 100, 200 and 400 ms); 2D ^{1}H-^{13}C multiplicity-edited HSQC (standard version in VNMRJ 2.3); 2D ^{1}H-^{15}N HSQC [169].

All spectra were recorded at 298 K with 12.5 mg/mL SET-M33 dissolved in H_2O/D_2O 9:1 with 0.5 µL TFA-*d* (99.5%D; Cambridge Isotope Laboratories, Tewksbury, MA, USA) with 5 µL 10 mM DSS (4,4-dimethyl-4-silapentane-1-sulfonic acid, 97%, Cambridge Isotope Laboratories) in D_2O added as the internal chemical shift calibration standard. NMR data were processed and analyzed using MestReNova 12.0.1–20560 (Mestrelab Research SL, Santiago de Compostela, Spain).

MIC determination

Antimicrobial susceptibility was assessed by determining MICs of SET-M33 acetate and SET-M33 chloride against *E. coli* TG-1 and *P. aeruginosa* PAO-1 using the broth microdilution technique according to 2017 EUCAST guidelines. The MIC assay measures visible inhibition of bacterial growth after 24 h exposure of bacteria to antibiotic in Mueller-Hinton (MH) broth. Assays were performed in triplicate using a bacterial inoculum of 5 x 10^4 CFU/well in a final volume of 100 µL. The twofold antibiotic concentration ranged from 0.1 µM to 12 µM for both peptides. MICs were read after 24 h of incubation at 35 °C.

Cytotoxicity

T24 human epithelial bladder cells, 16HBE14o- human bronchial epithelial cells and RAW264.7 mouse macrophages were plated at a density of 2.5 x 10^4 cells/well in 96-well microplates. The 16HBE14o- cells were previously incubated with coating solution (88% LHC basal medium, 10% bovine serum albumin, 30 µg/ml bovine collagen type I and 1% human fibronectin). Different concentrations of SET-M33 TFA, acetate and chloride were added 24 h after plating. Cells were grown for 48 h at 37°C. Their viability was assessed by MTT assay. EC50 values were obtained by dose-response variable slope analysis using GraphPad Prism 5.03 software (San Diego, CA, USA).

Acute toxicity

All animal experiments were conducted under the protocol approved by the Italian Ministry of Health at the Toscana Life Sciences Foundation animal facility in Siena, Italy (authorization n. 34/2016PR). Animals (10 CD1 mice/group, 20–22 g) were injected i.v. with SET-M33 acetate (group 1 and group 2) and SET-M33 chloride (group 3 and group 4), in a single dose. The doses were: group 1,25 mg/kg SET-M33 acetate; group 2, 30 mg/kg SET-M33 acetate; group 3, 20 mg/kg SET-M33 chloride and group 4, 30 mg/kg SET-M33 chloride. Animals were monitored for 96 h. Signs of toxicity were checked four times a day by visual inspection and were evaluated as not-observable, mild and severe. Mice were weighed every day from arrival to the last day of the experiment. Animals with clear signs of distress, like reduced mobility and weight loss greater than 20%, were anesthetized and sacrificed with carbon dioxide or by cervical dislocation.

Synthesis of SET-M33D-L-Ile, SET-M33D-Leu/Ile, SET-M33-Gly/Ala, SET-M33-PEG4 and SET-M33-DIM

SET-M33 analogues were performed by solid phase synthesis (SPPS), carried out by an automated Syro multiple peptide synthesizer (MultiSynTech, Witten, Germany), using standard 9-fluorenylmethyloxycarbonyl (Fmoc) strategy. Two solid support resins were used for the synthesis of the peptides, TentaGel cMAP 4 branch β-Ala (RAPP POLIMERE loading 0.45 mmol/g) SET-M33D-L-Ile, SET-M33D-Leu/Ile and SET-M33-Gly/Ala, in contrast to TentaGel S RAM (Iris Biotech GmbH loading 0.22 mmol/g) for the synthesis of SET-M33-PEG4 and SET-M33-DIM. Fmoc-Lys(Fmoc)-OH was used to build the dimeric core unlike the tetrameric core that is included in the resin. For the synthesis of SET-M33-PEG4 was used Fmoc-NH-PEG4-COOH as first coupling step. The respective amino acid sequences, in L or D version, were build up stepwise on the corresponding solid support resin by successive cycles of Fmoc deprotection with Piperidine 40%/dimethylformamide (DMF) and coupling of the following amino acid by the activation of respective carboxylic group with O-(benzotriazol- 1-yl)-N,N,N,N-tetramethyluronium hexafluorophosphate (HBTU)/1,3-isopropylethylamine (DIPEA) until completing the respective peptides. In all synthesis, side chain-protecting groups were 2,2,4,6,7-pentamethyldihydrobenzofuran-5-sulfonyl for R, t-butoxycarbonyl for K and t-butyl for S. The resin and protected Fmoc-amino-acids were purchased from RAPP Polymere and Iris Biotech, respectively. Peptides were cleaved from the solid support and deprotected in one step by treatment with Trifluoroacetic acid (TFA), containing triisopropylsilane and water (95/2,5/2,5), and precipitated with diethyl ether. Crude peptides were purified by reversed-phase HPLC chromatography on a Waters XBridge® Peptide BEH C18 OBD Prep column (300 Å 10 µm 19 x 250 mm), using 0.1% TFA/water as eluent A and acetonitrile as eluent B; linear gradient from 83:17 A/B to 70:30 A/B in 40 min was performed for the purification of SET-M33D-L-Ile, SET-M33D-Leu/Ile, SET-M33-PEG4 and SET-M33-Gly/Ala, in contrast to the purification of SET-M33-DIM that required a linear gradient from 85:15 A/B to 70:30 A/B in 40 min. At the end of the purification the peptides were obtained as trifluoroacetate. The exchange from trifluoroacetate to acetate form was carried out using a quaternary ammonium resin in acetate form (AG1-X8, 100-200 mesh, 1.2 meq/ml capacity, Biorad); resin and tetra-branched peptides (2000:1 molar ratio) and dimeric peptide (1000:1 molar ratio) were stirred for 1 h, then the resin was filtered off and washed thoroughly. The peptides were recovered and freeze dried. Final peptides purity was analyzed by reversed-phase HPLC chromatography on a Phenomenex Jupiter C18 analytical column (300 Å, 5 µm, 4,6 x 250 mm), using the same conditions of the respective purifications, and the identity of the peptides was confirmed by mass spectrometry MALDI ToF/ToF (Ultraflex III, Brucker Daltonics, Bremen Germany).

MIC determination of SET-M33 analogues

MIC values of SET-M33 analogues were determined against a collection of clinical isolates of major Gram-negative and Gram-positive pathogens. Isolates were selected from characterized collections of clinical isolates available at the Clinical Microbiology Unit of Careggi University Hospital in Florence or were collected during routine diagnostic procedures at the Microbiology and Virology Unit. Isolates were selected according to their phenotype or genotype (e.g. multidrug-resistant phenotype or carriage of specific resistance traits, such as resistance to carbapenems due to carbapenemases production and colistin due to the novel mcr transferable gene). Overall, 34 representative isolates were tested, including 18 Gram-negatives and 16 Gram-positives. MICs were determined in duplicate using a standard microdilution assay according to the guidelines of the Clinical and Laboratory Standards Institute. Briefly, assays were performed in cation-supplemented MHB (Becton Dickinson, Franklin Lakes, NJ, USA) using a bacterial inoculum of 5x104 CFU/well prepared in a final volume of 100 µL. MIC values were recorded after incubation at 35°C for 18–20 h. Tested concentrations were in the range 1-64 µg/mL (0,15-12 µM) for all peptides except for SET-M33-DIM for which the range was 0,3-22 µM.

Stability studies of SET-M33 analogues

The stability or "shelf-life" of the SET-M33 analogues was assessed with their storage at two temperatures, -20 and 25 °C in lyophilized form exclusively. Peptides stability was evaluated by antimicrobial activity in terms of MIC assays and by HPLC and MS resulting profiles at the following times: after synthesis (**T_0**) (peptides not stored at any temperature), 1 week (**T_1**), 2 weeks (**T_2**),1 month (**T_3**), 2 months (**T_4**), 4 months (**T_5**), 6 months (**T_6**). 6 mg of peptides SET-M33D-L-Ile, SET-M33D-Leu/Ile, SET-M33-PEG4 and SET-M33-Gly/Ala and 3 mg of SET-M33-DIM, just synthetized and purified, were dissolved in H_2O at the concentration of 200 µM; the respective solutions were filtered with a 0.2 µm sterile filter and divided in 20 aliquots for each peptide containing 200 µL, reaching a total of 100 aliquots. The filtered remainder of these solutions was used to perform the first MIC assay at time **T_0**. All aliquots were lyophilized for two nights. Then, samples were divided in two groups: ten of each peptide were stored at -20 °C and the others ten were stored at room temperature (25 °C). The MIC assays, at the appropriate time, were carried out against Gram-negative *Escherichia coli TG-1* strain using the following standard broth microdilution protocol according to the guidelines of the Clinical and Laboratory Standards Institute. The MIC assays were performed in triplicate with MHB, using a final bacterial inoculum of 5 x 10^4 CFU/well in a final volume of 100 µL. The scalar concentrations of all peptides ranged from 0.03 µM to 25 µM for all experiments. The determination of the respective MICs was revealed by visual inspection after 18-20 h of incubation at 35 ˚C. 85 µL of each peptide solution, at the tested times, were analyzed by reversed-phase HPLC chromatography, using the same conditions for their respective purification,

and by MS. The MS experiments were performed by MALDI TOF/TOF mass spectrometry up to T_4 and by ESI-Orbitrap mass spectrometry from T_5 to T_6.

DISCUSSION

Antimicrobial resistance is currently evaluated one of the main threats to global public health by the World Health Organization (WHO) [1], particularly for the global spread of multidrug-resistant (MDR) bacterial pathogens causing increases in nosocomial infections and in hospital mortality [2-5]. Since their isolation and characterization in 1980, antimicrobial peptides (AMPs) has been evaluated one of the most important solutions to overcome the crisis of antimicrobial resistance thanks to their antimicrobial, immunomodulatory and anti-inflammatory combined properties [19-25, 94]. AMPs are described as a promising alternative to traditional antibiotics, powerful to address the increasing problem of antibiotic resistance and hold promise to be developed as novel antibiotics [16]. These peptides are produced naturally by all organisms ranging from bacteria to plants, vertebrates and invertebrates or they also can be designed and chemically synthetized in the laboratory. The major part of antimicrobial peptides is amphipathic due to the balance of cationic and hydrophobic residues in the peptide sequence. This characteristic leads AMPs to have an electrostatic attraction with the bacterial membranes allowed by the interaction of the positively charged residues of AMPs, like lysine and arginine, with the negative charges of LPS or LTA which are on the outer surface of Gram-negative and Gram-positive bacteria, respectively [67-68]. This interaction leads to membrane perturbation, provokes cell permeation and causes bacterial death [11,106]. However, despite their desirable characteristic, antimicrobial peptides show limited pharmaceutical development due to their toxicity, instability and manufacturing costs; only a few of them have actually been approved for clinical use [41]. Thus, researchers and industry have been seeking news AMPs of natural or synthetic origin with low toxicity and longer half-life necessary for drug development. The SET-M33 peptide, optimized version of an artificial peptide sequence isolated from a random phage library [147], is a cationic non-natural peptide synthetized and used in multiple antigen peptide (MAP) form, with four copies of the same peptide sequence (KKIRVRLSA) mounted on a three-lysine core. This tetra-branched form provides more resistance to degradation in biological fluids and makes the peptide more suitable for clinical applications than the linear analogue peptide [109, 149]. The SET-M33 peptide has a strong *in vitro* antimicrobial activity against a several Gram-negative MDR clinical isolates, including many cystic fibrosis isolates [145, 146], *in vitro* anti-inflammatory activity thanks to its capacity to neutralize LPS-induced cytokine release [155] and *in vivo* antimicrobial activity preventing septic shock in animals infected with bacteria of clinical interest [145, 146]; in addition this peptide showed low hemolytic activity, lack of immunogenicity and ability in eradicating biofilms [152, 153]. Its mechanism of action is based on multistep interference with bacterial membranes [153]. First it was attracted to the bacterial surface by the anionic LPS coating. Close to the lipid double layer it took on amphipathic helix structure and became partially embedded in the bacterial plasma membrane, causing loss of membrane function [153].

Therefore, SET-M33 peptide is identified as a promising candidate for the treatment of multi-drug resistant bacteria, becoming a new possible antibacterial drug. SET-M33 peptide is currently in the late stage of preclinical characterization prior to clinical trials.

The aim of this PhD thesis was to improve biopharmaceutical development and manufacturing procedures of the peptide SET-M33.

First, the secondary structure of the peptide was investigated by NMR to predict potential aggregation in solution which can affect drug product design and formulation strategy. NMR studies of multiple branched peptides are extremely uncommon because their spectra are complex due to non-equivalent branches carrying the same amino acid sequence. The secondary structure of branched peptides in solution is therefore deducted from analogue linear peptides or studied using circular dichroism techniques [153]. The branched core, forcing the oligomers into parallel distribution, may induce a β-sheet secondary structure, that in turn could generate unwanted aggregation. Previous CD studies on SET-M33 and on a monomeric analogue, showed that helix formation is only observed in the presence of micelle-like structures [153]. It was therefore important to determine the secondary structure of SET-M33 in order to: 1) confirm the results obtained with a monomeric analogue [153], showing that a helix is only formed in the presence of micelles; 2) to investigate if a β-sheet forms in aqueous solution, so prepare a stable drug formulation. The result showed that no stable β-strand configuration of the peptide was revealed according with the chemical shift index method [160] nor supported by the NOESY data [158].

In developing a medicinal product, salt formulations are important. Most synthetic peptides are obtained using Fmoc–solid-phase procedures and are produced as TFA salts due to cleavage and purification conditions. TFA can be toxic for some eukaryotic cells and should therefore be removed from synthetic peptides [170-171]. TFA counter-ion is often removed using ion exchange resins by repeated addition of acetic acid alternating with freeze drying [163]. Preliminary studies, on the efficacy and toxicity of SET-M33 revealed that the acetate form of the peptide, SET-M33 acetate, was less toxic for human cells and animals than SET-M33 TFA [151]. Thus, at the end of the synthesis the peptide is normally converted into the acetate form using a quaternary ammonium salt resin. However, this counter-ion exchange required a rather lengthy procedure, involving some risk of lowering peptide yield or pKa of the peptide permitting, and high cost for industrial scaling [162]

Here it is described a simple procedure to prepare the chloride salt of a basic peptide in quantitative yield to remove the toxic TFA using a simple and economic procedure [158]. The complete exchange of TFA with chloride was confirmed by ^{19}F-NMR revealing an intensity of the fluorine signal, after the exchange, decreased by a factor of about 200 respect to that recorded before the exchange. The solubility of SET-M33 chloride improved seven-fold with respect to the acetate form [158].

The antimicrobial activity of SET-M33 chloride was assayed against two Gram-negative pathogens as *Escherichia coli TG-1* and *Pseudomonas aeruginosa PAO-1* and compared with that of the acetate form. The antimicrobial activity of SET-M33 chloride proved to be the same as that of the acetate, actually slightly better against *P. aeruginosa*, as shown by MIC results [158].

The toxicity of the peptide in chloride form was less than that of the TFA for mammalian cells and live mice. In mice, toxicity was similar to that of the acetate form, i.e., lower than the TFA [158].

In conclusion, the opportunity of using a chloride counter-ion is very convenient from a process development point of view since it allows to obtain a new salt form of the peptide using a simple and very cheap procedure. SET-M33 chloride retained and slightly improved the antimicrobial activity against Gram-negative bacteria and did not increase the toxicity in mammalian cells and in live mice. Besides, the unexpected large gain in solubility, almost seven times better than the acetate, could give the drug better pharmacokinetic features, making the new form of SET-M33 very promising.

To identify back-up molecules, new versions derived by modifications of SET-M33 sequence were assayed in order to obtain new molecules, with better performance in terms of pharmaceutical profile and manufacturing costs, without altering the positive residues of the peptide necessary for its antimicrobial activity. Thus, SET-M33 analogues like SET-M33D-L-Ile, SET-M33D-Leu/Ile, and SET-M33-Gly/Ala were synthetized and tested for their antimicrobial activity against many bacterial isolates. In addition, SET-M33-PEG4 and SET-M33-DIM for their very promising profile [145,157], were synthetized again and included in these analyses.
SET-M33D-L-Ile and SET-M33D-Leu/Ile peptides were synthesized in tetrameric form using amino-acids in D configuration and characterized by the replacement of D-Ile, the most expensive amino-acid in the sequence of SET-M33, with L-Ile and with D-Leu, respectively.
SET-M33-Gly/Ala peptide was synthetized in tetrameric form, using amino-acids in L configuration and characterized by the replacement of L-Ala with L-Gly; this replacement was attempted to eliminate the degradation site for bacterial proteases [152].
All SET-M33 analogues were successfully obtained by solid phase synthesis showing a high HPLC purity. The tetra-branched analogues retained the antimicrobial activity of the peptide SET-M33, traditionally synthetized in L configuration, and of SET-M33D, in D configuration. Moreover, SET-M33D-Leu/Ile resulted more efficient against *Klebsiella pneumoniae* strains than SET-M33 and SET-M33D peptides, as revealed by MIC results. The analogues showed a lower antimicrobial activity against Gram-positive bacteria than that observed for Gram-negatives with the exception of low MIC values showed for *S. saprophyticus* strains, compared to the traditional SET-M33 and SETM33D. Conversely SET-M33-DIM was characterized by the highest MIC values, against both Gram-negative and Gram-positive bacteria, probably due to less number of cationic amino-acids in the dimeric structure.
Among the tested peptides, SET-M33D-Leu/Ile was apparently the most active against both Gram-negative and Gram-positive bacteria.

In the early stages of the development of a pharmaceutical product a stability study, expressed as the time during which these products retain their physical, chemical, microbiological, pharmacokinetic properties and characteristics from the time of manufacture, is required for their approval and to determine their particular storage [166].
Therefore, an early stability study of all versions of SET-M33 was performed in order to evaluate their efficacy during the time and to determine their better storage conditions. This study was carried out, in particular, observing the respective antimicrobial activity against Gram-negative

E. coli TG-1 strain, in terms of MICs, the HPLC and the MS profiles, over a storage period of 6 months keeping the peptides stored at two temperatures, -20 and 25 °C, exclusively in lyophilizated form. The results demonstrated that peptides were more stable and slight more efficient when stored at -20 °C respect to 25 °C, as revealed by the HPLC profiles that showed a single pure peak with a higher area (%) up to 6 months, and slightly lower obtained MIC values. The storage of the peptides at 25 °C showed small HPLC peaks, suggesting a possible degradation during the time. SET-M33D-Leu/Ile, SET-M33-PEG4 and SET-M33-DIM peptides had the propensity to decrease their activity in MICs assays toward six months. This did not occur for SET-M33-Gly/Ala peptide that revealed small peaks in its HPLC profile already at two weeks without any activity modification. A special case occurred for SET-M33D-L-Ile stored at -20 °C that showed in its chromatogram a single pure peak with an area (%) higher than 98% up to six months showing, in both storage temperatures, a strong efficacy for all tested times, as revealed by the unchanged MIC of 0.7 μM.

In conclusion, all these results obtained on SET-M33 analogues are encouraging and deserve future elucidations. The opportunity of using SET-M33D-L-Ile and SET-M33D-Leu/Ile, in addition to their better resistance to bacterial proteases thanks to D-amino acids, will allow to decrease the costs in the synthesis process and SET-M33-Gly/Ala in L configuration, to eliminate the degradation site for bacterial proteases, without altering the strong original peptide antimicrobial activity.

Future *in vivo* experiments will be carried out to evaluate the toxicity of the three novel SET-M33 analogues. Moreover, it could be interesting to characterize the analogues synthetized in chloride form to enable, with a simpler procedure, a further reduction of costs in the synthesis process.

APPENDIX

During the last year of my PhD course I worked 8 months in the laboratories of Mechanistic Immunology of Professor Hao Wu at Boston Children's Hospital (BCH), affiliated with Harvard Medical School. The Wu Laboratory focuses on elucidating the molecular and cellular mechanisms that govern the assembly, regulation and therapeutic intervention of supramolecular complexes in innate immunity like inflammasomes. At BCH I learned and carried out different cloning strategies, expression systems, purifications and structural characterizations of various proteins of mammalian inflammasomes.

Inflammasomes

The innate immune system is the first line of host defense and the engagement of germline-encoded pattern-recognition receptors (PRRs) activates it in response to harmful stimuli, such as invading pathogens, dead cells, or environmental irritants [172]. PRRs recognize the presence of unique microbial components, called pathogen-associated molecular patterns (PAMPs) or damage-associated molecular patterns (DAMPs), which are generated by endogenous stress, and trigger downstream inflammatory pathways to eliminate microbial infection and repair damaged tissues. The major inflammatory pathway is the activation of several intracellular multimeric protein complexes, termed inflammasomes, that activate inflammatory caspase-1 [173]. In particular, an inflammasome is defined by its sensor protein (a PRR), which oligomerizes to form a pro-caspase-1 activating platform in response to DAMPs or PAMPs. Caspase-1 is activated via proximity-induced autocatalytic activation upon recruitment to an inflammasome. Active caspase-1 leads to the cleavage of cytokines pro-interleukin-1β (pro-IL-1β) and pro-IL-18 into their mature and biologically active forms [174-176]. IL-1β induces the expression of genes that control fever, pain threshold, vasodilatation, and hypotension, and its reception leads to an endothelial cell response that facilitates the infiltration of immune cells to infected or damaged tissues [177]. IL-18 is necessary for interferon-gamma (IFN-γ) production and it is a co-stimulatory cytokine that mediates adaptive immunity [177]. In addition, active caspase-1 also cleaves gasdermin D (GSDMD), which allows the N-terminal domain of GSDMD to form pores in the plasma membrane triggering a lytic, pro-inflammatory form of cell death, termed pyroptosis [178-181]. There are five members of PRRs that have been confirmed to form inflammasomes: the nucleotide-binding oligomerization domain (NBD), leucine-rich repeat (LRR)-containing proteins (NLR) family members NLRP1, NLRP3, and NLRC4, as well as absent-in-melanoma 2 (AIM2) and pyrin [182,183]. All members of the NLR family of proteins contain a central nucleotide-binding domain (NBD), and most also have a variable N-terminal domain and a C-terminal LRR domain [184]. Based on the presence of an N-terminal pyrin domain (PYD) or Caspase Activation Recruitment Domain (CARD), this family is further divided into NLRP or NLRC receptors. Upon pathogen detection, NLRs assemble and recruit caspase-1 via N-terminally located death domains: either directly through a CARD or indirectly through a PYD via the adaptor Apoptosis-associated Speck-like protein containing a CARD, termed ASC [185].

Human NLRP1 and CARD8 proteins

NLRP1 and CARD8 are related cytosolic sensors that upon activation form inflammasomes, resulting in caspase-1 activation, cytokine maturation and/or pyroptotic cell death [186]. Human NLRP1 contains both PYD and CARD domains, NBD domain also known as NACHT and LRR domain unlike human CARD8, considered a "minimized" NLRP1 ortholog, that has only the CARD domain [187] In contrast to most NLRs, one unusual feature of the NLRP1 and CARD8 CARD domains is their location at the C-terminus (Figure 45).

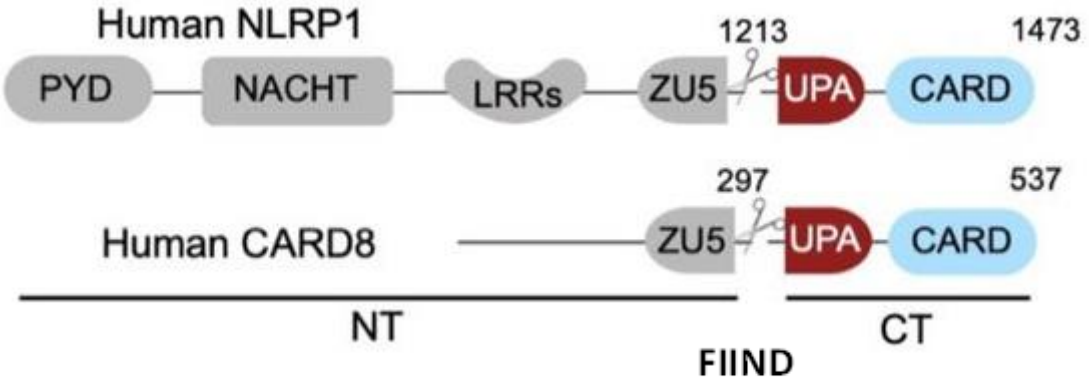

Figure 45. Domain architecture of human NLRP1 and CARD8 [186].

Distinct from all other NLRs, NLRP1 has a C-terminal CARD and an N-terminal PYD, which has been lost in some species, including mouse [187]. The other unusual feature of NLRP1 and CARD8 is FIIND (Function-to-find domain), which undergoes constitutive self-cleavage (henceforth referred to as auto-processing) resulting in two distinct polypeptides (ZU5 and UPA) that remain non-covalently associated with each other after auto-processing [187]. For reasons that have been unclear until recently, FIIND auto-processing is required for NLRP1 or CARD8 function [185]. NLRP1 and CARD8 use their C-terminal (CT) fragments containing a caspase recruitment domain (CARD) and the UPA subdomain of the FIIND for self-oligomerization and recruitment of the inflammasome adaptor ASC and/or caspase-1 [186]. CARD8 and NLRP1 undergo autoproteolytic cleavage at a conserved SF/S motif within the FIIND [187]. It was demonstrated that the substitution of Ser-1213 of NLRP1 or Ser-297 of CARD8 with alanine completely abrogated NLRP1 and CARD8 cleavage [187].

NLRP3

NLRP3 (NBD-, LRR- and pyrin domain-containing protein 3) is an intracellular sensor that detects a broad range of microbial motifs, endogenous danger signals and environmental irritants, resulting in the formation and activation of the NLRP3 inflammasome. It has an N-terminal pyrin domain, a

NACHT domain, which comprises an NBD, helical domain 1 (HD1), winged helix domain (WHD) and helical domain 2 (HD2), and a C-terminal LRR domain [188, 189]. The pyrin domain of NLRP3 interacts with the pyrin domain of ASC to initiate inflammasome assembly leading to caspase-1-dependent release of the pro-inflammatory cytokines IL-1β and IL-18, as well as to gasdermin D-mediated pyroptotic cell death (Figure 46) [190].

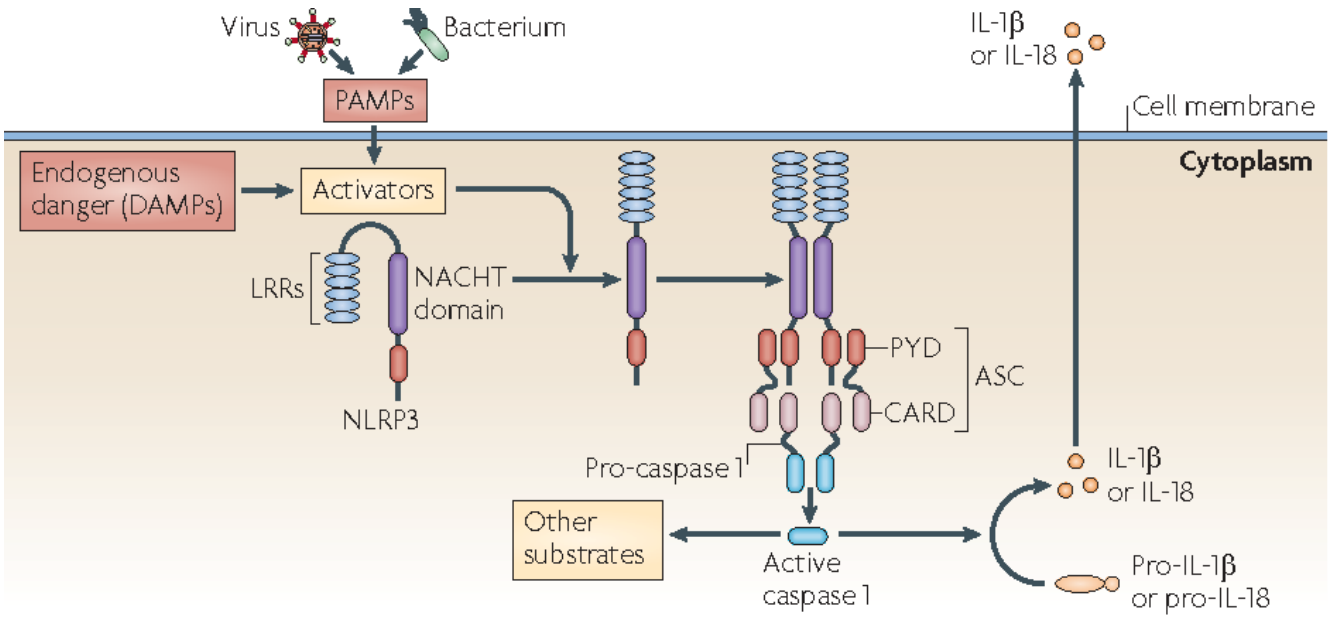

Figure 46. Mechanism of NLRP3 inflammasome complex formation [191].

NLRC3

NLRC3, a less studied member of the NLR family, is a negative regulator that reduces NF- kb activation [192], diminishes stimulator of interferon genes (STING) and TANK-binding kinase 1 (TBK1) activation of type I interferon (IFN-I) during infection [193]. NLRC3 has a C-terminal LRR domain, a central NACHT domain and a N-terminal CARD domain. It was demonstrated that NLRC3 binds viral DNA and other nucleic acids through its LRR domain [194]. DNA binding to NLRC3 increases its ATPase activity, and ATP-binding by NLRC3 diminishes its interaction with STING, thus licensing an IFN-I response (Figure 47) [194].

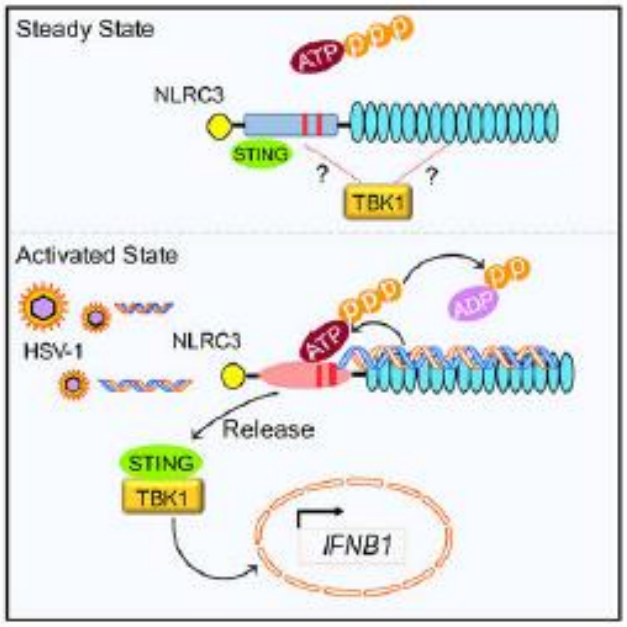

Figure 47. Binding of NLRC3 with viral DNA [194]

AIM2

AIM2 is a cytoplasmic sensor that recognizes dsDNA of microbial or host origin [195]. AIM2 is composed by C-terminal HIN-200 domain and N-terminal pyrin domain. AIM2 forms an inflammasome when the C-terminal HIN-200 domain binds double stranded DNA (either viral, bacterial, or even host) and acts as a cytosolic dsDNA sensor [196]. The N-terminal pyrin domain of AIM2 interacts with the pyrin domain of ASC; ASC also contains CARD domain that recruits procaspase-1 to the complex leading to the auto-activation of caspase-1 and the oligomerization of the AIM2 inflammasome complex (Figure 48) [197]. Previous structural studies revealed that mutants F27, L10 and L11 in the PYD domain were the major contributors of the interactions of AIM2 [198].

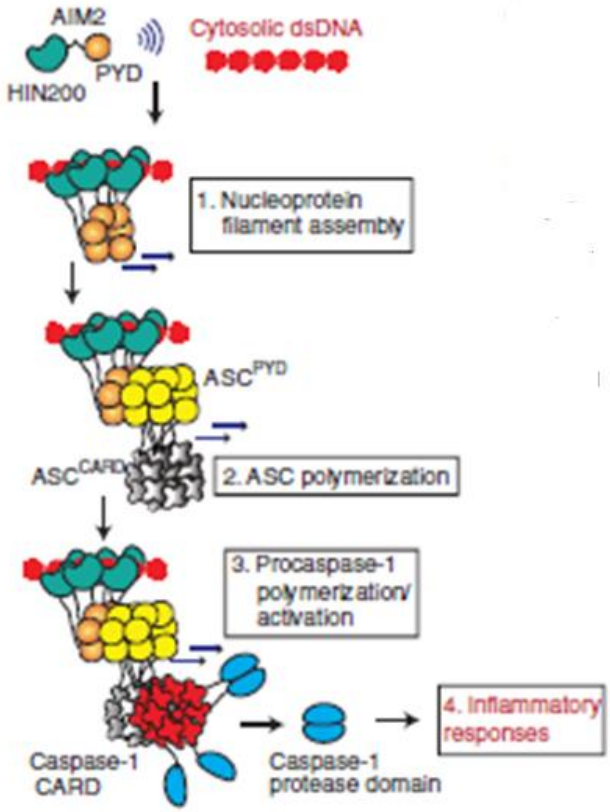

Figure 48. Mechanism for the assembly of the AIM2 inflammasome on foreign dsDNA [196].

Bac-to-Bac Baculovirus expression system

The Bac-to-Bac™ Baculovirus Expression System provides a rapid and highly effective method to generate recombinant baculoviruses based on site-specific transposition of an expression cassette into a baculovirus shuttle vector (bacmid) propagated in *E. coli* [199, 200]. The first major component of this System is a pFastBac™ vector into which the gene(s) of interest can be cloned. Depending on the selected pFastBac™ vector, expression of the gene(s) of interest is controlled by the Autographa californica multiple nuclear polyhedrosis virus (AcMNPV) polyhedrin (P_H) or p10 promoter for high-level expression in insect cells. This vector contains also left and right arms of Tn7, a gentamicin resistance gene and an SV40 polyadenylation signal to form a mini Tn7. The second major component of the System is the DH10Bac™ *E. coli* strain that is used as the host for the pFastBac™ vector. DH10Bac™ cells have a baculovirus shuttle vector (bacmid) containing a low-copy number mini-F replicon, the baculovirus genome, a kanamycin resistance marker and a segment of DNA encoding the LacZα peptide from a pUC-based cloning vector into which the attachment site for the bacterial transposon, Tn7 (mini-attTn7) has been inserted. The transposition is allowed by the helper plasmid that expresses the Tn7 transposase gene and confers resistance to tetracycline [201].

This technique is constituted by different steps, depicted in Figure 49. First, DH10Bac™ cells are transformed with the recombinant pFastBac™ vector and plated on LB agar with antibiotics, IPTG and Bluo-Gal. To identify the colony containing the recombinant plasmid is used the blue/white selection based on fact that the bacmid propagates in E. coli DH10Bac™ as a large plasmid that can complement a lacZα deletion present on the chromosome to form colonies that are blue (Lac+) in the presence of a chromogenic substrate and the inducer, IPTG. Insertions of the mini-Tn7 into the mini-attTn7 attachment site on the bacmid disrupt the expression of the LacZα peptide, so colonies containing the recombinant bacmid are white in a background of blue colonies carrying bacmid. Therefore, white colonies are picked and growth overnight in LB with antibiotics. Then the recombinant plasmid DNA is isolated and sequenced. Once DH10Bac™ cells are transformed with pFastBac™ expression plasmid transposition occurs between the mini-Tn7 element on the pFastBac™ vector and the mini-attTn7 target site on the bacmid to generate a recombinant bacmid. Then, the recombinant bacmid DNA is used for the transfection of insect cells, like Sf9 or Sf21. A cationic lipid formulation, Cellfectin® II Reagent is used for obtaining the highest transfection efficiencies and protein expression levels. P0, P1, P2 repeated phases of infection on insect cells are required in order to amplify the virus and to express the protein.

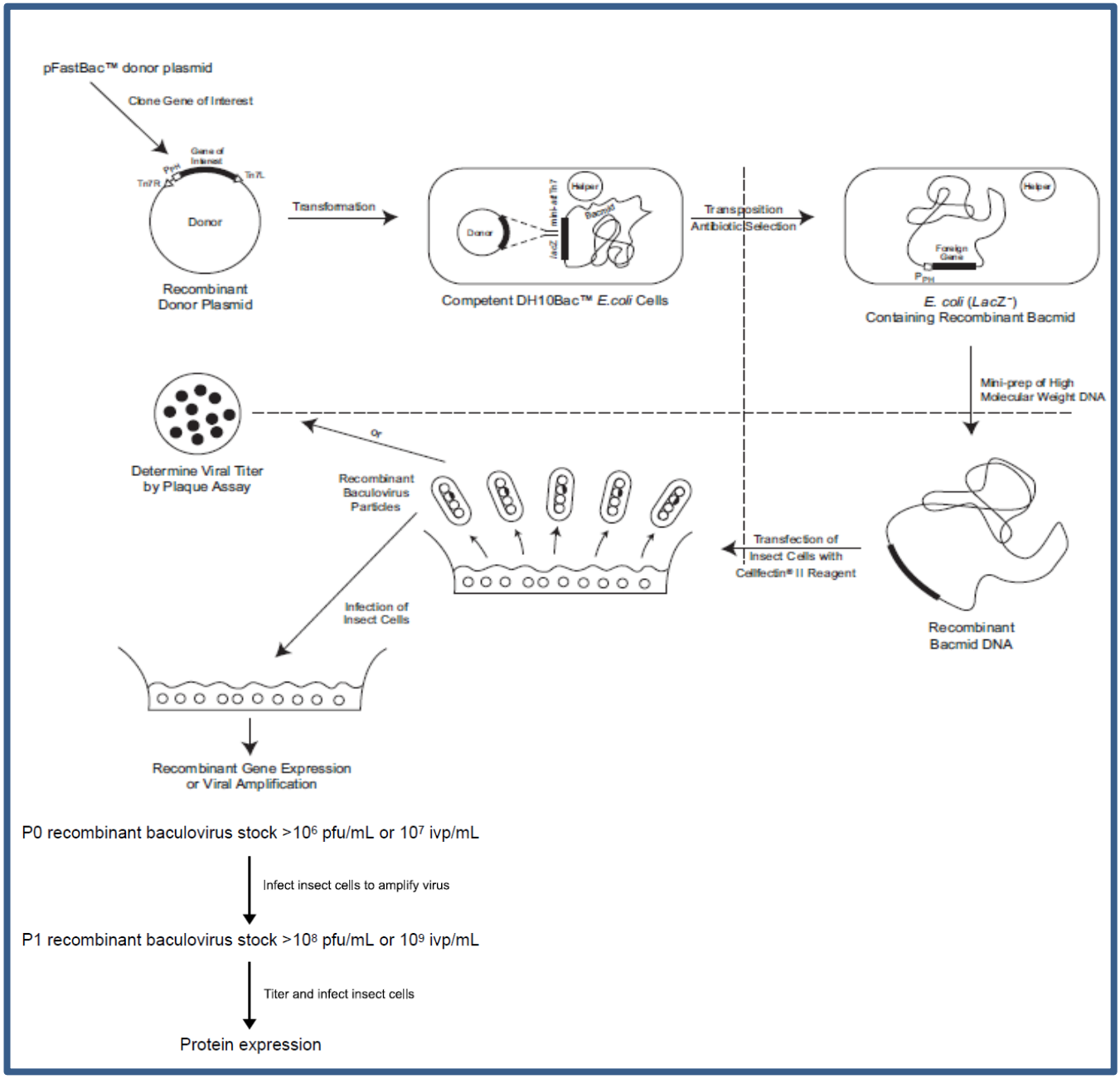

Figure 49. Generation of recombinant baculovirus and the expression of heterologous gene using the Bac-to-Bac™ Baculovirus Expression System.

I carried out cloning, transformation, baculovirus expression, purification and crystallization trials of the wild type full lenght NLRP3, wild type NLRP1 and CARD8 FIIND domains and, also, the mutated NLRP1 and CARD8 FIIND domains with the mutation S969A and S297A, respectively. I carried out transformation, bacterial expression and purification of three different constructs of AIM2 protein (full length, PYD domain and mutated L10A L11A PYD domain). I learned how to performing complexes between NLRC3 or AIM2 proteins and partners.

Cloning, expression and purification

The genes of all inflammasome proteins were synthesized by GENEWIZ.

All FIIND domains, wild type and mutants, and NLRP3 were generated by standard PCR-based cloning strategy or Gibson Assembly and cloned into a pFastBac-HTA vector with an N-terminal His-tag (FIIND domains) and MBP-tag (NLRP3). The mutations S969A and S297A were performed using Q5 polymerase (NEB) and Kinase Ligase DpnI (KLD) reaction. The identities of all plasmids were confirmed by Sanger sequencing. DH10Bac competent cells were transformed with the respective pFastBac-HTA plasmids to generate recombinant bacmid. Recombinant baculovirus expressing FIIND domains and NLRP3 was generated using the Bac-to-Bac system (Invitrogen). Sf9 insect cell culture and baculovirus infection were performed according to the manufacturer's protocols. In the last phase of baculovirus infection one liter of cells (2×10^6 cells mL^{-1} in HeyClone medium) was infected with 10 mL baculovirus at 28 ℃. After growth at 28 °C for 48 h, the cells were harvested by centrifugation (1200 rcf). All FIIND domains and NLRP3 full length were purified by affinity chromatography using Ni-NTA resin and amylose resin, respectively, as describe in the next parts.

Purification of NLRP1 and CARD8 wild type and mutated FIIND domain

The pellet was suspended in lysis buffer (50 mM Tris-HCl at pH 8, 150 mM NaCl, 1 mM TCEP, 20 mM Imidazole and SIGMAFAST protease inhibitor) and lysed by sonication (2 s on 6 s off, 4 min total on, 43% power, Branson). Then, the respective lysates were centrifuged at 40000 rpm at 4°C for 1 h. The clarified supernatant containing the respective protein was incubated with pre-equilibrated Ni-NTA resin (Qiagen) for 30 min at 4 °C. After incubation, the resin–supernatant mixture was poured into a gravity column and the resin was washed with lysis buffer. Proteins were eluted using lysis buffer supplemented with 500 mM imidazole and confirmed by SDS-PAGE analysis. The respective Ni-NTA eluate containing the proteins was concentrated until 600 µL (Amicon Ultra) and purified by size exclusion chromatography on a Superdex S200 Increase (10/300 GL) gel-filtration column (Cytiva) in 20 mM Tris-HCl at pH 8, 150 mM NaCl, 1 mM TCEP, to show their profile in terms of filament or monomer formation. The fractions of the gel filtration containing the protein were collected and incubated with TEV protease at 4 °C overnight in order to remove the His-Tag. Then proteins were concentrated until 600 µL (Amicon Ultra) and purified again by size exclusion chromatography, on a Superdex S200 Increase (10/300 GL) gel-filtration column (Cytiva) in the same buffer of the first size exclusion, to check the purest and monomeric fractions suitable for the crystallization. Therefore, fractions were concentrated around 10 mg/mL and used for making 500 different crystallization screens in order to obtain crystals.

Purification of NLRP3 full length

The pellet was suspended in lysis buffer (25 mM Tris-HCl pH 7.5, 150 mM NaCl, 1 mM TCEP, 50 µM ADP and SIGMAFAST protease inhibitor) and lysed by sonication (2 s on 6 s off, 4 min total on, 43% power, Branson). Cell lysate was then centrifuged at 40000 RPM at 4 °C for 1 h and the supernatant was incubated with pre-equilibrated amylose resin for 2 h at 4 °C. Bound resin was then washed by gravity flow with 50 column volume (CV) lysis buffer and eluted with 3 CV elution buffer (25 mM Tris-HCl pH 7.5, 150 mM NaCl, 1 mM TCEP, 50 mM maltose). Eluate from amylose resin was concentrated and purified on a Superdex S200 Increase (10/300 GL) gel-filtration column (Cytiva) in 20 mM Tris-HCl at pH 7.5, 150 mM NaCl, 1 mM TCEP and cleaved overnight with MBP-3C protease on ice. Then protein was concentrated until 600 µL (Amicon Ultra) and purified again by size exclusion chromatography, using the same column equilibrated with the same buffer of the first size exclusion, to check the purest and monomeric fractions suitable for the crystallization. Therefore, fractions were concentrated around 10 mg/mL and used for making 500 different crystallization screens in order to obtain crystals.

Expression and purification of AIM2 proteins

To generate AIM2 proteins, competent BL21(DE3) *E. coli* cells were transformed with expression plasmid pFS encoding the different constructs of AIM2 (full length, PYD and mutated L10A L11A PYD domain). Freshly transformed BL21(DE3) colonies were used to inoculate Terrific Broth media (TB) containing 100 mg/ml ampicillin (Amp). The cultures in TB were incubated at 37 °C with vigorous shaking and induced at $OD_{600\ nm}$ of ~ 0.8 by adding isopropyl 1-thio-β-D-galactopyranoside (IPTG) to a final concentration of 1 mM. The cultures were incubated at 18 °C o/n; the cells were harvested and the pellets were suspended in the buffer containing 50 mM Tris-HCl pH 8, 150 mM NaCl, 1mM TCEP, 20 mM Imidazole and SIGMAFAST protease inhibitor and lysed by sonication. Then, the respective lysates were centrifuged at 25000 rpm and the soluble fractions were incubated with nickel beads for 30 minutes at 4 °C; after the proteins were purified using affinity chromatography eluting with the lysis buffer supplemented with 250 mM of imidazole. The identity of proteins was confirmed by SDS-PAGE analysis. Therefore, proteins were checked and purified by gel filtration using Superdex S200 increase 10/300 GL. Finally, AIM2 proteins were used for interaction studies.

REFERENCES

1. WHO *Worldwide Country Situation Analysis: Response to Antimicrobial resistance;* Who Library Cataloguing-in-Publication Data; World Health Organization: Geneva, Switzerland, **2015**.
2. Gold, H.S.; Moellering, R.C. Antimicrobial-drug resistance. *N. Engl. J. Med.* **1996**, 335(19):1445–1453.
3. Willyard, C. The drug-resistant bacteria that pose the greatest health threats. *Nature* **2017**, 543(7643):15.
4. Alghoribi, M.F.; Gibreel, T.M.; Farnham, G.; Al Johani, S.M.; Balkhy, H.H.; Upton, M. Antibiotic-resistant ST38, ST131 and ST405 strains are the leading uropathogenic Escherichia coli clones in Riyadh, Saudi Arabia. *J. Antimicrob. Chemother*. **2015**, 70(10): 2757–2762.
5. Petty, N.K.; Zakour, B.N.L.; Stanton-Cook, M.; Skippington, E.; Totsika, M.; Forde, B.M.; Phan, M.D.; Gomes Moriel, D.; Peters, K.M.; Davies, M.; et al. Global dissemination of a multidrug resistant Escherichia coli clone. *Proc. Natl. Acad. Sci. USA* **2014**, 111(15):5694–5699.
6. Levin-Reisman, I.; Brauner, A.; Ronin, I.; Balaban, N.Q. Epistasis between antibiotic tolerance, persistence, and resistance mutations. *Proc. Natl. Acad. Sci. USA* **2019**, 116(29): 14734–14739.
7. Brauner, A.; Fridman, O.; Gefen, O.; Balaban, N.Q. Distinguishing between resistance, tolerance and persistence to antibiotic treatment. *Nat. Rev. Microbiol.* **2016**, 14(5): 320–330.
8. Rice, L.B. Federal funding for the study of antimicrobial resistance in nosocomial pathogens: No ESKAPE. *J. Infect. Dis.* **2008**, 197(8):1079–1081.
9. Bourlioux, P. Which alternatives are at our disposal in the anti-infectious therapeutics face to multi-drug resistant bacteria? *Ann. Pharm. Fr.* **2013**, 71(3): 150-158.
10. Schmidt, F.R. The challenge of multidrug resistance: actual strategies in the development of novel antibacterials. *Appl. Microbiol. Biotechol.* **2004**, 63(4): 335-343.
11. Mahlapuu, M.; Hakansson, J.; Ringstad, L.; Björn, C. Antimicrobial Peptides: An Emerging Category of Therapeutic Agents. *Front. Cell. and Infect. Microbiol.* **2016**, 6:194.
12. Steckbeck, J.D.; Deslouches, B.; Montelaro, R.C. Antimicrobial peptides: new drugs for bad bugs? *Expert Opin. Biol. Ther.* **2014**, 14(1):11-14.
13. Aminov, R.I. A brief history of the antibiotic era: lessons learned and challenges for the future. *Front. Microbiol.* **2010**, 1:134.
14. Hancock, R.E.; Haney, E.F.; Gill, E.E. The immunology of host defence peptides: beyond antimicrobial activity. *Nat. Rev. Immunol.* **2016**, 16(5):321-334.
15. Levy, S.B.; Marshall, B. Antibacterial resistance worldwide: causes, challenges and responses. *Nat. Med.* **2004**, 10(12Suppl.):S122–S129.
16. Hancock, R.E.W.; Sahl, H.-G. Antimicrobial and host-defense peptides as new anti-infective therapeutic strategies. *Nat. Biotechnol.* **2006**, 24(12):1551–1557.
17. Stanton, T.B. A call for antibiotic alternatives research. *Trends Microbiol.* **2013**, 21(3): 111-113.

18. Haney, E.F.; Straus, S.K.; Hancock, R.E.W. Reassessing the host defense peptide landscape. *Front. Chem.* **2019**, 7:43.
19. Hancock, R.E. Cationic peptides: effectors in innate immunity and novel antimicrobials. *Lancet. Infect. Dis.* **2001**, 1(3):156–164.
20. Zasloff, M. Antimicrobial peptides of multicellular organisms. *Nature* **2002**, 415(6870):389–395.
21. Straus, S.K.; Hancock, R.E.W. Mode of action of the new antibiotic for Gram-positive pathogens daptomycin: comparison with cationic antimicrobial peptides and lipopeptides. *Biochim. Biophys. Acta* **2006**, 1758(9):1215–1223.
22. Pan,Y-L.; Cheng, J.T-J.; Hale, J.; Pan, J.; Hancock, R.E.W.; Straus, S.K. Characterization of the structure and membrane interaction of the antimicrobial peptides aurein 2.2 and 2.3 from Australian southern bell frogs. *Biophys. J.* **2007**, 92(8):2854–2864.
23. Haney, E.F.; Nguyen, L.T.; Schibli, D.J.; Vogel, H.J. Design of a novel tryptophan-rich membrane-active antimicrobial peptide from the membrane proximal region of the HIV glycoprotein, gp41. *Beilstein J. Org. Chem.* **2012**, 8:1172–1184.
24. Haney, E.F.; Hancock, R.E.W. Peptide design for antimicrobial and immunomodulatory applications. *Biopolymers* **2013**, 100(6):572–583.
25. Uhlig, T.; Kyprianou, T.; Martinelli, F.G.; Oppici, C.A.; Heiligers, D.; Hills, D.; Calvo, X.R.; Verhaert, P. The emergence of peptides in the pharmaceutical business: from exploration to exploitation. *EuPA Open Proteom.* **2014**, 4:58–69.
26. Nuti, R.; Goud, N.S.; Saraswati, A.P.; Alvala, R.; Alvala, M. Antimicrobial Peptides: A Promising Therapeutic Strategy in Tackling Antimicrobial Resistance. *Curr. Med. Chem.* **2017**, 24(38):4303-4314.
27. Easton, D.M.; Nijnik, A.; Mayer, M.L.; Hancock, R.E.W. Potential of immunomodulatory host defense peptides as novel anti-infectives. *Trends Biotechnology* **2009**, 27(10):582-590.
28. Choi, K-Y.; Chow, L.N.Y.; Mookherjee, N. Cationic host defence peptides: multifaceted role in immune modulation and inflammation. *J. Innate Immun.* **2012**, 4(4):361-370.
29. Hamill, P.; Brown, K.; Jenssen, H.; Hancock, R.E.W. Novel anti-infectives: is host defence the answer? *Curr. Opin. Biotechnol.* **2008**, 19(6):628-636.
30. Madera, L.; Hoskin, D.W. Protocols for Studying Antimicrobial Peptides (AMPs) as Anticancer Agents. *Methods Mol. Biol.* **2017**, 1548:331-343.
31. Marr, A.K.; Gooderham, W.J.; Hancock, R.E. Antibacterial peptides for therapeutic use: Obstacles and realistic outlook. *Curr. Opin. Pharmacol.* **2006**, 6(5):468-472.
32. Bowdish, D.M.E.; Davidson, D.J.; Hancock, R.E.W. A re-evaluation of the role of host defence peptides in mammalian immunity. *Curr. Protein Pept. Sci.* **2005**, 6(1):35–51.
33. Nijnik, A.; Hancock, R. Host defence peptides: antimicrobial and immunomodulatory activity and potential applications for tackling antibiotic-resistant infections. *Emerg. Health Threats J.* **2009**, 2:e1.

34. Takahashi, D.; Shukla, S.K.; Prakash, O.; Zhang, G. Structural determinants of host defense peptides for antimicrobial activity and target cell selectivity. *Biochimie* **2010**, 92(9):1236–1241.
35. Hancock, R.E. Mechanisms of action of newer antibiotics for Gram positive pathogens. *Lancet Infect. Dis.* **2005**, 5(4):209–218.
36. Jenssen, H.; Hamill, P.; Hancock, R.E.W. Peptide antimicrobial agents. *Clin. Microbiol. Rev.* **2006**, 19(3):491–511.
37. Travkova, O.G.; Moehwald, H.; Brezesinski, G. The interaction of antimicrobial peptides with membranes. *Adv. Colloid Interface Sci.* **2017**, 247:521–532.
38. Harris, F.; Dennison, S.R.; Phoenix, D.A. Anionic antimicrobial peptides from eukaryotic organisms. *Curr. Protein Pept. Sci.* **2009**, 10(6):585–606.
39. Powers, S.J-P.; Hancock, R.E.W. The relationship between peptide structure and antibacterial activity. *Peptides* **2003**, 24(11):1681-91.
40. Kumar, P.; Kizhakkedathu, J.N.; Straus, S.K. Antimicrobial Peptides: Diversity, Mechanism of Action and Strategies to Improve the Activity and Biocompatibility in Vivo. *Biomolecules* **2018**, 8(1):4.
41. Chen, C.H.; Lu, T.K. Development and Challenges of Antimicrobial Peptides for Therapeutic Applications. *Antibiotics* **2020**, 9(1):24.
42. Guha, S.; Ghimire, J.; Wu, E.; Wimley, W.C. Mechanistic Landscape of Membrane-Permeabilizing Peptides. *Chem Rev.* **2019**, 119(9):6040–6085.
43. Lee, T.-H.; Hofferek, V.; Separovic, F.; Reid, G.E.; Aguilar, M.-I. The role of bacterial lipid diversity and membrane properties in modulating antimicrobial peptide activity and drug resistance. *Curr. Opin. Chem. Biol.* **2019**, 52:85–92.
44. Wang, G. Database-guided Discovery of Potent Peptides to Combat HIV-1 or Superbugs. *Pharmaceuticals (Basel)* **2013**, 6(6):728–758.
45. Brogden, K.A. Antimicrobial peptides: pore formers or metabolic inhibitors in bacteria? *Nat. Rev. Microbiol.* **2005**, 3(3):238–250.
46. Hancock, R.E.; Diamond, G. The role of cationic antimicrobial peptides in innate host defences. *Trends Microbiol.* **2000**, 8(9):402-10.
47. Langen, G.; Imani, J.; Altincicek, B.; Kieseritzky, G.; Kogel, K.-H.; Vilcinskas, A. Transgenic expression of gallerimycin, a novel antifungal insect defensin from the greater wax moth Galleria mellonella, confers resistance to pathogenic fungi in tobacco. *Biol. Chem.* **2006**, 387(5):549-57.
48. Wang, G. Structures of human host defense cathelicidin ll-37 and its smallest antimicrobial peptide kr-12 in lipid micelles. *J. Biol. Chem.* **2008**, 283(47):32637–32643.
49. Hancock, R.E.; Haney, E.F.; Gill, E.E. The immunology of host defence peptides: beyond antimicrobial activity. *Nat. Rev. Immunol.* **2016**, 16(5):321-334.
50. Zairi, A.; Tangy, F.; Bouassida, K.; Hani, K. Dermaseptins and magainins: antimicrobial peptides from frogs' skin-new sources for a promising spermicides microbicides-a mini review. *J. Biomed. Biotechnol.* **2009**, 2009:452567.

51. Lee, T.-H.; Hall, K.N.; Aguilar, M.-I. Antimicrobial Peptide Structure and Mechanism of Action: A Focus on the Role of Membrane Structure. *Curr. Top. Med. Chem.* **2016**, 16(1): 25–39.
52. Powers, S.J.-P.; Rozek, A.; Hancock, R.E.W. Structure-activity relationships for the beta-hairpin cationic antimicrobial peptide polyphemusin I. *Biochim. Biophys. Acta* **2004**, 1698(2):239– 250.
53. Miyata, T.; Tokunaga, F.; Yoneya, T.; Yoshikawa, K.; Iwanaga, S.; Niwa, M.; Takao, T.; Shimonishi, Y. Antimicrobial peptides, isolated from horseshoe crab hemocytes, tachyplesin II, and polyphemusins I and II: chemical structures and biological activity. *J. Biochem.* **1989**, 106 (4), 663-668.
54. Rozek, A.; Friedrich, C.L.; Hancock, R.E. Structure of the bovine antimicrobial peptide indolicidin bound to dodecylphosphocholine and sodium dodecyl sulfate micelles. *Biochemistry* **2000**, 39(51):15765–15774.
55. Falla, T.J.; Karunaratne, D.N.; Hancock, R.E. Mode of action of the antimicrobial peptide indolicidin. *J. Biol. Chem.* **1996**, 271(32):19298–19303.
56. Rokitskaya, T.I.; Kolodkin, N.I.; Kotova, E.A.; Antonenko, Y.N. Indolicidin action on membrane permeability: carrier mechanism versus pore formation. *Biochim. Biophys. Acta* **2011**, 1808(1):91–97.
57. Sawai, M.V.; Jia, H.P.; Liu, L.; Aseyev, V.; Wiencek, J.M.; McCray Jr, P.B.; Ganz, T.; Kearney, W.R.; Tack, B.F. The NMR structure of human beta-defensin-2 reveals a novel alpha-helical segment. *Biochemistry* **2001**, 40(13): 3810–3816.
58. Otte, J.-M.; Werner, I.; Brand, S.; Chromik, A.M.; Schmitz, F.; Kleine, M.; Schmidt, W.E. Human beta defensin 2 promotes intestinal wound healing *in vitro*. *J. Cell. Biochem.* **2008**, 104(6):2286–97.
59. Ulm, H.; Wilmes, M.; Shai, Y.; Sahl, H.-G. Antimicrobial Host Defensins—Specific Antibiotic Activities and Innate Defense Modulation. *Front. Immunol.* **2012**, 3:249.
60. Zhang, L.; Rozek, A.; Hancock, R.E. Interaction of cationic antimicrobial peptides with model membranes. *J. Biol. Chem.* **2001**, 276(38):35714–35722.
61. Guilhelmelli, F.; Vilela, N.; Albuquerque, P.; Derengowski L, S.; Silva-Pereira, I.; Kyaw, C.M. Antibiotic development challenges: the various mechanisms of action of antimicrobial peptides and of bacterial resistance. *Front. Microbiol.* **2013**, 4:353.
62. Matsuzaki, K.; Sugishita, K.; Ishibe, N.; Ueha, M.; Nakata, S.; Miyajima, K.; Epand, R.M. Relationship of Membrane Curvature to the Formation of Pores by Magainin 2. *Biochemistry* **1998**, 37(34):11856–11863.
63. Epand, R.M.; Vogel, H.J. Diversity of antimicrobial peptides and their mechanisms of action. *Biochim. Biophys. Acta* **1999**, 1462(1-2);11–28.
64. Jouhet, J. Importance of the hexagonal lipid phase in biological membrane organization. *Front. Plant Sci.* **2013**, 4:494.
65. Drin, G.; Antonny, B. Amphipathic helices and membrane curvature. *FEBS Lett.* **2010**, 584(9):1840–1847.

66. Schmidt, N.W.; Wong, G.C.L. Antimicrobial peptides and induced membrane curvature: Geometry, coordination chemistry, and molecular engineering. *Curr. Opin. Solid State Mater. Sci.* **2013**, 17(4):151–163.
67. Yeaman, M.R.; Yount, N.Y. Mechanisms of Antimicrobial Peptide Action and Resistance. *Pharmacol. Rev.* **2003**, 55(1):27–55.
68. Shai, Y. Mode of action of membrane active antimicrobial peptides. *Biopolymers* **2002**, 66(4):236–248.
69. Hancock, R.E.; Chapple, D.S. Peptide antibiotics. *Antimicrob. Agents Chemother.* **1999**, 43(6):1317-1323.
70. Clifton, L.A.; Skoda, M.W.A.; Le Brun, A. P.; Ciesielski, F.; Kuzmenko, I.; Holt, S.A.; Lakey, J.H. Effect of divalent cation removal on the structure of gram-negative bacterial outer membrane models. *Langmuir* **2015**, 31(1):404–412.
71. Hancock, R.E.W. Peptide antibiotics. *Lancet* **1997**, 349(9049):418-422.
72. Epand, R.M.; Walker, C.; Epand, R.F.; Magarvey, N.A. Molecular mechanisms of membrane targeting antibiotics. *Biochim. Biophys. Acta* **2016**, 1858(5):980–987.
73. Andersson, D.I.; Hughes, D.; Kubicek-Sutherland, J.Z. Mechanisms and consequences of bacterial resistance to antimicrobial peptides. *Drug Resist. Updat.* **2016**, 26:43–57.
74. Ehrenstein, G.; Lecar, H. Electrically gated ionic channels in lipid bilayers. *Q. Rev. Biophys.* **1977**, 10(1):1-34.
75. Brogden, K.A. Antimicrobial peptides: pore formers or metabolic inhibitors in bacteria? *Nat. Rev. Microbiol.* **2005**, 3(3):238–250.
76. Breukink, E.; de Kruijff, B. The lantibiotic nisin, a special case or not? *Biochim. Biophys. Acta* **1999**, 1462(1-2):223–234.
77. Wimley, W.C. Describing the Mechanism of Antimicrobial Peptide Action with the Interfacial Activity Model. *ACS Chem. Biol.* **2010**, 5(10):905–917.
78. Uematsu, N.; Matsuzaki, K. Polar Angle as a Determinant of Amphipathic-Helix-Lipid Interactions: A Model Peptide Study. *Biophys. J.* **2000**, 79(4):2075–2083.
79. Melo, M. N.; Ferre, R.; Castanho, M.A.R.B. Antimicrobial peptides: linking partition, activity and high membrane-bound concentrations. *Nat. Rev. Microbiol.* **2009**, 7(3):245–250.
80. Matsuzaki, K.; Sugishita, K.; Harada, M.; Fujii, N.; Mikajima, K. Interactions of an antimicrobial peptide, magainin 2, with outer and inner membranes of Gram-negative bacteria. *Biochim. Biophys. Acta* **1997**, 1327(1):119-130.
81. Breukink, E.; Wiedemann, I.; van Kraaij, C.; Kuipers, O.P.; Sahl, H.G.; de Kruijff, B. Use of the cell wall precursor lipid II by a pore-forming peptide antibiotic. *Science* **1999**, 286(5448): 2361–2364.
82. Hilchie, A.L.; Wuerth, K.; Hancock, R.E.W. Immune modulation by multifaceted cationic host defense (antimicrobial) peptides. *Nat. Chem. Biol.* **2013**, 9(12):761–768.
83. Afacan, N.J.; Yeung, A.T.Y.; Pena, O.M.; Hancock, R.E.W. Therapeutic potential of host defense peptides in antibiotic-resistant infections. *Curr. Pharm. Des.* **2012**, 18(6):807–819.

84. Mader, J.S.; Hoskin, D.W. Cationic antimicrobial peptides as novel cytotoxic agents for cancer treatment. *Expert Opin. Investig. Drugs* **2006**, 15(8): 933–946.
85. Lai, Y.; Gallo, R.L. AMPed up immunity: how antimicrobial peptides have multiple roles in immune defense. *Trends Immunol.* **2009**, 30(3):131–141.
86. Hancock, R.E.W.; Nijnik, A.; Philpott, D.J. Modulating immunity as a therapy for bacterial infections. *Nat. Rev. Microbiol.* **2012**, 10(4):243–254.
87. Lee, E.Y.; Lee, M.W.; Wong, G.C.L. Modulation of toll-like receptor signaling by antimicrobial peptides. *Semin. Cell Dev. Biol.* **2019**, 88:173–184.
88. Van Harten, R.M.; van Woudenbergh, E.; van Dijk, A.; Haagsman, H.P. Cathelicidins: Immunomodulatory Antimicrobials. *Vaccines* **2018**, 6(3):63.
89. Nijnik, A.; Madera, L.; Ma, S.; Waldbrook, M.; Elliott, M.R.; Easton, D.M.; Mayer, M.L.; Mullaly, S.C.; Kindrachuk, J.; Jenssen, H.; Hancock, R.E.W. Synthetic Cationic Peptide IDR-1002 Provides Protection against Bacterial Infections through Chemokine Induction and Enhanced Leukocyte Recruitment. *J. Immunol.* **2010**, 184(5):2539–2550.
90. Scott, M.G.; Dullaghan, E.; Mookherjee, N.; Glavas, N.; Waldbrook, M.; Thompson, A.; Wang, A.; Lee, K.; Doria, S.; Hamill, P.; et al. An anti-infective peptide that selectively modulates the innate immune response. *Nat. Biotechnol.* **2007**, 25(4):465–472.
91. Steinstraesser, L.; Kraneburg, U.; Jacobsen, F.; Al-Benna, S. Host defense peptides and their antimicrobial-immunomodulatory duality. *Immunobiology* **2011**, 216(3):322-333.
92. Hu, Z.; Murakami, T.; Suzuki, K.; Tamura, H.; Kuwahara-Arai, K.; Iba, T.; Nagaoka, I. Antimicrobial cathelicidin peptide LL-37 inhibits the LPS/ATP-induced pyroptosis of macrophages by dual mechanism. *PLoS One* **2014**, 9(1):e85765.
93. Zhang, L.; Dhillon, P.; Yan, H.; Farmer, S.; Hancock, R.E. Interactions of bacterial cationic peptide antibiotics with outer and cytoplasmic membranes of Pseudomonas aeruginosa. *Antimicrob. Agents Chemother.* **2000**, 44(12):3317–3321.
94. Mansour, S.C.; Pena, O.M.; Hancock, R.E. Host defense peptides: front-line immunomodulators. *Trends Immunol.* **2014**, 35(9):443-450.
95. Vaara, M. New approaches in peptide antibiotics. *Curr. Opin. Pharmacol.* **2009**, 9(5):571–576.
96. Gentilucci, L.; De Marco, R.; Cerisoli, L. Chemical modifications designed to improve peptide stability: incorporation of non-natural amino acids, pseudo-peptide bonds, and cyclization. *Curr. Pharm. Des.* **2010**, 16(28):3185–3203.
97. Nordström, R.; Malmsten, M. Delivery systems for antimicrobial peptides. *Adv. Colloid Interface Sci.* **2017**, 242:17–34.
98. Davies, J.S.; Elmore, D.T. Amino Acids, Peptides and Proteins. Volume 36, A Review of the Literature Published during 2003-2004; RSC Pub: Cambridge, UK, 2007; ISBN 9781847558459.
99. Berthold, N.; Czihal, P.; Fritsche, S.; Sauer, U.; Schiffer, G.; Knappe, D.; Alber, G.; Hoffmann, R. Novel Apidaecin 1b Analogs with Superior Serum Stabilities for Treatment of

Infections by Gram-Negative Pathogens. *Antimicrob. Agents Chemother.* **2013**, 57(1):402–409.

100. Nguyen, L.T.; Chau, J.K.; Perry, N.A.; de Boer, L.; Zaat, S.A.J.; Vogel, H.J. Serum Stabilities of Short Tryptophan- and Arginine-Rich Antimicrobial Peptide Analogs. *PLoS ONE* **2010**, 5(9):e12684.
101. Papanastasiou, E.A.; Hua, Q.; Sandouk, A.; Son, U.H.; Christenson, A.J.; Van Hoek, M.L.; Bishop, B.M. Role of acetylation and charge in antimicrobial peptides based on human-defensin-3. *APMIS* **2009**, 117(7):492–499.
102. Jayawardene, D.S.; Dass, C. The effect of N-terminal acetylation and the inhibition activity of acetylated enkephalins on the aminopeptidase M-catalyzed hydrolysis of enkephalins. *Peptides* **1999**, 20(8): 963–970.
103. Reinhardt, A.; Neundorf, I. Design and Application of Antimicrobial Peptide Conjugates. *Int. J. Mol. Sci.* **2016**, 17(5):701.
104. Veronese, F.M.; Mero, A. The Impact of PEGylation on Biological Therapies. *BioDrugs* **2008**, 22(15):315–329.
105. Guiotto, A.; Pozzobon, M.; Canevari, M.; Manganelli, R.; Scarin, M.; Veronese, F.M. PEGylation of the antimicrobial peptide nisin A: problems and perspectives. *Farmaco* **2003**, 58(1):45–50.
106. Som, A.; Vemparala, S.; Ivanov, I.; Tew, G.N. Synthetic mimics of antimicrobial peptides. *Biopolymers* **2008**, 90(2):83–93.
107. Rotem, S.; Mor, A. Antimicrobial peptide mimics for improved therapeutic properties. *Biochim. Biophys. Acta Biomembr.* **2009**, 1788(8):1582–1592.
108. Giuliani, A.; Rinaldi, A.C. Beyond natural antimicrobial peptides: multimeric peptides and other peptidomimetic approaches. *Cell. Mol. Life Sci.* **2011**, 68(13):2255–2266.
109. Bracci, L.; Falciani, C.; Lelli, B.; Lozzi, L.; Runci, Y.; Pini, A.; De Montis, M.G.; Tagliamonte, A.; Neri, P. Synthetic Peptides in the Form of Dendrimers Become Resistant to Protease Activity. *The Journal of Biological Chemistry.* **2003**, 278(47): 46590–46595.
110. Syryamina, V.N.; Samoilova, R.I.; Tsvetkov, Y.D.; Ischenko, A.V.; De Zotti, M.; Gobbo, M.; Toniolo, C.; Formaggio, F.; Dzuba, S.A. Peptides on the Surface: Spin-Label EPR and PELDOR Study of Adsorption of the Antimicrobial Peptides Trichogin GA IV and Ampullosporin A on the Silica Nanoparticles. *Appl. Magn. Reson.* **2016**, 47:309–320.
111. Godoy-Gallardo, M.; Mas-Moruno, C.; Yu, K.; Manero, J.M.; Gil, F.J.; Kizhakkedathu, J.N.; Rodriguez, D. Antibacterial Properties of hLf1–11 Peptide onto Titanium Surfaces: A Comparison Study Between Silanization and Surface Initiated Polymerization. *Biomacromolecules* **2015**, 16(2):483–496.
112. Chen, W.-Y.; Chang, H.-Y.; Lu, J.-K.; Huang, Y.-C.; Harroun, S.G.; Tseng, Y.-T.; Li, Y.-J.; Huang, C.-C.; Chang, H.-T. Self-Assembly of Antimicrobial Peptides on Gold Nanodots: Against Multidrug-Resistant Bacteria and Wound-Healing Application. *Adv. Funct. Mater.* **2015**, 25:7189–7199.

113. Chaudhari, A.A.; Ashmore, D.; deb Nath, S.; Kate, K.; Dennis, V.; Singh, S.R.; Owen, D.R.; Palazzo, C.; Arnold, R.D.; Miller, M.E.; Pillai, S.R. A novel covalent approach to bio-conjugate silver coated single walled carbon nanotubes with antimicrobial peptide. *J. Nanobiotechnology* **2016**, 14, 58.

114. Galdiero, E.; Siciliano, A.; Maselli, V.; Gesuele, R.; Guida, M.; Fulgione, D.; Galdiero, S.; Lombardi, L.; Falanga, A. An integrated study on antimicrobial activity and ecotoxicity of quantum dots and quantum dots coated with the antimicrobial peptide indolicidin. *Int. J. Nanomedicine* **2016**, 11:4199–4211.

115. Kanchanapally, R.; Viraka Nellore, B.P.; Sinha, S.S.; Pedraza, F.; Jones, S.J.; Pramanik, A.; Chavva, S.R.; Tchounwou, C.; Shi, Y.; Vangara, A.; Sardar, D.; Ray, P.C. Antimicrobial Peptide-Conjugated Graphene Oxide Membrane for Efficient Removal and Effective Killing of Multiple Drug Resistant Bacteria. *RSC Adv.* **2015**, 5(24):18881–18887.

116. Dostalova, S.; Moulick, A.; Milosavljevic, V.; Guran, R.; Kominkova, M.; Cihalova, K.; Heger, Z.; Blazkova, L.; Kopel, P.; Hynek, D.; Vaculovicova, M.; Adam, V.; Kizek, R. Antiviral activity of fullerene C60 nanocrystals modified with derivatives of anionic antimicrobial peptide maximin H5. *Monatshefte für Chem. Chem. Mon.* **2016**, 147:905–918.

117. D'Angelo, I.; Casciaro, B.; Miro, A.; Quaglia, F.; Mangoni, M.L.; Ungaro, F. Overcoming barriers in Pseudomonas aeruginosa lung infections: Engineered nanoparticles for local delivery of a cationic antimicrobial peptide. *Colloids Surf. B Biointerfaces* **2015**, 135:717–725.

118. Lim, L.M.; Ly, N.; Anderson, D.; Yang, J.C.; Macander, L.; Jarkowski 3rd, A.; Forrest, A.; Bulitta, J.B.; Tsuji, B.T. Resurgence of colistin: A review of resistance, toxicity, pharmacodynamics, and dosing. *Pharmacotherapy* **2010**, 30(12):1279–1291.

119. Velkov, T.; Thompson, P.E.; Nation, R.L.; Li, J. Structure—Activity relationships of polymyxin antibiotics. *J. Med. Chem.* **2010**, 53(5):1898–1916.

120. Mohamed, Y.F.; Abou-Shleib, H.M.; Khalil, A.M.; El-Guink, N.M.; El-Nakeeb, M.A. Membrane permeabilization of colistin toward pan-drug resistant Gram-negative isolates. *Braz. J. Microbiol.* **2016**, 47(2):381–388.

121. Hallett, J.W.; Wolkowicz, M.I.; Leopold, I.H. Ophthalmic use of neosporin. *Am. J. Ophthalmol.* **1956**, 41(5):850–853.

122. Eliopoulos, G.M.; Willey, S.; Reiszner, E.; Spitzer, P.G.; Caputo, G.; Moellering, Jr. R.C. In vitro and in vivo activity of LY 146032, a new cyclic lipopeptide antibiotic. *Antimicrob. Agents Chemother.* **1986**, 30(4):532–535.

123. Carpenter, C.F.; Chambers, H.F. Daptomycin: Another novel agent for treating infections due to drug-resistant gram-positive pathogens. *Clin. Infect. Dis.* **2004**, 38(7):994–1000.

124. Chen, A.Y.; Zervos, M.J.; Vazquez, J.A. Dalbavancin: A novel antimicrobial. *Int. J. Clin. Pract.* **2007**, 61(5):853–863.

125. Zhanel, G.G.; Calic, D.; Schweizer, F.; Zelenitsky, S.; Adam, H.; Lagacé-Wiens, P.R.; Rubinstein, E.; Gin, A.S.; Hoban, D.J.; Karlowsky, J.A. New lipoglycopeptides: A Comparative Review of Dalbavancin, Oritavancin and Telavancin. *Drugs* **2010**, 70(7): 859–886.

126. Saravolatz, L.D.; Stein, G.E.; Johnson, L.B. Telavancin: A Novel Lipoglycopeptide. *Clin. Infect. Dis.* **2009**, 49(12):1908–1914.

127. Higgins, D.L.; Chang, R.; Debabov, D.V.; Leung, J.; Wu, T.; Krause, K.M.; Sandvik, E.; Hubbard, J.M.; Kaniga, K.; Schmidt Jr, D.E.; Gao, Q.; Cass, R.T.; Karr, D.E.; Benton, B.M.; Humphrey, P.P. Telavancin, a Multifunctional Lipoglycopeptide, Disrupts both Cell Wall Synthesis and Cell Membrane Integrity in Methicillin-Resistant Staphylococcus aureus. *Antimicrob. Agents Chemother.* **2005**, 49(3):1127–1134.

128. Cochrane, S.A.; Vederas, J.C. Lipopeptides from Bacillus and Paenibacillus spp.: A Gold Mine of Antibiotic Candidates. *Med. Res. Rev.* **2016**, 36(1): 4–31.

129. Hamamoto, K.; Kida, Y.; Zhang, Y.; Shimizu, T.; Kuwano, K. Antimicrobial activity and stability to proteolysis of small linear cationic peptides with D-amino acid substitutions. *Microbiol. Immunol.* **2002,** 46(11):741–749.

130. Wang, J.; Yadav, V.; Smart, A.L.; Tajiri, S.; Basit, A.W. Toward Oral Delivery of Biopharmaceuticals: An Assessment of the Gastrointestinal Stability of 17 Peptide Drugs. *Mol. Pharm.* **2015**, 12(3):966–973.

131. Wang, J.; Yadav, V.; Smart, A.L.; Tajiri, S.; Basit, A.W. Stability of peptide drugs in the colon. *Eur. J. Pharm. Sci.* **2015**, 78:31–36.

132. Vlieghe, P.; Lisowski, V.; Martinez, J.; Khrestchatisky, M. Synthetic therapeutic peptides: science and market. *Drug Discov. Today* **2010**, 15(1-2): 40–56.

133. Scheinfeld, N. Dalbavancin: A review. *Drugs Today (Barc)* **2007**, 43(5):305–316.

134. Rosenthal, S.; Decano, A.G.; Bandali, A.; Lai, D.; Malat, G.E.; Bias, T.E. Oritavancin (Orbactiv): A New-Generation Lipoglycopeptide for the Treatment of Acute Bacterial Skin and Skin Structure Infections. *Pharm. Ther.* **2018**, 43(3):143–179.

135. Smith, J.R.; Roberts, K.D.; Rybak, M.J. Dalbavancin: A Novel Lipoglycopeptide Antibiotic with Extended Activity Against Gram-Positive Infections. *Infect. Dis. Ther.* **2015**, 4(3):245–258.

136. Cavanaugh, C.; Moeckel, G.W.; Perazella, M.A. Telavancin-associated acute kidney injury. *Clin. Nephrol.* **2019**, 91(3):187–191.

137. Nnedu, O.N.; Pankey, G.A. Update on the emerging role of telavancin in hospital-acquired infections. *Ther. Clin. Risk Manag.* **2015**, 11:605–610.

138. Wolinsky, E.; Hines, J.D. Neurotoxic and nephrotoxic effects of colistin in patients with renal disease. *N. Engl. J. Med.* **1962**, 266:759–762.

139. Poirel, L.; Jayol, A.; Nordmann, P. Polymyxins: Antibacterial Activity, Susceptibility Testing, and Resistance Mechanisms Encoded by Plasmids or Chromosomes. *Clin. Microbiol. Rev.* **2017**, 30(2):557–596.

140. Fox, J.L. Antimicrobial peptides stage a comeback. *Nat. Biotechnol.* **2013**, 31(5):379–382.

141. Fjell, C.D.; Hiss, J.A.; Hancock, R.E.W.; Schneider, G. Designing antimicrobial peptides: form follows function. *Nat. Rev. Drug Discov.* **2011**, 11(1)37-51.

142. Novarifyn® (NP432) is antibacterial peptide with a number of key benefits over conventional antibiotic therapies and the clear potential to succeed where existing treatments for a number of bacterial infections, including those caused by MRSA, *P. aeruginosa*, and *C. difficile*, are

failing. [(accessed on 18 August 2017)]; available online: http://www.novabiotics.co.uk/pipeline/novarifyn-np432.

143. Myhrman, E.; Hakansson, J.; Lindgren, K.; Björn, C.; Sjöstrand, V.; Mahlapuu, M. The novel antimicrobial peptide PXL150 in the local treatment of skin and soft tissue infections. *Appl. Microbial. Biotechnol.* **2013,** 97(7):3085-3096.

144. Ghobrial, O.G.; Derendorf, H.; Hillman, J.D. Pharmacodynamic activity of the lantibiotic MU1140. *Int. J. Antimicrob. Agents* **2009**, 33(1):70–74.

145. Brunetti, J.; Falciani, C.; Roscia, G.; Pollini, S.; Bindi, S.; Scali, S.; Arrieta, U.C.; Gómez-Vallejo, V.; Quercini, L.; Ibba, E.; Prato, M.; Rossolini, G.M.; Llop, J.; Bracci, L.; Pini, A. In vitro and in vivo efficacy, toxicity, bio-distribution and resistance selection of a novel antibacterial drug candidate. *Sci. Rep.* **2016**, 6:26077.

146. Pini, A.; Falciani, C.; Mantengoli, E.; Bindi, S.; Brunetti, J.; Iozzi, S.; Rossolini, G.M.; Bracci, L. A novel tetrabranched antimicrobial peptide that neutralizes bacterial lipopolysaccharide and prevents septic shock in vivo. *FASEB J.* **2010**, 24(4):1015-1022.

147. Pini, A.; Giuliani, A.; Falciani, C.; Runci, Y.; Ricci, C.; Lelli, B.; Malossi, M.; Neri, P.; Rossolini, G.M.; Bracci, L. Antimicrobial activity of novel dendrimeric peptides obtained by phage display selection and rational modification. *Antimicrob. Agents Chemother.* **2005**, 49(7): 2665-2672.

148. Tam, J.P. Synthetic peptide vaccine design: synthesis and properties of a high-density multiple antigenic peptide system. *Proc. Natl. Acad. Sci. USA* **1988**, 85(15):5409-5413.

149. Falciani, C.; Lozzi, L.; Pini, A.; Corti, F.; Fabbrini, M.; Bernini, A.; Lelli, B.; Niccolai, N.; Bracci, L. Molecular basis of branched peptides resistance to enzyme proteolysis. *Chem. Biol. Drug Des.* **2007**, 69(3):216-221.

150. Mäde, V.; Els-Heindl, S.; Beck-Sickinger, A.G. Automated solid-phase peptide synthesis to obtain therapeutic peptides. *Beilstein J. Org. Chem.* **2014**, 10:1197–1212.

151. Pini, A.; Lozzi, L.; Bernini, A.; Brunetti, J.; Falciani, C.; Scali, S.; Bindi, S.; Di Maggio, T.; Rossolini, G.M.; Niccolai, N.; Bracci, L. Efficacy and toxicity of the antimicrobial peptide M33 produced with different counter-ions. *Amino Acids* **2012**, 43(1):467-473.

152. Falciani, C.; Lozzi, L.; Pollini, S.; Luca, V.; Carnicelli, V.; Brunetti, J.; Lelli, B.; Bindi, S.; Scali, S.; Di Giulio, A.; Rossolini, G.M.; Mangoni, M.L.; Bracci, L.; Pini, A. Isomerization of an Antimicrobial Peptide Broadens Antimicrobial Spectrum to Gram-Positive Bacterial Pathogens. *Plos one* **2012**, 7(10): e46259.

153. Van der Weide, H.; Brunetti, J.; Pini, A.; Bracci, L.; Ambrosini, C.; Lupetti, P.; Paccagnini, E.; Gentile, M.; Bernini, A.; Niccolai, N.; Vermeulen-de Jongh, D.; Bakker-Woudenberg, I.A.J.M.; Goessens, W.H.F.; Hays, J.P.; Falciani, C. Investigations into the killing activity of an antimicrobial peptide active against extensively antibiotic-resistant K. pneumoniae and P. aeruginosa. *Biochim. Biophys. Acta* **2017**, 1859(10):1796–1804.

154. Froes, F.; Roche, N.; Blasi, F. Pneumococcal vaccination and chronic respiratory diseases, *Int. J. Chron. Obstruct. Pulmon. Dis.* **2017**, 12: 3457–3468.

155. Brunetti, J.; Roscia, G.; Lampronti, I.; Gambari, R.; Quercini, L.; Falciani, C.; Bracci, L.; Pini, A. Immunomodulatory and Anti-inflammatory Activity in Vitro and in Vivo of a Novel Antimicrobial Candidate. *J. Biol. Chem.* **2016**, 291(49):25742-25748.

156. Ryan, S.M.; Mantovani, G.; Wang, X.; Haddleton, D.M.; Brayden, D.J. Advances in PEGylation of important biotech molecules: delivery aspects. *Expert Opin. Drug Deliv.* **2008**, 5(4):371-83.

157. Quercini, L.; Brunetti, J.; Riolo, G.; Bindi, S.; Scali, S.; Lampronti, I.; D'Aversa, E.; Wronski, S.; Pollini, S.; Gentile, M.; Lupetti, P.; Rossolini, G.M.; Falciani, C.; Bracci, L.; Pini, A. An antimicrobial molecule mitigates signs of sepsis in vivo and eradicates infections from lung tissue. *FASEB J.* **2020**, 34(1):192-207.

158. Castiglia, F.; Zevolini, F.; Riolo, G.; Brunetti, J.; De Lazzari, A.; Moretto, A.; Manetto, G.; Fragai, M.; Algotsson, J.; Evenäs, J.;Bracci, L.; Pini, A.; Falciani, C. NMR Study of the Secondary Structure and Biopharmaceutical Formulation of an Active Branched Antimicrobial Peptide. *Molecules* **2019**, 24(23):4290.

159. Wüthrich, K. NMR of Proteins and Nucleic Acids, 1st ed.; Wiley: Hoboken, NJ, USA, **1986**, pp. 1–292.

160. Wishart, D.S.; Sykes, B.D.; Richards, F.M. The chemical shift index: A fast and simple method for the assignment of protein secondary structure through NMR spectroscopy. *Biochemistry* **1992**, 31(6):1647–1651.

161. Wishart, D.S.; Sykes, B.D. The ^{13}C chemical-shift index: A simple method for the identification of protein secondary structure using ^{13}C chemical-shift data. *J. Biomol. NMR* **1994**, 4(2):171–180.

162. Roux, S.; Zékri, E.; Rousseau, B.; Paternostre, M.; Cintrat, J.-C.; Fay, N. Elimination and exchange of trifluoroacetate counter-ion from cationic peptides: a critical evaluation of different approaches. *J. Pept. Sci.* **2008**, 14(3):354–359.

163. Andrushchenko, V.V.; Vogel, H.J.; Prenner, E.J. Optimization of the hydrochloric acid concentration used for trifluoroacetate removal from synthetic peptides. *J. Pept. Sci.* **2007**, 13(1):37–43.

164. Sani, M.-A.; Loudet, C.; Gröbner, G.; Dufourc, E.J. Pro-apoptotic bax-alpha1 synthesis and evidence for beta-sheet to alpha-helix conformational change as triggered by negatively charged lipid membranes. *J. Pept. Sci.* **2007**, 13(2):100–106.

165. Beck, A.; Bussat, M.C.; Klinquer-Hamour, C.; Goetsch, L.; Aubry, J.P.; Champion, T.; Julien, E.; Haeuw, J.F.; Bonnefoy, J.Y.; Corvaia, N. Stability and CTL activity of N-terminal glutamic acid containing peptides. *J. Pept. Res.* **2001**, 57(6):528–538.

166. Aashigari, S.; Goud, R.; Sneha, S.; Vykuntam, U.; Potnuri, N. Stability studies of pharmaceutical products. *World J. Pharm. Res.* **2019**, 8(8):479-492.

167. Little, M.J.; Aubry, N.; Beaudoin, M.-E.; Goudreau, N.; LaPlante, S.R. Quantifying trifluoroacetic acid as counterion in drug discovery by ^{19}F NMR and capillary electrophoresis. *J. Pharm. Biomed. Anal.* **2007**, 43(4):1324–1330.

168. Preiss, A.; Kruppa, J.; Buschmann, J.; Mügge, C. The determination of trifluoroacetic acid in rat milk samples by ^{19}F-NMR spectroscopy and capillary gas chromatography. *J. Pharm. Biomed. Anal.* **1998**, 16(8):1381–1385.

169. Zhang, O.; Kay, L.E.; Olivier, J.P.; Forman-Kay, J.D. Backbone ^{1}H and ^{15}N resonance assignments of the N-terminal SH3 domain of drk in folded and unfolded states using enhanced-sensitivity pulsed field gradient NMR techniques. *J. Biomol. NMR.* **1994**, 4(6):845–858.

170. Sikora, K.; Neubauer, D.; Jàskiewicz, M.; Kamysz, W. Citropin 1.1 Trifluoroacetate to Chloride Counter-Ion Exchange in HCl-Saturated Organic Solutions: An Alternative Approach. *Int. J. Pept. Res. Ther.* **2018**, 24(2):265–270.

171. Cornish, J.; Callon, K.E.; Lin, C.Q.; Xiao, C.L.; Mulvey, T.B.; Cooper, G.J.; Reid, I.R. Trifluoroacetate, a contaminant in purified proteins, inhibits proliferation of osteoblasts and chondrocytes. *Am. J. Phisyol.* **1999**, 277(5):E779–E783.

172. Takeuchi, O.; Akira, S. Pattern recognition receptors and inflammation. *Cell.* **2010**, 140(6): 805–820.

173. Franchi, L.; Eigenbrod, T.; Muñoz-Planillo, R.; Nuñez, G. The Inflammasome: A Caspase-1 Activation Platform Regulating Immune Responses and Disease Pathogenesis. *Nat. Immunol.* **2009**, 10(3):241-247.

174. Manji, G.A.; Wang, L.; Geddes, B.J.; Brown, M.; Merriam, S.; Al-Garawi, A.; Mak, S.; Lora, J.M.; Briskin, M.; Jurman, M.; Cao, J.; DiStefano, P.S.; Bertin, J. PYPAF1, a PYRIN-containing Apaf1-like protein that assembles with ASC and regulates activation of NF-kappa B. *J. Biol. Chem.* **2002**, 277(13):11570–11575.

175. Franchi, L.; Warner, N.; Viani, K.; Nuñez, G. Function of Nod-like receptors in microbial recognition and host defense. *Immunol. Rev.* **2009**, 227(1):106–128.

176. Martinon, F.; Burns, K.; Tschopp, J. The Inflammasome: A Molecular Platform Triggering Activation of Inflammatory Caspases and Processing of proIL-β. *Mol. Cell* **2002**, 10(2):417–426.

177. Dinarello, C.A. Immunological and Inflammatory Functions of the Interleukin-1 Family. *Annu. Rev. Immunol.* **2009**, 27:519–550.

178. Fink, S.L.; Cookson, B.T. Caspase-1-dependent pore formation during pyroptosis leads to osmotic lysis of infected host macrophages. *Cell. Microbiol.* **2006**, 8(11):1812–1825.

179. Shi, J.; Zhao, Y.;Wang, K.; Shi, X.;Wang, Y.; Huang, H.; Zhuang, Y.; Cai, T.; Wang, F.; Shao, F. Cleavage of GSDMD by inflammatory caspases determines pyroptotic cell death. *Nature* **2015**, 526(7575):660–665.

180. Kayagaki, N.; Stowe, I.B.; Lee, B.L.; O'Rourke, K.; Anderson, K.; Warming, S.; Cuellar, T.; Haley, B.; Roose-Girma, M.; Phung, Q.T.; et al. Caspase-11 cleaves gasdermin D for non-canonical inflammasome signalling. *Nature* **2015**, 526(7575):666–671.

181. He, W.; Wan, H.; Hu, L.; Chen, P.; Wang, X.; Huang, Z.; Yang, Z.-H.; Zhong, C.-Q.; Han, J. Gasdermin D is an executor of pyroptosis and required for interleukin-1β secretion. *Cell Res.* **2015**, 25(12):1285–1298.

182. Sharma, D.; Kanneganti, T.-D. The cell biology of inflammasomes: Mechanisms of inflammasome activation and regulation. *J. Cell Biol.* **2016**, 213(6): 617–629.

183. Lamkanfi, M.; Dixit, V.M. Mechanisms and Functions of Inflammasomes. *Cell* **2014**, 157(5):1013–1022.

184. Malik, A.; Kanneganti, T.-D. Inflammasome activation and assembly at a glance. *J. Cell Sci.* **2017**, 130(23):3955–3963.

185. Mitchell, P.S.; Sandstrom, A.; Vance, R.E. The NLRP1 inflammasome: new mechanistic insights and unresolved mysteries. *Curr. Opin. Immunol.* **2019**, 60:37–45.

186. Hollingsworth, L.R.; David, L.; Li, Y.; Griswold, A.R.; Ruan, J.; Sharif, H.; Fontana, P.; Orth-He, E.L.; Fu, T.-M.; Bachovchin, D.A.; Wu, H. Mechanism of filament formation in UPA-promoted CARD8 and NLRP1 inflammasomes. *Nat. Commun.* **2021**, 12(1):189.

187. D'Osualdo, A.; Weichenberger, C.X.; Wagner, R.N.; Godzik, A.; Wooley, J.; Reed, J.C.; CARD8 and NLRP1 undergo autoproteolytic processing through a ZU5-like domain. *PLoS One* **2011**, 6(11):e27396.

188. Sharif, H.; Wang, L.; Wang, W.L.; Magupalli, V.G.; Andreeva, L.; Qiao, Q.; Hauenstein, A.V.; Wu, Z.; Nunez, G.; Mao, Y.; Wu, H. Structural mechanism for NEK7-licensed NLRP3 inflammasome activation. *Nature* **2019,** 570(7761):338–343.

189. Kelley, N.; Jeltema, D.; Duan, Y.; He, Y. The NLRP3 Inflammasome: An Overview of Mechanisms of Activation and Regulation. *Int. J. Mol. Sci.* **2019**, 20(13):3328.

190. Vajjhala, P.R.; Mirams, R.E.; Hill, J.M. Multiple binding sites on the pyrin domain of ASC protein allow self-association and interaction with NLRP3 protein. *J. Biol. Chem.* **2012**, 287(50):41732–41743.

191. Tschopp, J.; Schroder, K. NLRP3 inflammasome activation: The convergence of multiple signalling pathways on ROS production? *Nat. Rev. Imunol.* **2010**, 10(3):210-215.

192. Schneider, M.; Zimmermann, A.G.; Roberts, R.A.; Zhang, L.; Swanson, K.V.; Wen, H.; Davis, B.K.; Allen, I.C.; Holl, E.K.; Ye, Z.; et al. The innate immune sensor NLRC3 attenuates Toll-like receptor signaling via modification of the signaling adaptor TRAF6 and transcription factor NF-kb. *Nat. Immunol.* **2012**, 13(9):823–831.

193. Zhang, L.; Mo, J.; Swanson, K.V.; Wen, H.; Petrucelli, A.; Gregory, S.M.; Zhang, Z.; Schneider, M.; Jiang, Y.; Fitzgerald, K.A., et al. NLRC3, a member of the NLR family of proteins, is a negative regulator of innate immune signaling induced by the DNA sensor STING. *Immunity* **2014,** 40(3):329–341.

194. Li, X.; Deng, M.; Petrucelli, A.S.; Zhu, C.; Mo, J.; Zhang, L.; Tam, J.W.; Ariel, P.; Zhao, B.; Zhang, S.; Ke, H.; Li, P.; Dokholyan, N.V.; Duncan, J.A.; Ting, J.P.-Y. J. Viral DNA Binding to NLRC3, an Inhibitory Nucleic Acid Sensor, Unleashes STING, a Cyclic Dinucleotide Receptor that Activates Type I Interferon. *Immunity.* **2019**, 50(3):591–599.

195. Man, S.M.; Karki, R.; Kanneganti, T.-D. AIM2 inflammasome in infection, cancer and autoimmunity: role in DNA sensing, inflammation and innate immunity. *Eur. J. Immunol.* **2016**, 46(2):269–280.

196. Morrone, S.R.; Matyszewski, M.; Yu, X.; Delannoy, M.; Egelman, E.H.; Sohn, J. Assembly-driven activation of the AIM2 foreign-dsDNA sensor provides a polymerization template for downstream ASC. *Nat. Comm.* **2015**, 6:7827.

197. Man, S.M.; Kanneganti, T.-D. Regulation of inflammasome activation. *Immunol. Rev.* **2015**, 265(1):6–21.

198. Lu, A.; Kabaleeswaran, V.; Fu, T.; Magupalli, V.G.; Wu, H. Crystal structure of the F27G AIM2 PYD mutant and similarities of its self-association to DED/DED interactions. *J. Mol. Biol.* **2014**, 426(7):1420-1427.

199. Ciccarone, V.C.; Polayes, D.; Luckow, V.A. Generation of Recombinant Baculovirus DNA in *E. coli* Using Baculovirus Shuttle Vector. *Methods Mol. Med.* **1998**, 13:213-235.

200. Luckow, V.A.; Lee, S.C.; Barry, G.F.; Olins, P.O. Efficient Generation of Infectious Recombinant Baculoviruses by Site-Specific Transposon-Mediated Insertion of Foreign Genes into a Baculovirus Genome Propagated in Escherichia coli. *J. Virol.* **1993**, 67(8):4566-4579.

201. Barry, G. F. A broad host-range shuttle system for gene insertion into the chromosomes of Gram-negative bacteria. *Gene* **1988**, 71(1):75-84.

ACKNOWLEDGEMENTS

I would like to thank my tutor, Prof. Alessandro Pini, for giving me the opportunity to work in a friendly and intellectually stimulating research environment that allowed me to grow both scientifically and personally. I would like to thank him for being a friend and not only a Professor and for helping me to follow my inspirations.

I would like to thank Silvia Scali for teaching me how synthetize peptides in the laboratory and for supporting me every moment. I always remember the good moments spent in the laboratory with her, full of important teachings

I would like to thank all the other people that supported me in my laboratory: Luisa Bracci, Chiara Falciani, Luisa Lozzi, Lorenzo Depau, Leila Quercini and Stefano Bindi.

I would like to thank Giovanni, Elisabetta, Laura and Marta to make me always feel in the right place and for having created a beautiful friendship. I love you guys.

To my family, especially to my mother Anna Maria, for encouraging me to reach all of my pursuits, making right decisions and inspiring me to follow my dreams. You are the strongest person that I have ever met and the more special in my life, you know it.

To all my friends, especially to my best friend Elisa for always being close to me, even when I was overseas, and for all our laughs.

To my cats

I would like to thank Professor Hao Wu for giving me the opportunity to work in the laboratories of Boston Children's Hospital and Harvard Medical School, for introducing me in a new hard and very competitive reality and for teaching me many techniques along with leading researchers. My sincere thanks go to Liron David, Liudmila Andreeva, Ying Dong and Bobby Hollingsworth.

Finally, I would like to give special thanks to my American flatmates: the Afroamerican Amina, the Chinese Zheng and the Japanese Takuma for their precious support for almost one year and to make me always feel at home during the terrible and very hard 2020 months, very far from my home, for teaching me other cultures and for confirming that is not important the color of the skin because WE ARE ALL THE SAME.

Another special thank goes to the multi-cultural cat, Bella, wherewith I spent my American lockdown at home.

I really miss you Jamaica Plain, thank you for all.